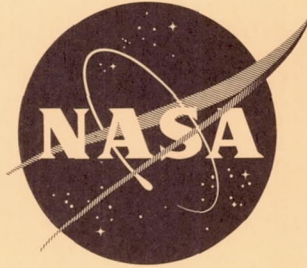N 63-10734

55 1165

886

NASA

TECHNICAL NOTE

D-1433

ANALYSIS OF GUIDANCE PERTURBATIONS FOR A LOW-THRUST

MARS ORBITER MISSION USING SNAP-8

By Alan L. Friedlander

Lewis Research Center
Cleveland, Ohio

NATIONAL AERONAUTICS AND SPACE ADMINISTRATION

WASHINGTON   December 1962

NATIONAL AERONAUTICS AND SPACE ADMINISTRATION

TECHNICAL NOTE D-1433

ANALYSIS OF GUIDANCE PERTURBATIONS FOR A LOW-THRUST

MARS ORBITER MISSION USING SNAP-8

By Alan L. Friedlander

SUMMARY

A typical low-thrust Mars orbiter mission using the Snap-8 power-generating system has been studied from a guidance viewpoint. The mission trajectory was divided into the three characteristic phases, namely, the outward escape spiral, the heliocentric transfer, and the inward capture spiral. The sensitivity of the final trajectory state (velocity, position, and mass) due to errors in the initial trajectory state and to thrust-vector errors was determined for each phase of the mission. The analysis and numerical solutions are based on the methods of linear perturbations and adjoint functions.

During the escape-spiral phase, any of the following minimum errors, if left uncorrected, is sufficient to cause the escape direction to be $180°$ out of phase: a 0.1-percent error in either initial orbital altitude or initial vehicle mass, a 0.1-percent error in the thrust magnitude acting over the entire trajectory, or a $2.8°$ error in the thrust angle acting over the entire trajectory.

During the heliocentric transfer, final position and velocity errors of the order of several hundred thousand kilometers and 10 meters per second will result from either an escape-direction error of $1/2°$, a thrust-magnitude error of 1 percent, or a thrust-angle error of $1/2°$.

During the capture-spiral phase, if the initial velocity vector were in error by only 1 meter per second and 1 milliradian, and if the nominal thrust program were followed exactly, the vehicle would spiral down into the Martian surface.

In general, low-thrust trajectories are highly sensitive to errors. Open-loop trajectory control is thus completely out of the question; that is, repetitive trajectory determination and corrective guidance maneuvers are required to ensure a successful mission.

INTRODUCTION

In the past several years, theoretical and experimental analyses have shown that electric rocket systems are practical and offer high performance in advanced space missions. First-generation spacecraft flights are scheduled to begin around 1965 with an ion engine powered by the Snap-8 nuclear turboelectric system currently under development. A feasible mission that has been proposed for the 60-kilowatt version of Snap-8 is a scientifically instrumented Mars orbiter. Such a mission would begin in a low-altitude Earth-satellite orbit and end in a similar orbit about Mars. Since the vehicle would penetrate a large portion of the near-Martian space as it slowly transverses the capture-spiral trajectory, an accurate survey of radiation and surface conditions may be obtained and transmitted back to Earth.

The question of how accurately the vehicle can be guided to its given target is of great consequence to the success of the mission. As yet, little attention has been given to the problem of low-thrust guidance in the presence of random or systematic perturbations arising from such error sources as thrust-vector control, navigational measurements, and an approximate system model. In a preliminary analysis of this subject (ref. 1), linear perturbation theory and the method of adjoint functions were used to derive the fundamental guidance equation for low-thrust trajectories. This equation provides a means of studying the effect of error perturbations and corrective guidance perturbations. The specific problem treated in reference 1 is an error analysis of the heliocentric-transfer trajectory between Earth and Mars covering a wide range of propulsion characteristics and transfer times. This report is an investigation of the guidance problem for a typical Mars orbiter mission considering, in turn, the escape-spiral phase, the heliocentric-transfer phase, and the capture-spiral phase. The purpose of this investigation is to determine the sensitivity of the final trajectory state for each phase to initial trajectory state errors and thrust vector errors. It should be emphasized that this study is a fixed-time analysis; that is, perturbations refer to the difference between the actual and reference trajectories at a particular instant of time. The choice of time as the independent variable is computationally convenient and is a good criterion of comparison for the problem at hand.

SYMBOLS

a   semimajor axis, m

c   jet velocity, m/sec

e   eccentricity

F thrust force, newtons

f_i function of thrust vector perturbations (eq. (19))

GM gravitational constant of central attracting body, m^3/sec^2

m vehicle mass, kg

p semilatus rectum, m

r radial position, m

r_a apogee distance, m

r_p perigee distance, m

t time, sec or days

u radial velocity, m/sec

V total velocity, m/sec

W matrix of weighting functions

w thrust-error weighting function

x general trajectory state variable

y general thrust-vector perturbation variable

β thrust angle, radians or deg

$\Delta(\ )$ large variation from reference quantity $(\ )$

$\delta(\ )$ small variation from reference quantity $(\ )$

Λ matrix of sensitivity coefficients

λ error sensitivity coefficient, variable in adjoint equations (8) to (12)

φ angular position, radians

ω angular velocity, radians/sec

$\cdot$ scalar product of vectors

Subscripts:

c   beginning of coast period

des   design thrust level

E   Earth

f   final value

ij   general indexes

M   Mars

n   values at t_n - beginning of control interval

o   initial value

Superscripts:

T   transpose of matrix

'   second-order perturbation

·   time derivative

‾   vector

ANALYSIS

Vehicle and Mission Characteristics

In this report an investigation of the trajectory sensitivity and control problem for a particular Earth-Mars instrumented space probe utilizing the Snap-8 electric propulsion system is presented. Rather than proceeding directly to the analysis, it is appropriate here to present the propulsion characteristics of the vehicle that have been assumed and to discuss briefly the mission and trajectory characteristics.

Vehicle-propulsion characteristics (unpublished NASA data). - The Snap-8 vehicle will be placed into a nearly circular, low-altitude satellite orbit utilizing a multistaged chemical booster. Typically, an initial gross weight of 4080 kilograms (9000 lb) is placed in a 927-kilometer (500-naut.-mile) orbit. The design electric power and specific powerplant mass are 60 kilowatts and 22.7 kilograms per kilowatt, respectively, and the resulting powerplant - initial-gross-weight

ratio is 1/3. With a propellant utilization of 90 percent and a power efficiency of 76.2 percent assumed, a design specific impulse of 3600 seconds is obtained. The available thrust force is 2.32 newtons (0.524 lb), and the propellant mass rate is 5.68 kilograms per day.

Mission characteristics. - The mission under consideration is a 415.4-day, one-way trip to Mars beginning in a 927-kilometer Earth-satellite orbit and terminating in a similar satellite orbit about Mars. Figure 1 is a schematic illustration of the overall interplanetary-transfer maneuver. It is convenient to discuss the mission in terms of three distinct phases, namely, the escape spiral, the heliocentric transfer, and the capture spiral.

(1) During the first 139 days of the trip the vehicle increases its energy relative to Earth according to a continuous-power tangential-thrust program. Solar gravitational effects are neglected during this phase.

(2) At the hyperbolic-escape condition, the gravitational effect of the Earth is neglected, and the vehicle initiates a 223-day heliocentric transfer employing an optimum constant-thrust program. The power-coast-power sequence is 27.7, 160, 35.3 days, respectively. The heliocentric-transfer angle is 159°.

(3) At 362 days the vehicle is in the vicinity of Mars and initiates the energy-decreasing capture spiral, again employing a continuous-power-tangential-thrust program. After 53.4 days, the 927-kilometer satellite orbit has been established. Solar gravitational effects are neglected during this phase.

The overall trajectory has been pieced together from a series of two-body solutions in order to simplify the analysis. This procedure has been commonly used by investigators of the low-thrust interplanetary mission. In most cases, the approach taken is to terminate the escape spiral when parabolic escape energy has been attained. After this, the vehicle is assumed to be moving in the Earth's orbit with Earth's orbital velocity relative to the sun, and the Earth's gravitational effect is then neglected. A similar procedure is used at Mars. Frequently, the parabolic energy condition occurs at a position well within the planet's sphere of influence. The essential difference in the approach taken in this analysis is an extension of the escape- and capture-spiral phases past the parabolic energy condition. Transformation to or from the heliocentric system is arbitrarily made at a point where the solar and the planetary gravitational effects are approximately equal. The main reason for extension of the spiral phases is that in the vicinity of the hyperbolic escape or capture condition the motion of the vehicle is approximately along the asymptote of a hyperbola, which is a useful target criterion for guidance purposes.

Figure 2 describes the escape-spiral trajectory in detail, where the last of 500 revolutions about Earth is plotted. Parabolic escape energy is reached at a distance of about 100 Earth radii and at a time of 125.5 days after launch. At a distance of 298 Earth radii, the escape phase is terminated, and, at this point, the relative velocity of the vehicle is 1577 meters per second. The direction of the velocity vector was arbitrarily chosen to be parallel to Earth's velocity. The perpendicular distance from the center of the Earth to the hyperbolic asymptote is referred to as the asymptotic displacement and, in this case, is 0.675×10^9 meters.

As previously mentioned, the heliocentric-transfer trajectory is of the optimum constant-thrust type; that is, the thrust program employed was one that minimized the propellant expenditure subject to the following constraints: (1) The thrust must be equal to its maximum design value or equal to zero, and (2) the transfer is to take place in a specified time, namely, 223 days. Details of the optimization procedure are fully presented in reference 2.

A plot of the capture-spiral trajectory is shown in figure 3. Initially, the vehicle's relative position and velocity are 418 Mars radii and 1454 meters per second, respectively. The direction of relative velocity is parallel but opposite to Mars' orbital velocity. Thus, the planet is catching up with the vehicle. The asymptote of the capture hyperbola is displaced by 0.209×10^9 meters. With the use of reverse tangential thrust, a 927-kilometer satellite orbit is achieved during the 109th spiral turn.

Trajectory Sensitivity Analysis

The motion of the vehicle during each phase of the mission is described by a set of nonlinear differential equations. Consider that a solution of such a set corresponding to a specified thrust program and satisfying prescribed boundary conditions has been obtained and is termed the reference solution. If the major assumption is made that perturbations (e.g., guidance errors) are sufficiently small so that the actual vehicle trajectory does not vary significantly from the reference trajectory, it is possible to study these variations and the required corrective maneuvers by linear perturbation techniques. The perturbed differential equations of motion represent a linear system with time-varying coefficients, which are determined from the known reference trajectory. The general solution of the perturbed equations is best facilitated by the method of adjoint functions as suggested in reference 3. Application of the adjoint method to various trajectory sensitivity and control problems is found extensively throughout the literature, for example, references 1, 4, and 5.

Equations of motion. - During each phase of the mission, the vehicle is assumed to travel in a vacuum under the influence of an inverse-square central gravitational field in addition to its own thrust acceleration. A two-dimensional geometry is used, and the vehicle motion is described in a rotating polar coordinate system centered at the appropriate central body. With reference to figure 4, the differential equations of motion to be satisfied along the flight path are given as

$$\dot{u} = r\omega^2 - \frac{GM}{r^2} + \frac{F}{m} \sin \beta \tag{1}$$

$$\dot{\omega} = \frac{-2u\omega}{r} + \frac{F}{rm} \cos \beta \tag{2}$$

$$\dot{r} = u \tag{3}$$

$$\dot{\varphi} = \omega \tag{4}$$

$$\dot{m} = -\frac{F}{c} \tag{5}$$

Differentiation with respect to the independent variable time is denoted by a superscribed dot. The state variables of interest are radial velocity u, angular velocity ω, radial position r, angular position φ, and mass m. The propulsion or control variables are the thrust magnitude F and the thrust angle β, which is measured with respect to the local horizontal (circumferential) direction. The effective jet velocity c is equal to the product of specific impulse and a conversion factor and is considered constant in this analysis.

The fact that the angular position φ does not appear in the non-linear equations of motion is very significant in that large variations in φ may be admitted without invalidating the linear perturbation analysis. The possibility of very large variations in this quantity, relative to 2π radians, during the escape-spiral phase is evident, since the vehicle makes several hundred revolutions around Earth in the process of escaping.

Fundamental guidance equation. - The derivation of the linearized equations of motion and their solution by adjoint methods are reported in reference 1. The development needed for the present study is presented in appendix A. In the following discussion, the symbol δ is used to represent small variations from reference quantities, that is, by definition

$$\delta x(t) = x(t) - x^*(t)$$

where x is any state or control variable, and the asterisk denotes the reference value.

The fundamental guidance equation expresses the variation in state variables at the final reference time t_f in terms of the variation in state variables at some time t along the path and in terms of the integrated effect of thrust-vector variations during the interval (t, t_f) . This equation is written with the use of matrix notation for conciseness, as

$$
\begin{bmatrix} \delta u_f \\ \delta \omega_f \\ \delta r_f \\ \delta \varphi_f \\ \delta m_f \end{bmatrix} = \Lambda(t) \begin{bmatrix} \delta u(t) \\ \delta \omega(t) \\ \delta r(t) \\ \delta \varphi(t) \\ \delta m(t) \end{bmatrix} + \int_t^{t_f} W \begin{bmatrix} \delta F \\ \delta \beta \end{bmatrix} dt \tag{6}
$$

where Λ is a 5 by 5 matrix of sensitivity coefficients and W is a 5 by 2 matrix of thrust sensitivity or weighting functions. By definition

$$
\Lambda = \begin{bmatrix} \overline{\lambda}_1 \\ \cdot \\ \cdot \\ \cdot \\ \overline{\lambda}_5 \end{bmatrix} = \begin{bmatrix} \lambda_{11} \ \lambda_{12} \ \cdot \ \cdot \ \lambda_{15} \\ \lambda_{21} \ \cdot \ \cdot \ \cdot \ \lambda_{25} \\ \cdot \\ \cdot \\ \lambda_{51} \qquad\qquad \lambda_{55} \end{bmatrix} ; \ W = \begin{bmatrix} \overline{w}_1 \\ \cdot \\ \cdot \\ \cdot \\ \overline{w}_5 \end{bmatrix} = \begin{bmatrix} w_{11} \ w_{12} \\ \cdot \ \cdot \\ \cdot \ \cdot \\ \cdot \ \cdot \\ w_{51} \ w_{52} \end{bmatrix} \tag{7}
$$

The elements λ_{ij} and w_{ij} are determined from a set of adjoint differential equations discussed in the next section.

The fundamental guidance equation has two basic interpretations. First, the sensitivity of final conditions due to a variety of error sources may be determined, and the analyst thereby provided with information regarding the navigational and control-accuracy requirements. For example, if the final variations have some prescribed tolerance level, $(\delta F, \delta \beta)$ may be regarded as constant bias or random variations acting over the path, and their tolerance level may be computed. Also, if at time t the variations δu, $\delta \omega$, and so forth are measured, the uncertainty in these variations due to instrumentation errors causes uncertainty in the knowledge of final conditions that may be determined from equation (6). Thus, something might be inferred about the measurement accuracy requirements. The second interpretation of the equation has to do with the formulation of an active guidance technique. With the assumption that corrective maneuvers are required to null some or all final variations, which have been determined by measurements $\delta u(t)$,

δω(t), and so forth, the necessary corrective-thrust program is implicitly contained in the integral terms of equation (6). The form of (δF, δβ) will depend on the particular control criteria and constraints imposed.

In this report the major concern in the evaluation of the effect of errors in initial conditions and thrust vector on the final-state variables, that is, the evaluation of the right side of equation (6) when $t = t_O$. For example, if the error in radial velocity at t_f is of interest equation (6) yields

$$\delta u_f = (\lambda_{11}\delta u + \lambda_{12}\delta\omega + \lambda_{13}\delta r + \lambda_{14}\delta\varphi + \lambda_{15}\delta m)_{t_O}$$

$$+ \int_{t_O}^{t_f} (w_{11}\delta F + w_{12}\delta\beta)dt$$

From the form of this equation, the sensitivity coefficients may be interpreted as partial derivatives; for example,

$$\lambda_{11}(t_O) \equiv \frac{\partial u_f}{\partial u_O}$$

Also, if δF and $\delta\beta$ are constant along the path, the following partial derivatives could be defined as

$$\frac{\partial u_f}{\partial F} \equiv \int_{t_O}^{t_f} w_{11}\, dt$$

$$\frac{\partial u_f}{\partial\beta} \equiv \int_{t_O}^{t_f} w_{12}\, dt$$

The extension of these definitions to the remaining variables follows directly.

Adjoint equations. - The sensitivity coefficients $\lambda_{ij}(t)$ are determined from the solution of the following adjoint differential equations (see appendix A):

$$\dot{\lambda}_{i1} = \left(\frac{2\omega}{r}\right)\lambda_{i2} - \lambda_{i3} \tag{8}$$

$$\dot{\lambda}_{i2} = -(2r\omega)\lambda_{i1} + \left(2\frac{u}{r}\right)\lambda_{i2} - \lambda_{i4} \tag{9}$$

$$\dot{\lambda}_{i3} = -\left(\frac{2GM}{r^3} + \omega^2\right)\lambda_{i1} - \left(\frac{2u\omega}{r^2} - \frac{F \cos \beta}{r^2 m}\right)\lambda_{i2} \tag{10}$$

$$\dot{\lambda}_{i4} = 0 \tag{11}$$

$$\dot{\lambda}_{i5} = \left(\frac{F \sin \beta}{m^2}\right)\lambda_{i1} + \left(\frac{F \cos \beta}{rm^2}\right)\lambda_{i2} \tag{12}$$

The time-varying coefficients in parenthesis are known from the particular reference trajectory of interest. These equations were integrated backward in time from t_f. The initial conditions specified at t_f have the form

$$\lambda_{ii}(t_f) = 1; \ \lambda_{ij}(t_f) = 0 \qquad j \neq i$$

that is,

$$\Lambda(t_f) = I(\text{unit matrix}) \tag{13}$$

The sensitivity coefficients and β are continuous functions of time even if a discontinuity in F is admitted, as it is during nominal coasting periods (see ref. 2). From equations (11) and (12) it is noted that λ_{i4} is a constant and that λ_{i5} is constant during coasting periods ($F = 0$). When boundary conditions are specified as in equation (13), the fourth column and the fifth row of the matrix Λ are time invariant and may be given directly without numerical integration:

$$\left.\begin{aligned} (\lambda_{14}, \ \lambda_{24}, \ \lambda_{34}, \ \lambda_{44}, \ \lambda_{54}) = (0,0,0,1,0) \\ (\lambda_{51}, \ \lambda_{52}, \ \lambda_{53}, \ \lambda_{54}, \ \lambda_{55}) = (0,0,0,0,1) \end{aligned}\right\} \tag{14}$$

The elements of the matrix W are, from appendix A,

$$w_{i1} = \frac{\lambda_{i1}}{m} \sin \beta + \frac{\lambda_{i2}}{rm} \cos \beta - \frac{\lambda_{i5}}{c} \tag{15}$$

$$w_{i2} = \frac{F}{m}\left(\lambda_{i1} \cos \beta - \frac{\lambda_{i2}}{r} \sin \beta\right) \tag{16}$$

On substitution from the second of equations (14), w_{51} and w_{52} simplify to

$$w_{51} = -\frac{1}{c}; \quad w_{52} = 0 \tag{17}$$

The thrust-angle weighting function w_{i2} is continuous only during the nominal powered periods and is zero during the nominal coast period ($F = 0$). A discontinuity exists at the initiation and the termination of the coast period. This result is as it should be, since thrust-angle variations have no physical meaning when thrust is shut off.

Nonlinear thrust-vector perturbations. - In the derivation of the fundamental guidance equation (eq. (6)), it is assumed herein that thrust-vector perturbations are sufficiently small so that only first-order or linear variations need be considered. If, however, large variations in thrust magnitude or direction are allowed, the linear form of the integrand in equation (6) must be modified; that is,

$$W\begin{bmatrix}\delta F \\ \delta \beta\end{bmatrix} \rightarrow [f_i(\Delta F, \Delta \beta)] \qquad i = 1,\ldots,5$$

where ΔF and $\Delta \beta$ may be considered large variations. The need for such modification arises when consideration is made of the problem of guidance maneuvers (corrective thrust programs). For example, if the guidance maneuver requires that thrust be cut off for a specified time during the nominal powered period or that thrust be turned on during a nominal coast period, than $\Delta F = \mp F$, which is certainly not small. Another reason for deriving the exact f_i functions is that a check on the conclusions drawn from the linear-sensitivity analysis is available when the first-order sensitivities appear to be negligible.

The perturbation analysis (see appendix A) involves two essentially unrelated types of linearization, that is, linearization of the state variables and linearization of the control variables. This separation is evident in the results of equation (6). The validity of the trajectory perturbation solution, however, depends only on the validity of the linearization of state variables. Note that the adjoint solution $\Lambda(t)$ is independent of control-variable linearizations. Consequently, as long as large thrust-vector perturbations do not result in large trajectory perturbations, it is necessary to modify only the integrand terms in equation (6). From appendix A the result is

$$\delta \bar{x}(t_f) = \Lambda(t)\delta \bar{x}(t) + \int_t^{t_f} [f_i]dt \tag{18}$$

where

$$f_i = \frac{\lambda_{i1}}{m} \left[(F + \Delta F)\sin(\beta + \Delta\beta) - F\sin\beta \right]$$

$$+ \frac{\lambda_{i2}}{rm} \left[(F + \Delta F)\cos(\beta + \Delta\beta) - F\cos\beta \right] - \frac{\lambda_{i5}}{c} \left[(F + \Delta F) - F \right]$$

After expansion of the trigonometric functions and with the use of equations (15) and (16), the alternative form is

$$f_i = \left(w_{i1} + \frac{\lambda_{i5}}{c} \right)\Delta F \cos\Delta\beta + \left(\frac{w_{i2}}{F} \right)\Delta F \sin\Delta\beta - \left(\frac{\lambda_{i5}}{c} \right)\Delta F$$

$$+ F\left(w_{i1} + \frac{\lambda_{i5}}{c} \right)(\cos\Delta\beta - 1) + (w_{i2})\sin\Delta\beta \qquad (19)$$

When ΔF and $\Delta\beta$ are small, $\Delta F \approx \delta F$, $\sin\Delta\beta \approx \delta\beta$, and $\cos\Delta\beta \approx 1$. Equation (19) thus degenerates into the approximate linear form derived previously:

$$f_i \approx w_{i1}\delta F + w_{i2}\delta\beta$$

In the previous section it is noted that w_{i2} is discontinuous at the beginning and at the end of a coast period ($F = 0$) and is zero during this period. The quantity w_{i2}/F, which appears in equation (19), however, is always continuous and, in general, is nonzero, as can be seen from equation (16).

Several special cases of equation (19), used later in this report are as follows:

$F = 0$; $\Delta F = F_{des}$; $\Delta\beta$ arbitrary

$$f_i = F_{des} \left[\left(w_{i1} + \frac{\lambda_{i5}}{c} \right)\cos\Delta\beta + \left(\frac{w_{i2}}{F} \right)\sin\Delta\beta - \left(\frac{\lambda_{i5}}{c} \right) \right] \qquad (20)$$

$\Delta\beta = 0$; ΔF arbitrary

$$f_i = w_{i1} \Delta F \qquad (21)$$

$F = F_{des}$; $\Delta F = \delta F \ll F$; $\Delta\beta = \delta\beta$, small but second-order effects significant; $\sin\Delta\beta \approx \delta\beta$; $\cos\Delta\beta - 1 \approx -\frac{1}{2}\delta\beta^2$

$$f_i = w_{i1}\delta F + w_{i2}\delta\beta - \frac{F_{des}}{2}\left(w_{i1} + \frac{\lambda_{15}}{c}\right)\delta\beta^2 \tag{22}$$

RESULTS AND DISCUSSION

The overall low-thrust trajectory for the 415.4-day Mars orbiter mission has been pieced together from a series of two-body solutions. The equations needed to calculate the reference trajectories were programmed for an IBM 704 digital computer. Numerical integration was performed by the Runge-Kutta technique with an automatic step-size control to limit truncation error. The computer program was developed for the study presented in reference 2, and only minor modifications were required to adapt it to this investigation. Basically, this modification involved increasing the integration loop by the addition of the adjoint equations (8) to (12).

In the following sections, each phase of the mission is considered separately, and the results show the sensitivity of the final trajectory state due to errors in the initial trajectory state and thrust-magnitude and -direction errors. Two examples of simple corrective guidance are presented.

Trajectory Sensitivity - Escape-Spiral Phase

Reference trajectory. - Characteristic parameters of the escape-spiral trajectory are given in figure 5. The thrust angle β, which corresponds to the tangential-thrust program, is plotted in figure 5(a). Thrust direction is seen to be within 2° of the horizontal throughout the first 100 days, and thus a circumferential-thrust program would result in approximately the same trajectory up to this point as the tangential program. Aside from the fact that tangential thrust is very efficient in terms of propellant expenditure, trajectory control is enhanced, since the local vertical (local horizontal) may be easily sensed. Past the knee of the curve, β increases at an average of about 3° per day.

Radial velocity is shown as a function of time in figure 5(b), and the similarity to the thrust-angle program is noted. The vehicle's orbit is essentially circular up to 100 days at which point the eccentricity is only 0.028. A characteristic of the function $u(t)$, which is entirely masked out in figure 5(b), is its oscillatory nature over the flat region of the curve. A close examination of the digital-computer results, in a region where output is called for at every integrating step, shows that u oscillates with an increasing period and decreasing amplitude as time increases. The period is approximately equal to the orbital period

during a given revolution. Initially, the amplitude of oscillation is of the order of several meters per second. At $t = 25$ days, the amplitude has decayed to a small fraction of 1 meter per second. A corresponding oscillation is also exhibited by the thrust angle and the eccentricity.

The angular velocity ω decreases with time by almost four decades, as shown by figure 5(c). An approximation of the average orbital period may be made at any time by $2\pi/\omega$. For example, at $t = 15$ days 1 revolution is made in about 0.1 day, while at $t = 82$ days one revolution requires about 1 day. Figures 5(d) and (e) show the time histories of radial and angular positions, respectively.

Initial-condition variations. - With reference to equation (6), the effect of errors in velocity, position, and mass at $t = t_0 = 0$ on these same quantities at $t_f = 139$ days is given by $\Lambda(t_0)$. The elements of this matrix have been obtained from the adjoint-equation solution and are given as

$$\Lambda(t_0) = \begin{array}{c} \delta u_f \\ \delta \omega_f \\ \delta r_f \\ \delta \varphi_f \\ \delta m_f \end{array} \begin{array}{|c|c|c|c|c|} \hline \delta u_0 & \delta \omega_0 & \delta r_0 & \delta \varphi_0 & \delta m_0 \\ \hline 7.39 \times 10^{-4} & 7.20 \times 10^{6} & 1.99 \times 10^{-3} & 0 & -2.13 \\ \hline 5.69 \times 10^{-13} & -2.01 \times 10^{-3} & -5.43 \times 10^{-13} & 0 & 5.19 \times 10^{-10} \\ \hline 1.51 \times 10^{2} & 1.44 \times 10^{13} & 4.00 \times 10^{3} & 0 & -3.80 \times 10^{6} \\ \hline -4.41 \times 10^{-4} & -1.23 \times 10^{7} & -3.41 \times 10^{-3} & 1 & 0.768 \\ \hline 0 & 0 & 0 & 0 & 1 \\ \hline \end{array}$$

(23)

Consider, for example, a variation in the initial-circular-orbit altitude of 10 kilometers, that is, $\delta r_0 = 10^4$ meters. Assume also that $\delta u_0 = \delta \varphi_0 = \delta m_0 = 0$. Since

$$\omega_0 = \sqrt{\frac{GM_E}{r_0^3}}$$

the variation in ω_0 is

$$\delta \omega_0 = -\frac{3}{2}\sqrt{\frac{GM_E}{r_0^5}}\, \delta r_0 = -\frac{3}{2}\frac{\omega_0}{r_0}\, \delta r_0 = -2.08 \times 10^{-6} \text{ radian/sec}$$

From the second and third columns of $\Lambda(t_o)$ the following are obtained:

$$\delta u_f = 5.00 \text{ m/sec}$$

$$\delta \omega_f = -1.25 \times 10^{-9} \text{ radian/sec}$$

$$\delta r_f = 1.00 \times 10^7 \text{ m}$$

$$\delta \varphi_f = -8.49 \equiv -2.21 \text{ radians} \equiv -127^{\circ}$$

The final errors δu_f, $\delta \omega_f$, and δr_f are each of the order of 1/2 percent. If there were no error in the angular position, a transformation to heliocentric coordinates would show an extremely small perturbation on the initial heliocentric conditions. This is not the case, however, since φ_f is the parameter that is related to a heliocentric reference direction and is in error by -127°. The perturbed escape trajectory may be visualized by a 127° clockwise rotation of the reference trajectory in figure 2. Qualitatively, the result is a very significant error in heliocentric coordinates.

The preceding example has served to focus attention on the extreme sensitivity of final angular position relative to the sensitivity of the other state variables. There is, however, an essential difference in the nature of the sensitivities. That is, the magnitudes of δu_f, $\delta \omega_f$, and δr_f increase proportionally with initial-condition errors, whereas the principal magnitude of $\delta \varphi_f$ varies between 0 and π in a cyclical, triangular fashion. As an example, consider each initial-condition error independently and compute the error magnitudes that cause φ_f to be π radians out of phase. From the fourth row of the matrix $\Lambda(t_o)$ if $\delta \varphi_f = \pm(2n + 1)\pi$, where $n = 0, 1, 2, \ldots$,

$$\delta u_o = \mp \frac{\delta \varphi_f}{4.41 \times 10^{-4}} = \mp (2n + 1)(7.10 \times 10^3) \text{ m/sec}$$

$$\delta \omega_o = \mp \frac{\delta \varphi_f}{1.23 \times 10^7} = \mp (2n + 1)(2.55 \times 10^{-7}) \text{ radian/sec}$$

$$\delta r_o = \mp \frac{\delta \varphi_f}{3.41 \times 10^{-3}} = \mp (2n + 1)(9.21 \times 10^2) \text{ m}$$

$$\delta \varphi_o = \pm \frac{\delta \varphi_f}{1} = \pm (2n + 1)\pi \text{ radians}$$

$$\delta m_o = \pm \frac{\delta \varphi_f}{0.768} = \pm (2n + 1)(4.09) \text{ kg}$$

The minimum errors are found when $n = 0$. From the previous results, it may be concluded that δu_0 is several orders of magnitude greater than any reasonable error that may be expected. In contrast, a 0.04-percent error in ω_0 or a 0.1-percent error in either the initial orbital altitude or m_0 is sufficient, if left uncorrected, to reverse the direction of the escape asymptote.

Thrust-vector variations. - Consider next the sensitivity of velocity and position components at the nominal escape condition to variations in thrust magnitude and direction. This information is expressed by the integral terms in equation (6), where the elements of the weighting matrix W are given by equations (15) and (16) and are plotted against time in figure 6. Each weighting function, except w_{41}, exhibits an oscillatory characteristic the amplitude and period of which increase with time. As in the case of the radial-velocity characteristic, the period of oscillation approximately coincides with the orbit rotational period of the vehicle. In figure 6, only the last cycle of the weighting functions is shown; however, the envelope of oscillation is plotted.

Qualitatively, the weighting functions illustrate the relative sensitivity to thrust-vector errors during any two arbitrary time intervals. Figures 6(b), (d), (f), and (h) show that final velocity and position components are relatively insensitive to first-order thrust-angle errors during the first half of the escape phase, whereas figures 6(a), (c), and (e) show a significant and essentially constant sensitivity to thrust-magnitude errors during this same interval. In particular, figure 6(g) illustrates a result that could easily have been predicted, namely, that φ_f is most sensitive to δF occurring during the early tightly wound spirals and that the sensitivity is essentially zero during the last spiral turn ($t > 120$ days).

A convenient quantitative measure of the sensitivity to thrust errors is obtained by considering δF and $\delta \beta$ to be constant; thus, the time integrals of the weighting functions yield the desired sensitivity. The results are presented in the following matrix form, where δF and $\delta \beta$ are measured in newtons and radians, respectively:

$$\left[\int_{t_0}^{t_f} w_{ij} \, dt \right] = \begin{array}{c} \\ \delta u_f \\ \delta \omega_f \\ \delta r_f \\ \delta \varphi_f \end{array} \begin{array}{|c|c|} \multicolumn{1}{c}{\delta F} & \multicolumn{1}{c}{\delta \beta} \\ \hline 3.73 \times 10^3 & 11.7 \\ \hline -9.11 \times 10^{-7} & -2.77 \times 10^{-7} \\ \hline 6.68 \times 10^9 & 7.32 \times 10^7 \\ \hline -1.35 \times 10^3 & -2.92 \\ \hline \end{array} \tag{24}$$

Consider the effects of a thrust-magnitude error first. Since an appreciation for the serious consequences of a large error in φ_f has been gained, the sequence of δF values, which causes φ_f to be π radians out of phase, are computed. From equation (24)

$$\delta F = \pm \frac{(2n + 1)\pi}{1.35 \times 10^3} = \pm (2n + 1)(2.33 \times 10^{-3}) \text{ newton} \qquad n = 0,1,2,\ldots$$

The minimum value of δF required is thus 2.33×10^{-3} newton, or a 0.1-percent error. Since it is unlikely that such accurate thrust control is possible, it must be concluded that the requirement of guided flight is of major importance for low-thrust missions.

The effects of a ±0.1-percent error in F on the velocity and radial-position components at t_f are

$$\delta u_f = \pm (3.73 \times 10^3)(2.33 \times 10^{-3}) = \pm 8.70 \text{ m/sec}$$

$$\delta \omega_f = \pm (-9.11 \times 10^{-7})(2.33 \times 10^{-3}) = \mp 2.12 \times 10^{-9} \text{ radian/sec}$$

$$\delta r_f = \pm (6.68 \times 10^9)(2.33 \times 10^{-3}) = \pm 1.56 \times 10^7 \text{ m}$$

Each of these final variations when divided by its respective reference quantity represents an error of less than 1 percent; therefore, the resultant perturbation on the heliocentric trajectory is due almost entirely to $\delta \varphi_f = \pi$.

For discussion of the effects of a thrust-angle error, an error of ±10 milliradians, or about $1/2^\circ$, is assumed as a typical order of magnitude. The final velocity and position errors that result are then given by equation (24) as

$$\delta u_f = \pm 0.117 \text{ m/sec}$$

$$\delta \omega_f = \mp 2.77 \times 10^{-9} \text{ radian/sec}$$

$$\delta r_f = \pm 7.32 \times 10^5 \text{ m}$$

$$\delta \varphi_f = \mp 0.0292 \text{ radian} = \mp 1.67^\circ$$

which are all first-order effects. The error magnitudes due to the first-order variation of β appear to be quite small; however, before a conclusion can be drawn the effects of second-order variations of β must be computed. From equation (22),

$$\delta x_i^!(t_f) \equiv \delta x_i(t_f) \text{ due to } \delta\beta^2 = -\frac{F_{des}}{2}\delta\beta^2 \int_{t_o}^{t_f}\left(w_{i1} + \frac{\lambda_{i5}}{c}\right)dt$$

In this study, $F_{des}/2$ is of the order of unity. Also, computer results show that λ_{i5}/c is small compared with w_{i1} for all values of i. Thus, the second-order effects are very well approximated by the integrals of w_{i1}, which are given in the first column of the matrix equation (24), multiplied by $\delta\beta^2 = 10^{-4}$:

$$\delta u_f^! = -0.373 \text{ m/sec}$$

$$\delta\omega_f^! = 9.11 \times 10^{-11} \text{ radian/sec}$$

$$\delta r_f^! = -6.68 \times 10^5 \text{ m}$$

$$\delta\varphi_f^! = 0.135 \text{ radian} = 7.74^o$$

A comparison of the first- and second-order effects shows that second-order effects are of the same magnitude or greater except in the case of angular-velocity errors. The total errors in velocity and radial-position components are quite small. The total angular-position error is less than 10°. If, however, $\delta\beta$ were increased to 2.8^o, the final angular-position error would increase to about 180°.

Trajectory Sensitivity - Heliocentric-Transfer Phase

Reference trajectory. - The time required to transfer between planetary orbits was chosen as 223 days, and the trajectory was optimized to minimize the propellant expenditure. The constraint imposed here was that the thrust must be equal either to the design value or to zero. Characteristic variables of the reference trajectory are plotted in figure 7 where the time scale chosen has been reinitialized to zero. The optimum-thrust-angle program is shown in figure 7(a). Thrust direction is outward with an average rate of change of 0.86^o per day during the first powered period and inward with an average rate of change of 0.56^o per day during the second powered period. Velocity and position time histories are shown in figures 7(b) to (e).

Initial-condition variations. - Digital-computer solutions of the adjoint equations (8) to (12), which correspond to the boundary conditions

$\Lambda(t_f)$ = unit matrix, are plotted as functions of time in figure 8. The effects of initial-condition variations on final conditions are given by $\Lambda(t_o)$:

$$\Lambda(t_o) = \begin{array}{c} \delta u_f \\ \delta \omega_f \\ \delta r_f \\ \delta \varphi_f \\ \delta m_f \end{array}$$

	δu_o	$\delta \omega_o$	δr_o	$\delta \varphi_o$	δm_o
δu_f	-0.366	2.63×10^{11}	6.46×10^{-7}	0	-0.149
$\delta \omega_f$	-1.84×10^{-12}	-3.48	-8.07×10^{-18}	0	8.07×10^{-12}
δr_f	2.20×10^{6}	4.57×10^{18}	10.9	0	-1.27×10^{7}
$\delta \varphi_f$	-1.02×10^{-4}	-3.11×10^{7}	-8.44×10^{-11}	1	1.00×10^{-4}
δm_f	0	0	0	0	1

$$(25)$$

Variations in initial velocity, position, and mass will be due to errors incurred during the escape-spiral phase. Expressions are derived in appendix B that relate the two sets of errors. Suppose, for example, at the termination of the escape phase that the angular position is in error by only 10 milliradians, while all other errors are zero. With the use of equations (B6), (B7), (B12), and (B14), the initial-heliocentric-velocity and -position errors are found to be

$$\delta u_o = -15.8 \text{ m/sec}$$

$$\delta \omega_o = 2.47 \times 10^{-11} \text{ radian/sec}$$

$$\delta r_o = -1.78 \times 10^{7} \text{ m}$$

$$\delta \varphi_o = 4.50 \times 10^{-5} \text{ radian}$$

$$\delta m_o = 0$$

Then from equation (25) the final-condition errors will be

$$\delta u_f = 0.770 \text{ m/sec}$$

$$\delta \omega_f = 8.69 \times 10^{-11} \text{ radian/sec}$$

$$\delta r_f = -1.16 \times 10^{8} \text{ m}$$

$$\delta\varphi_f = 2.39 \times 10^{-3} \text{ radian}; \quad r_f\delta\varphi_f = 5.43 \times 10^8 \text{ m}$$

$$\delta m_f = 0$$

With reference to figure 3, the resultant errors show that at the nominal final time the vehicle is both below and ahead of its nominal position, and its motion relative to Mars is essentially parallel to the nominal capture trajectory. Hence, the incoming asymptotic displacement is in error by some 1.16×10^8 meters. The requirement for midcourse corrective guidance to compensate for the escape errors is evident.

Thrust-vector variations. - The elements of the matrix W are plotted as functions of time in figure 9. Recall that the nominal coasting period extends over the interval $27.7 \leq t \leq 187.7$ days. Since it is reasonable to assume that no thrust errors will occur during this interval, the weighting functions are of interest here only during the nominal powered periods. The significant result illustrated by figure 9 is that the final velocity and position components are relatively more sensitive to thrust-vector errors that occur during the first powered period. In particular, the radial-position perturbation due to either δF or $\delta\beta$ is relatively 15 times greater during the first powered period, while the angular-position perturbation due to δF is relatively 25 times greater.

The time integrals of the weighting functions over the powered regions of flight have been evaluated as

$$\left[\int_{\substack{\text{powered} \\ \text{periods}}} w_{ij}\, dt\right] = \begin{array}{c} \\ \delta u_f \\ \delta\omega_f \\ \delta r_f \\ \delta\varphi_f \end{array} \begin{array}{|c|c|} \hline \delta F & \delta\beta \\ \hline 211 & -604 \\ \hline -1.14 \times 10^{-8} & 2.45 \times 10^{-8} \\ \hline 1.80 \times 10^{10} & -2.15 \times 10^{10} \\ \hline -0.142 & 0.0384 \\ \hline \end{array} \qquad (26)$$

As an example, the velocity and position perturbations resulting from a 1-percent error in thrust magnitude or a 10-milliradian error in thrust angle are

$$\delta F = 2.32 \times 10^{-2} \text{ newton} \qquad \delta\beta = 10^{-2} \text{ radian}$$

$$\delta u_f = 4.90 \text{ m/sec} \qquad \delta u_f = -6.04 \text{ m/sec}$$

$$\delta\omega_f = -2.64 \times 10^{-10} \text{ radian/sec} \qquad \delta\omega_f = 2.45 \times 10^{-10} \text{ radian/sec}$$

$$\delta r_f = 4.17 \times 10^{8} \text{ m} \qquad \delta r_f = -2.15 \times 10^{8} \text{ m}$$

$$\delta\varphi_f = -3.29 \times 10^{-3} \text{ radian} \qquad \delta\varphi_f = 0.384 \times 10^{-3} \text{ radian}$$

The resultant errors and, in particular, the position errors are of sufficient magnitude to require midcourse guidance corrections.

Trajectory Sensitivity - Capture-Spiral Phase

Reference trajectory. - Variables that describe the capture-spiral trajectory are plotted as a function of time in figure 10. The thrust angle β, corresponding to the energy-decreasing tangential-thrust program, is shown in figure 10(a) in which β is shown as a second quadrant angle, since the thrust vector in this case is parallel but opposite to velocity vector. As in the case of the escape-spiral trajectory, the thrust direction is essentially circumferential over a large region. In this region, $t > 25$ days, the vehicle travels in a nearly circular orbit with a decreasing semimajor axis. These results may readily be inferred from the radial-velocity and -position curves shown in figures 10(b) and (d). Again, as in the case of the escape spiral, a characteristic of the function $u(t)$, which is entirely masked out in figure 10(b), is its oscillatory nature over the flat region of the curve. The period and amplitude of oscillation decrease and increase, respectively, with time, although the largest amplitude is quite small.

Variational parameters of final satellite orbit. - It may be more illuminating to consider the sensitivity of the final satellite orbit about Mars in terms of orbital parameters such as semilatus rectum p, semimajor axis a, eccentricity e, perigee r_p, or apogee r_a. If the orbital orientation is not of interest, any two of these parameters will define the orbit. The parameters a_f and p_f may be expressed in terms of the radial-position and -velocity components as

$$a_f = \cfrac{1}{\cfrac{2}{r_f} - \cfrac{u_f^2 + (r_f\omega_f)^2}{GM_M}}$$

$$p_f = \frac{r_f^4 \omega_f^2}{GM_M}$$

The eccentricity, perigee, and apogee are given as

$$e_f^2 = 1 - \frac{p_f}{a_f}$$

$$r_{p,f} = a_f(1 - e_f)$$

$$r_{a,f} = a_f(1 + e_f)$$

When the reference orbit is circular, the following special relations occur:

$$u_f = e_f = 0$$

$$a_f = p_f = r_{p,f} = r_{a,f} = r_f$$

$$V_f = r_f \omega_f = \left(\frac{GM_M}{r_f}\right)^{1/2}$$

Expansion of a_f and p_f in a Taylor series keeping only first- and second-order terms and utilization of the previous special relations yields

$$\Delta a_f = \left(\frac{2r_f}{\omega_f}\right)\delta\omega_f + 4\delta r_f + \left(\frac{r_f}{V_f^2}\right)\delta u_f^2 + \left(\frac{5r_f}{\omega_f^2}\right)\delta\omega_f^2 + \left(\frac{15}{r_f}\right)\delta r_f^2 + \left(\frac{20}{\omega_f}\right)\delta\omega_f \delta r_f \tag{27}$$

$$\Delta p_f = \left(\frac{2r_f}{\omega_f}\right)\delta\omega_f + 4\delta r_f + \left(\frac{r_f}{\omega_f^2}\right)\delta\omega_f^2 + \left(\frac{6}{r_f}\right)\delta r_f^2 + \left(\frac{8}{\omega_f}\right)\delta\omega_f \delta r_f \tag{28}$$

Variations in eccentricity, perigee, and apogee may then be calculated from

$$\Delta e_f^2 = \frac{\Delta a_f - \Delta p_f}{r_f + \Delta a_f} \tag{29}$$

$$\Delta r_{p,f} = \Delta a_f - (r_f \, \Delta e_f + \Delta a_f \, \Delta e_f) \tag{30}$$

$$\Delta r_{a,f} = \Delta a_f + (r_f \, \Delta e_f + \Delta a_f \, \Delta e_f) \tag{31}$$

Note that, even for very small variations in velocity and position, equations (29) to (31) are essentially nonlinear when expressed in terms of these variations. This result is due to the fact that the final reference orbit is circular.

Initial-condition variations. - Solution of the adjoint equations for the capture-spiral trajectory yields the following $\Lambda(t_O)$ matrix:

$$\Lambda(t_O) = \begin{array}{c} \\ \delta u_f \\ \delta\omega_f \\ \delta r_f \\ \delta\varphi_f \\ \delta m_f \end{array}
\begin{array}{c} \delta u_O \\ \hline -24.2 \\ -2.02\times10^{-4} \\ 5.73\times10^{5} \\ \text{-----} \\ 0 \end{array}
\begin{array}{c} \delta\omega_O \\ 9.67\times10^{11} \\ 2.01\times10^{5} \\ -5.77\times10^{14} \\ \text{-----} \\ 0 \end{array}
\begin{array}{c} \delta r_O \\ 5.37\times10^{-5} \\ -1.10\times10^{-10} \\ 0.311 \\ \text{-----} \\ 0 \end{array}
\begin{array}{c} \delta\varphi_O \\ 0 \\ 0 \\ 0 \\ 1 \\ 0 \end{array}
\begin{array}{c} \delta m_O \\ 7.16 \\ 4.87\times10^{-5} \\ -1.39\times10^{5} \\ \text{-----} \\ 1 \end{array}$$

(32)

The magnitudes of the sensitivity coefficients in equation (32) indicate the extreme sensitivity of the capture trajectory to errors in initial conditions. A sample calculation illustrates this point. Consider a situation where the vehicle is at the influence sphere ($\delta r_O = 0$), but the velocity components are in error by $\delta u_O = 1$ meter per second and $\delta\omega_O = -10^{-9}$ radian per second. This corresponds to the initial velocity vector having an error of about 1 meter per second in magnitude and 1 milliradian in direction. Assume also that $\delta m_O = 0$. From equation (32), the final variables will be in error by

$$\delta u_f = -24.2 - 997 = -991 \text{ m/sec}$$

$$\delta\omega_f = -2.02\times10^{-4} - 2.01\times10^{-4} = -4.03\times10^{-4} \text{ radian/sec}$$

$$\delta r_f = 5.73\times10^{5} + 5.77\times10^{5} = 1.15\times10^{6} \text{ m} = 1150 \text{ km}$$

These errors represent a significant perturbation of the trajectory. Evaluation of equations (27) to (30) shows the eccentricity to be about 0.5 and the perigee to be well within the Martian surface. Actually, the errors are large enough to invalidate the linear perturbation approach.

An interesting result may be found from the matrix $\Lambda(t_O)$ if in any given column the element of the second row is divided by the element

of the third row. These ratios are very nearly the same, about
-3.5×10^{-10}. Within the validity of the first-order approximation, this
result means that $\delta \omega_f$ is not independent of δr_f; that is, no matter
what set of initial errors leads to a given δr_f, $\delta \omega_f \approx -3.5 \times 10^{-10} \delta r_f$.
This common ratio is not unique to the time $t_o = 0$, since an examination
of the matrix $\Lambda(t)$ shows approximately the same result over a large
portion of the trajectory.

A further result is that the quantity $2\omega_f/r_f$ is equal to
3.54×10^{-10}; thus, $\delta \omega_f \approx -(2\omega_f/r_f)\delta r_f$. This result is not explained in a
rigorous manner; however, a relation of this form and order of magnitude
may be deduced from the following argument. If the errors δu_f, $\delta \omega_f$,
and δr_f are quite small, the final perturbed orbit is very nearly
circular. Since for a circular orbit

$$\omega_f = \left(\frac{GM_M}{r_f^3}\right)^{1/2}$$

the relation between $\delta \omega_f$ and δr_f required to maintain a circular
orbit of slightly different size is

$$\delta \omega_f = -\left(\frac{3}{2}\frac{\omega_f}{r_f}\right)\delta r_f$$

The 25-percent discrepancy in the coefficient δr_f may be ascribed to
the fact that the final perturbed orbit is not exactly circular.

Thrust-vector variations. - The sensitivities of final-velocity
and -radial-position components to variations in thrust magnitude and
direction are given by the weighting functions, which are plotted in
figure 11. As in the case of the escape-spiral phase, the functions
exhibit an oscillatory characteristic, the envelope of which is shown.
The major qualitative result to be gained from figure 11 is one that
may have been anticipated: the maximum sensitivity to thrust errors
occurs in the vicinity of t_o when the vehicle is far from the planet
and moving asymptotically, and the sensitivity decreases to a negligible
amount as the final satellite orbit is approached. The guidance impli-
cations are clearly understood. Trajectory perturbations due to initial-
condition errors are most efficiently corrected early in the capture
phase, provided, of course, that accurate guidance information is
available to the vehicle at such large distances from the target planet.

A quantitative measure of the sensitivity to thrust variations is provided by the time integrals of the weighting functions:

$$\left[\int_{t_o}^{t_f} w_{ij}\ dt\right] = \begin{array}{c} \delta u_f \\ \delta \omega_f \\ \delta r_f \end{array} \begin{array}{|c|c|} \hline \delta F & \delta\beta \\ \hline -9.03\text{X}10^3 & -3.44\text{X}10^5 \\ \hline -6.15\text{X}10^{-2} & -7.83\text{X}10^{-2} \\ \hline 1.75\text{X}10^8 & 2.23\text{X}10^8 \\ \hline \end{array} \qquad (33)$$

A simple calculation shows that a significant perturbation of the final satellite orbit results from thrust errors as small as 0.1 percent in magnitude and 1 milliradian in direction. For $\delta F = 2.32\text{X}10^{-3}$, the final-velocity and -position errors are -20.9 meters per second, $-1.43\text{X}10^{-4}$ radian per second, and $4.05\text{X}10^5$ meters, respectively. For $\delta\beta = 10^{-3}$, the final errors are -344 meters per second, $-0.783\text{X}10^{-4}$ radian per second, and $2.23\text{X}10^5$ meters, respectively. In the last case the eccentricity of the perturbed orbit is about 0.1, and the perigee altitude has been decreased from the nominal 927 to 390 kilometers.

For reasons previously discussed, the second-order effects of thrust-angle variations may be approximated by the product of $\delta\beta^2$ and the integrals of w_{i1} given in the first column of equation (33). Since the integrals of w_{i1} are of smaller magnitude than the integrals of w_{i2}, the second order effects are negligible for $\delta\beta < 0.1$ radian.

Note from equation (33) that the ratios of the elements taken from the second and third rows are both equal to $-3.51\text{X}10^{-10}$. Thus, from the arguments of the previous section $\delta\omega_f \approx -(2\omega_f/r_f)\delta r_f$ for any small values of constant δF and $\delta\beta$.

Examples of Simple Guidance

Escape guidance in one variable. - The basic result of the sensitivity analysis of the escape-spiral trajectory is that a very small perturbation in thrust magnitude is sufficient to rotate the asymptotic escape direction through a large angle. Specifically, if a 0.1-percent systematic error exists and no corrective maneuver is made, the escape asymptote will lie on the sun's side of the Earth's orbit and will be directed opposite to Earth's orbital velocity. This condition is equivalent to a 25-percent loss in heliocentric energy, which would most likely result in a mission failure. The objective of escape guidance is to prevent such a condition from occurring.

As an example, consider a simple guidance scheme that employs constant thrust ΔF as the control variable and a single-variable guidance criterion, namely, to null $\Delta\varphi_f$. A constant-thrust-magnitude error (unknown to the vehicle) of 0.1 percent is arbitrarily assumed as the uncontrolled perturbing function, and repetitive corrective action is to be taken at 20-day intervals based on perfect trajectory determination. The calculation is simplified by restricting the control interval Δt to within 1 day, where the thrust weighting functions are essentially constant over this interval. The details of the thrust-control system are left unspecified, and results are given in the form of thrust impulse $\Delta F \Delta t$ measured in newton-seconds. Depending on the control required, then, consideration may be given to the possibilities of throttling the low-thrust engine, shutting it off completely, or using a medium-thrust chemical rocket.

The guidance equation involving angular position only may be extracted from equation (6). At the beginning of any control interval t_n the final-angular-position error predicted from measurements is denoted as $\delta\varphi_f(t_n)$. The result of equation (21) is substituted for the integrand term in equation (6); hence, the guidance equation may be written as

$$\Delta\varphi_f(t_n + \Delta t_n) = \Delta\varphi_f(t_n) + \int_{t_n}^{t_n + \Delta t_n} w_{41}\Delta F_n \, dt$$

$$= \Delta\varphi_f(t_n) + w_{41}(t_n)\Delta F_n \, \Delta t_n$$

Since $\Delta\varphi_f(t_n + \Delta t_n) = 0$ is desired, the control thrust impulse is

$$\Delta F_n \, \Delta t_n = - \frac{\Delta\varphi_f(t_n)}{w_{41}(t_n)}$$

If corrective action were taken at the previous control instant t_{n-1} to null $\Delta\varphi_f$, $\Delta\varphi_f(t_n)$ is due to the perturbing function δF acting over the interval (t_{n-1}, t_n). For the purpose of the calculation herein,

$$\Delta F_n \, \Delta t_n = - \frac{\delta F \int_{t_{n-1}}^{t_n} w_{41} \, dt}{w_{41}(t_n)}$$

Figure 12(a) illustrates the results of this simple-final-value guidance scheme. A constant-thrust perturbation $\delta F = 2.32 \times 10^{-3}$ newton (0.1 percent) and five control intervals at 20, 40, 60, 80, and 100 days

are assumed. The uncorrected $\Delta\varphi_f$ characteristic is shown for comparison. Although the last corrective action was taken at 100 days, the angular-position error increases to an acceptable final value of less than 1° during the interval 100 to 139 days. Since a positive perturbation was assumed, the control impulse must be negative to make up for the lag in angular position. This impulse increases in magnitude slightly with each successive correction from 5.08×10^3 to 8.34×10^3 newton-seconds. Consider the correction at $t = 20$ days. If the low-thrust engine is shut off completely ($\Delta F = -2.32$), the shutoff time Δt is 2.18×10^3 seconds, or about 0.6 hour. If the engine is throttled down by 5 percent, the control interval is about 12 hours.

The effect of the guidance maneuvers on the uncontrolled final variables δu_f, $\delta \omega_f$, and δr_f is shown in figures 12(b) to (d). Control stability results in each case, and a comparison with the uncorrected characteristics shows a significant reduction in the final errors.

Midcourse guidance in two variables. - As a second example of how the fundamental guidance equation may be used to prescribe corrective maneuvers, guidance action taken during the nominal coast period of the heliocentric-transfer phase is considered. The coast period begins 27.7 days after heliocentric injection, and this time instant is denoted t_c. If the powered period is extended over the interval $(t_c, t_c + \Delta t)$, where Δt is arbitrary but less than several days, and if the thrust-angle correction $\Delta\beta$ is constant during this interval, any two of the final-velocity and -position error components may be nulled. The position errors were chosen to be nulled.

The guidance equations involving position errors only are taken from equation (6) and are written as

$$\delta r_f(t_c + \Delta t) = \delta r_f(t_c) + \int_{t_c}^{t_c + \Delta t} f_3 \, dt$$

$$\delta \varphi_f(t_c + \Delta t) = \delta \varphi_f(t_c) + \int_{t_0}^{t_c + \Delta t} f_4 \, dt$$

where $\delta r_f(t_c)$ and $\delta\varphi_f(t_c)$ are the final-position errors predicted at time t_c from navigational measurements, and the integrands f_3 and f_4 are given by equation (20). For the purpose of calculation, the integrands may be approximated by dropping the terms λ_{15}/c, since

results have shown them to be quite small in comparison with the other terms. Therefore, since $\delta r_f(t_c + \Delta t) = \delta\varphi_f(t_c + \Delta t) = 0$ is desired, and Δt is small,

$$\delta r_f(t_c) + F_{des}\,\Delta t\left[w_{31}(t_c)\cos\Delta\beta + \frac{w_{32}(t_c)}{F}\sin\Delta\beta\right] = 0$$

and

$$\delta\varphi_f(t_c) + F_{des}\,\Delta t\left[w_{41}(t_c)\cos\Delta\beta + \frac{w_{42}(t_c)}{F}\sin\Delta\beta\right] = 0$$

The solutions for $\Delta\beta$ and Δt are

$$\tan\Delta\beta = \frac{w_{41}(t_c)\delta r_f(t_c) - w_{31}(t_c)\delta\varphi_f(t_c)}{\dfrac{w_{32}(t_c)}{F}\delta\varphi_f(t_c) - \dfrac{w_{42}(t_c)}{F}\delta r_f(t_c)}$$

$$\Delta t = \frac{-\delta r_f(t_c)}{F_{des}\left[w_{31}(t_c)\cos\Delta\beta + \dfrac{w_{32}(t_c)}{F}\sin\Delta\beta\right]}$$

where the quadrant of $\Delta\beta$ is chosen such that Δt is positive. The effect of the corrective maneuver on the final-velocity errors may be determined from

$$\delta u_f(t_c + \Delta t) = \delta u_f(t_c) + F_{des}\,\Delta t\left[w_{11}(t_c)\cos\Delta\beta + \frac{w_{12}(t_c)}{F}\sin\Delta\beta\right]$$

$$\delta\omega_f(t_c + \Delta t) = \delta\omega_f(t_c) + F_{des}\,\Delta t\left[w_{21}(t_c)\cos\Delta\beta + \frac{w_{22}(t_c)}{F}\sin\Delta\beta\right]$$

As a numerical example, assume the final errors determined at time t_c to be due to the residual escape-guidance errors and to a constant 0.1-percent-thrust-magnitude perturbation δF acting over the interval $t_0 = 0$ to $t_c = 27.7$ days. The final-escape errors from the previous section are transformed to initial heliocentric errors with the use of equations (B6), (B7), (B12), and (B14). Then, from the results of the heliocentric-trajectory-sensitivity analysis

$$\delta u_f(t_c) = 0.240 \text{ m/sec}$$

$$\delta\omega_f(t_c) = -1.58\times10^{-10} \text{ radian/sec}$$

$$\delta r_f(t_c) = 2.08 \times 10^8 \text{ m}$$

$$\delta \varphi_f(t_c) = -3.93 \times 10^{-3} \text{ radian}$$

The midcourse corrective maneuver requires that

$$\Delta\beta = 3.91 \text{ radians} \equiv 224^{\circ}$$

$$\Delta t = 5.66 \times 10^4 \text{ sec} \equiv 0.656 \text{ day}$$

The actual thrust direction is found by adding $\Delta\beta$ to the reference thrust direction at t_c (see fig. 7(a)); hence,

$$\beta = 0.850 + 3.91 = 4.76 \text{ radians} \equiv 273^{\circ}$$

The mass loss due to the corrective maneuver is

$$\Delta m = \dot{m} \, \Delta t$$

$$= (-5.68 \text{ kg/day})(0.656 \text{ day})$$

$$= -3.73 \text{ kg}$$

The final-velocity errors after the correction become

$$\delta u_f(t_c + \Delta t) = 9.83 \text{ m/sec}$$

$$\delta \omega_f(t_c + \Delta t) = 2.25 \times 10^{-11} \text{ radian/sec}$$

CONCLUDING REMARKS

A typical low-thrust Mars orbiter mission using the Snap-8 power-generating system is studied from a guidance viewpoint. The mission trajectory is divided into the three characteristic phases, namely, the outward escape spiral, the heliocentric transfer, and the inward capture spiral. For each trajectory phase, the sensitivity of the final trajectory state (velocity, position, and mass) due to errors in the initial trajectory state and to thrust-vector errors is determined. This information is expressed by the fundamental guidance equation, the derivation and solution of which is based on linear perturbation theory and the method of adjoint functions. In addition to providing a means of investigating the perturbative effect due to a number of error sources, which is the major objective of this report, the guidance equation may also be used to determine requirements for corrective guidance.

The escape-spiral trajectory is designed so that the hyperbolic escape asymptote is pointed in a prescribed direction relative to the

Earth-sun line. In other words, the last spiral turn must be oriented properly. Since the vehicle makes several hundred revolutions about the Earth in the process of escaping, it might be expected that the escape direction would be highly sensitive to errors. This expectation is amply verified by the results of the sensitivity analysis. For example, a 0.1-percent error in either the initial-orbital altitude or the initial mass, if left uncorrected, is sufficient to reverse the direction of escape. A minimum error of 0.1 percent in the thrust magnitude acting over the entire trajectory will also result in a 180° misorientation. The effects of thrust-angle errors during the escape phase are found to be nonlinear for errors larger than a fraction of 1°, so that second-order terms are required. Results show, for example, that thrust-angle errors of 1/2° and 2.8° acting over the entire trajectory cause the escape direction to be in error by about 10° and 180°, respectively. Because of the small control errors involved, specifically the thrust-magnitude error, the vehicle must have the capability of corrective-guidance programming.

The sensitivity analysis of the heliocentric transfer phase shows that the nature and magnitude of trajectory perturbations are not unlike those for free-fall trajectories. The exception, of course, is that an error in the vehicle's mass will perturb the low-thrust trajectory. An error of 10 kilograms at the initial-trajectory state results in a final-position error of several hundred thousand kilometers. Either a 1/2° error in the escape direction, a 1-percent error in thrust magnitude, or a 1/2° error in thrust angle, will result in final position and velocity errors of the order of several hundred thousand kilometers and 10 meters per second, respectively. These errors are of sufficient magnitude to require midcourse corrective maneuvers.

The capture spiral, like the escape spiral, is highly sensitive to errors both in the initial trajectory state and in thrust-vector control. These two phases of the mission are essentially duals of each other. In the escape phase, the final velocity and radial position are not too sensitive to guidance errors. The important parameter is the final angular position, which is strongly related to the escape direction. In the capture phase, however, the final angular position is of little consequence compared with the size of the final satellite orbit. Hence, the final velocity and radial position are the important parameters, and results have shown these to be very sensitive. For example, if the initial-velocity magnitude and direction were in error by only 1 meter per second and 1 milliradian, respectively, and if the reference thrust program were followed exactly, the vehicle would spiral down into the Martian surface instead of establishing the nominal 927-kilometer circular orbit. A constant-thrust-angle error of only 1 milliradian acts to decrease the final perigee altitude by about 400 kilometers.

In summary, the results of this analysis indicate that the low-thrust trajectory is extremely sensitive to relatively small error

magnitudes. It should not be concluded, however, that accurate guidance
is unachievable. As the trajectory is affected by error perturbations,
it is likewise affected by controlled perturbations, that is, by correc-
tive thrust programming. The proper conclusion to be drawn from this
study is that the electrically propelled space vehicle incurs the job
of repetitive trajectory determination and corrective guidance maneuvers.

Lewis Research Center
    National Aeronautics and Space Administration
        Cleveland, Ohio, July 16, 1962

APPENDIX A

PERTURBATION ANALYSIS

The motion of the vehicle during each phase of the mission is described by a set of nonlinear differential equations. Consider that a solution of such a set corresponding to a specified thrust program and satisfying prescribed boundary conditions has been obtained and is termed the reference solution. If the major assumption is made that extraneous perturbations (e.g., guidance errors) are sufficiently small so that the actual vehicle trajectory does not vary significantly from the reference trajectory, it is possible to study these variations and the required corrective maneuvers by linear perturbation techniques. The perturbed differential equations of motion represent a linear system with time-varying coefficients, which are expressed as known functions of position, velocity, thrust and gravity forces, and mass along the reference trajectory.

The following analysis shows the derivation of the linearized system equations and the use of adjoint methods in obtaining the variational solution and expressing the fundamental guidance equation. In the following discussion, the symbol δ is used to represent small variations from reference quantities, and matrix notation is used for the purpose of compactness and ease in algebraic manipulation.

System Equations

During each phase of the mission, the vehicle is assumed to travel in a vacuum under the influence of an inverse-square central gravitational field in addition to its own thrust acceleration. A two-dimensional geometry is used, and the vehicle motion is described in a rotating polar coordinate system centered at the appropriate central body. With reference to figure 1, the differential equations of motion to be satisfied along the flight path are given as

$$\dot{u} = r\omega^2 - \frac{GM}{r^2} + \frac{F}{m} \sin \beta \tag{1}$$

$$\dot{\omega} = \frac{-2u\omega}{r} + \frac{F}{rm} \cos \beta \tag{2}$$

$$\dot{r} = u \tag{3}$$

$$\dot{\varphi} = \omega \tag{4}$$

$$\dot{m} = -\frac{F}{c} \tag{5}$$

Differentiation with respect to the independent variable time is denoted by a superscribed dot. The state variables of interest are radial velocity u, angular velocity ω, radial position r, angular position φ, and mass m. The propulsion or control variables are the thrust magnitude F, and the thrust angle β, which is measured with respect to the local horizontal (circumferential) direction. The effective jet velocity c is equal to the product of specific impulse and a conversion factor, and is considered constant herein.

At this point, it is convenient to define the following column matrices or vectors:

$$\overline{x} = \begin{bmatrix} x_1 \\ x_2 \\ x_3 \\ x_4 \\ x_5 \end{bmatrix} = \begin{bmatrix} u \\ \omega \\ r \\ \varphi \\ m \end{bmatrix} ; \quad \overline{y} = \begin{bmatrix} y_1 \\ y_2 \end{bmatrix} \quad \begin{bmatrix} F \\ \beta \end{bmatrix} \tag{A1}$$

and to write equations (1) to (5) as

$$\dot{x}_i = g_i(x_1, \ldots, x_5, y_1, y_2) \qquad i = 1, \ldots, 5 \tag{A2}$$

The perturbed system of equations is obtained by taking the first-order variations of (A2)

$$\delta\dot{x}_i = \sum_{j=1}^{5} \frac{\partial g_i}{\partial x_j} \delta x_j + \sum_{j=1}^{2} \frac{\partial g_i}{\partial y_j} \delta y_j \qquad i = 1, \ldots, 5 \tag{A3}$$

which is, in matrix notation,

$$\frac{d}{dt} \delta\overline{x} - A\delta\overline{x} = B\delta\overline{y} \tag{A4}$$

where A and B are (5 by 5) and (5 by 2) coefficient matrices, respectively, whose ij^{th} elements are given by $\partial g_i/\partial x_j$ and $\partial g_i/\partial y_j$, respectively; thus,

$$
A = \left[\frac{\partial g_i}{\partial x_j}\right] = \begin{bmatrix}
0 & 2r\omega & \left(\dfrac{2GM}{r^3} + \omega^2\right) & 0 & \dfrac{-F}{m^2}\sin\beta \\[2ex]
\dfrac{-2\omega}{r} & \dfrac{-2u}{r} & \left(\dfrac{2u\omega}{r^2} - \dfrac{F\cos\beta}{mr^2}\right) & 0 & \dfrac{-F}{rm^2}\cos\beta \\[2ex]
1 & 0 & 0 & 0 & 0 \\[1ex]
0 & 1 & 0 & 0 & 0 \\[1ex]
0 & 0 & 0 & 0 & 0
\end{bmatrix} \tag{A5}
$$

$$
B = \left[\frac{\partial g_i}{\partial y_j}\right] = \begin{bmatrix}
\dfrac{\sin\beta}{m} & \dfrac{F\cos\beta}{m} \\[2ex]
\dfrac{\cos\beta}{rm} & \dfrac{-F\sin\beta}{rm} \\[2ex]
0 & 0 \\[1ex]
0 & 0 \\[1ex]
\dfrac{-1}{c} & 0
\end{bmatrix} \tag{A6}
$$

Note that A and B are time-varying matrices evaluated along the known reference trajectory.

Solution by Adjoint Methods

The solution of equation (A4) can best be facilitated by the method of adjoint functions, as suggested in reference 3, by introduction of a 5 by 1 vector of Lagrangian multipliers $\overline{\lambda}_i$, which satisfies a system of equations defined to be adjoint to equation (A4):

$$
\frac{d}{dt}\,\overline{\lambda}_i + A^T\overline{\lambda}_i = 0 \tag{A7}
$$

where

$$
\overline{\lambda}_i = \begin{bmatrix} \lambda_{i1} \\ \cdot \\ \cdot \\ \cdot \\ \lambda_{i5} \end{bmatrix}
$$

In equation (A7,) A^T is the transpose of the matrix A. The desired relation between equations (A4) and (A7) is obtained by taking the scalar product of (A4) with $\overline{\lambda}_i$, the scalar product of (A7) with $\delta\overline{x}$, and adding the results:

$$\overline{\lambda}_i \cdot \left(\frac{d}{dt}\, \delta\overline{x}\right) - \overline{\lambda}_i \cdot (A\delta\overline{x}) + \left(\frac{d}{dt}\, \overline{\lambda}_i\right) \cdot \delta\overline{x} + \left(A^T\overline{\lambda}_i\right) \cdot \delta\overline{x} = \overline{\lambda}_i \cdot (B\delta\overline{y})$$

It is easily shown, however, that

$$\overline{\lambda}_i \cdot (A\delta\overline{x}) = \left(A^T\overline{\lambda}_i\right) \cdot \delta\overline{x}$$

$$\overline{\lambda}_i \cdot (B\delta\overline{y}) = \left(B^T\overline{\lambda}_i\right) \cdot \delta\overline{y}$$

$$\frac{d}{dt}\, (\overline{\lambda}_i \cdot \delta\overline{x}) = \overline{\lambda}_i \cdot \left(\frac{d}{dt}\, \delta\overline{x}\right) + \left(\frac{d}{dt}\, \overline{\lambda}_i\right) \cdot \delta\overline{x}$$

Therefore

$$\frac{d}{dt}\, (\overline{\lambda}_i \cdot \delta\overline{x}) = \left(B^T\overline{\lambda}_i\right) \cdot \delta\overline{y} \tag{A8}$$

Define a 2 by 1 weighting vector $\overline{w}_i$:

$$\overline{w}_i = \begin{bmatrix} w_{i1} \\ w_{i2} \end{bmatrix} = B^T\overline{\lambda}_i \tag{A9}$$

and integrate both sides of equation (A8) between the general time t and the nominal final time t_f:

$$\overline{\lambda}_i(t_f) \cdot \delta\overline{x}(t_f) = \overline{\lambda}_i(t) \cdot \delta\overline{x}(t) + \int_t^{t_f} (\overline{w}_i \cdot \delta\overline{y})dt \tag{A10}$$

Equation (A10) expresses a linear function of variations in final conditions in terms of variations in state variables at any point along the path and the integrated effect of future thrust variations over the path. For the purpose of analysis it is desirable to separate the effect of variations on each quantity individually. This is possible by a proper interpretation of the boundary conditions on the Lagrangian multipliers. For example, let the variation δx_i be of interest at the final time t_f. If the following boundary conditions at t_f are specified,

$$\lambda_{ii}(t_f) = 1; \; \lambda_{ij}(t_f) = 0 \qquad \text{for} \quad j \neq i \tag{A11}$$

the adjoint equations (A7) can be integrated backward from t_f to yield numerical values for the multipliers at each time instant t. The variation of interest is then given explicitly from (A10):

$$\delta x_i(t_f) = \overline{\lambda}_i(t) \cdot \delta \overline{x}(t) + \int_t^{t_f} (\overline{w}_i \cdot \delta \overline{y})dt \qquad (A12)$$

If this procedure is followed for $i = 1, \ldots, 5$, the complete solution for the variations in final-state variables may be expressed in the matrix form

$$\delta \overline{x}(t_f) = \Lambda(t)\delta \overline{x}(t) + \int_t^{t_f} (W\delta \overline{y})dt \qquad (A13)$$

where the rows of Λ and W are made up of the elements of $\overline{\lambda}$ and $\overline{w}_i$, respectively:

$$\Lambda = \begin{bmatrix} \overline{\lambda}_1 \\ \cdot \\ \cdot \\ \cdot \\ \overline{\lambda}_5 \end{bmatrix} = \begin{bmatrix} \lambda_{11} & \lambda_{12} & \cdot & \cdot & \lambda_{15} \\ \lambda_{21} & \cdot & \cdot & \cdot & \lambda_{25} \\ \cdot & & & & \cdot \\ \cdot & & & & \cdot \\ \lambda_{51} & & & & \lambda_{55} \end{bmatrix} ; \quad W = \begin{bmatrix} \overline{w}_1 \\ \cdot \\ \cdot \\ \cdot \\ \overline{w}_5 \end{bmatrix} = \begin{bmatrix} w_{11} & w_{12} \\ \cdot & \cdot \\ \cdot & \cdot \\ \cdot & \cdot \\ w_{51} & w_{52} \end{bmatrix} \qquad (7)$$

Because of the form of equation (7), the elements of Λ can be interpreted as partial derivatives or sensitivity coefficients; thus,

$$\lambda_{ij}(t) = \frac{\partial x_i(t_f)}{\partial x_j(t)} \qquad \begin{cases} i = 1, \ldots, 5 \\ j = 1, \ldots, 5 \end{cases} \qquad (A14)$$

Now that the general results have been established with the help of matrix notation, it would be well to write out equations (A7) and (A9) in terms of the variables of interest in this study. The set of adjoint equations is determined from (A7) and (A5):

$$\dot{\lambda}_{i1} = \left(\frac{2\omega}{r}\right) \lambda_{i2} - \lambda_{i3} \qquad (8)$$

$$\dot{\lambda}_{i2} = -(2r\omega)\lambda_{i1} + \left(2 \frac{u}{r}\right)\lambda_{i2} - \lambda_{i4} \qquad (9)$$

$$\dot{\lambda}_{i3} = -\left(\frac{2GM}{r^3} + \omega^2\right)\lambda_{i1} - \left(\frac{2u\omega}{r^2} - \frac{F \cos \beta}{r^2 m}\right)\lambda_{i2} \qquad (10)$$

$$\dot{\lambda}_{i4} = 0 \qquad (11)$$

$$\dot{\lambda}_{i5} = \left(\frac{F \sin \beta}{m^2}\right)\lambda_{i1} + \left(\frac{F \cos \beta}{rm^2}\right)\lambda_{i2} \qquad (12)$$

The weighting functions are found from (A9) and (A6):

$$w_{i1} = \frac{\lambda_{i1}}{m} \sin \beta + \frac{\lambda_{i2}}{rm} \cos \beta - \frac{\lambda_{i5}}{c} \tag{15}$$

$$w_{i2} = \frac{F}{m}\left(\lambda_{i1} \cos \beta - \frac{\lambda_{i2}}{r} \sin \beta\right) \tag{16}$$

Nonlinear Thrust-Vector Perturbations

The previous results were derived with consideration given only to first-order variations in the state variables and the thrust vector. It is possible that relatively large variations in thrust magnitude and direction will occur in such a way that the deviation between actual and reference trajectories still remains small; that is, the linearization of state variables is still valid. The integrand in equation (A13) must be modified from its linear form to account for this situation.

When exact variations in thrust magnitude and direction (ΔF and $\Delta \beta$) are considered, the right side of equation (A4) becomes

$$B\delta\overline{y} \rightarrow \begin{bmatrix} \frac{F + \Delta F}{m} \sin (\beta + \Delta\beta) - \frac{F}{m} \sin \beta \\[2ex] \frac{(F + \Delta F)}{rm} \cos (\beta + \Delta\beta) - \frac{F}{rm} \cos \beta \\[2ex] 0 \\[1ex] 0 \\[2ex] -\frac{(F + \Delta F)}{c} + \frac{F}{c} \end{bmatrix}$$

Correspondingly, from the definition of equation (A9), the integrand term of equation (A12) becomes

$$(\overline{w}_i \cdot \delta\overline{y}) \rightarrow f_i = \frac{\lambda_{i1}}{m} [(F + \Delta F) \sin (\beta + \Delta\beta) - F \sin \beta]$$

$$+ \frac{\lambda_{i2}}{rm} [(F + \Delta F) \cos (\beta + \Delta\beta) - F \cos \beta] - \frac{\lambda_{i5}}{c} [(F + \Delta F) - F]$$

Equation (A13) then becomes

$$\delta \overline{x}(t_f) = \Lambda(t)\delta \overline{x}(t) + \int_t^{t_f} (f_i)dt \qquad (18)$$

APPENDIX B

ERROR TRANSFORMATION BETWEEN ESCAPE AND

HELIOCENTRIC MISSION PHASES

The relations between final escape errors and initial heliocentric errors are presented. The Earth-referenced velocity and position components at the termination of the escape phase are denoted as u_{f1}, ω_{f1}, r_{f1}, and φ_{f1} and the sun-referenced components at the initiation of the heliocentric phase as u_{02}, ω_{02}, r_{02}, and φ_{02}. Only first-order variations in u_{f1}, ω_{f1}, and r_{f1} are considered; however, large variations in φ_{f1} are to be allowed.

Position Errors

The geometric configuration of the Earth-centered reference position $\overline{r}_{f1}$ and the actual position $\overline{r}_{f1} + \delta\overline{r}_{f1}$ is shown in the following sketch. The coordinate frame has $\overline{i}_r$ as a unit vector away from the sun, and $\overline{i}_\varphi$ as a unit vector in the direction of Earth's orbital velocity.
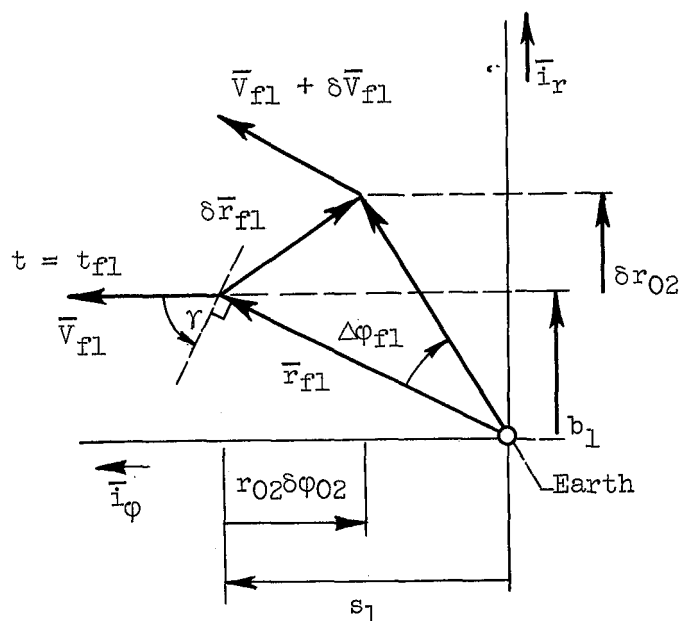
The quantities b_1 and s_1 are components of the reference-position vector. Since it has been arbitrarily assumed that the hyperbolic escape direction is parallel to $\bar{i}_\varphi$, the asymptotic displacement of the escape hyperbola is represented by b_1.

The heliocentric position of the vehicle at time t_{f1} is

$$\bar{r}_{02} = \bar{r}_E + \bar{r}_{f1}$$

so that

$$\delta\bar{r}_{02} = \delta\bar{r}_{f1} = (\delta r_{02})\bar{i}_r + (r_{02}\delta\varphi_{02})\bar{i}_\varphi$$

The components of $\delta\bar{r}_{02}$, which may easily be found from the sketch, are given by

$$\delta r_{02} = \frac{b_1}{r_{f1}}\left[r_{f1}(\cos\Delta\varphi_{f1} - 1) + \cos\Delta\varphi_{f1}\delta r_{f1}\right] - s_1\sin\Delta\varphi_{f1} \quad \text{(B1)}$$

$$r_{02}\delta\varphi_{02} = \frac{s_1}{r_{f1}}\left[r_{f1}(\cos\Delta\varphi_{f1} - 1) + \cos\Delta\varphi_{f1}\delta r_{f1}\right] + b_1\sin\Delta\varphi_{f1}$$
$$\text{(B2)}$$

where

$$b_1 = r_{f1}\left(\frac{r_{f1}\omega_{f1}}{V_{f1}}\right) \quad \text{(B3)}$$

$$s_1 = r_{f1}\left(\frac{u_{f1}}{V_{f1}}\right) \quad \text{(B4)}$$

$$r_{02} \approx r_E + b_1 \quad \text{(B5)}$$

If $\Delta\varphi_{f1}$ is very small $(\Delta\varphi_{f1} \rightarrow \delta\varphi_{f1})$, equations (B1) and (B2) are approximated by

$$\delta r_{02} = \left(\frac{b_1}{r_{f1}}\right)\delta r_{f1} - (s_1)\delta\varphi_{f1} \quad \text{(B6)}$$

$$r_{02}\delta\varphi_{02} = \left(\frac{s_1}{r_{f1}}\right)\delta r_{f1} + (b_1)\delta\varphi_{f1} \quad \text{(B7)}$$

Positive $\Delta\varphi_{fl}$ is measured counterclockwise, so $\Delta\varphi_{fl}$ is a negative angle, as indicated by the sketch.

Velocity Errors

The heliocentric velocity of the vehicle at time t_{fl} is

$$\overline{V}_{02} = \overline{V}_E + \overline{V}_{fl}$$

so that

$$\delta\overline{V}_{02} = \delta\overline{V}_{fl} = (\delta u_{02})\overline{i}_r + \delta(r_{02}\omega_{02})\overline{i}_\varphi$$

where

$$\delta(r_{02}\omega_{02}) = r_{02}\delta\omega_{02} + \omega_{02}\delta r_{02}$$

The magnitude of $\delta\overline{V}_{fl}$ may be found as follows:

$$V_{fl}^2 = u_{fl}^2 + (r_{fl}\omega_{fl})^2$$

$$\delta V_{fl} = \left(\frac{u_{fl}}{V_{fl}}\right)\delta u_{fl} + \left(\frac{r_{fl}^2\omega_{fl}}{V_{fl}}\right)\delta\omega_{fl} + \left(\frac{r_{fl}^2\omega_{fl}}{V_{fl}}\right)\delta r_{fl}$$

or from (B3) and (B4)

$$\delta V_{fl} = \left(\frac{s_1}{r_{fl}}\right)\delta u_{fl} + (b_1)\delta\omega_{fl} + \left(\frac{b_1\omega_{fl}}{r_{fl}}\right)\delta r_{fl}$$

$$\left.\begin{array}{c}\\\\\\\\\\\\\\\end{array}\right\} \quad (B8)$$

The angle between the velocity vector and the Earth-centered local horizontal is denoted by γ in the sketch. The variation in this angle may be expressed in terms of δu_{fl}, $\delta\omega_{fl}$, and δr_{fl} as follows:

$$\tan\gamma = \frac{u_{fl}}{r_{fl}\omega_{fl}}$$

$$\delta\gamma = \cos^2\gamma\left[\left(\frac{1}{r_{fl}\omega_{fl}}\right)\delta u_{fl} - \left(\frac{u_{fl}}{r_{fl}\omega_{fl}^2}\right)\delta\omega_{fl} - \left(\frac{u_{fl}}{r_{fl}^2\omega_{fl}}\right)\delta r_{fl}\right]$$

42

since

$$\cos \gamma = \frac{r_{f1}\omega_{f1}}{V_{f1}}$$

$$\delta\gamma = \left(\frac{r_{f1}\omega_{f1}}{V_{f1}^2}\right)\delta u_{f1} - \left(\frac{u_{f1}r_{f1}}{V_{f1}^2}\right)\delta\omega_{f1} - \left(\frac{u_{f1}\omega_{f1}}{V_{f1}^2}\right)\delta r_{f1} \qquad (B9)$$

Now, the directional variation between $\overline{V}_{f1}$ and $\overline{V}_{f1} + \delta\overline{V}_{f1}$ is in part due to $\delta\gamma$ and in part due to $\Delta\varphi_{f1}$. Specifically, the angle between the latter vector and $\overline{I}_\varphi$ is $\delta\gamma - \Delta\varphi_{f1}$ measured counterclockwise positive from $\overline{V}_{f1} + \delta\overline{V}_{f1}$. Now the heliocentric components of $\delta\overline{V}_{f1}$ may be expressed as

$$\delta u_{02} = (V_{f1} + \delta V_{f1})\sin(\delta\gamma - \Delta\varphi_{f1})$$

$$\delta(r_{02}\omega_{02}) = (V_{f1} + \delta V_{f1})\cos(\delta\gamma - \Delta\varphi_{f1}) - V_{f1}$$

Since $\delta V_{f1} \ll V_{f1}$ and $\delta\gamma$ is very small, the following approximations are valid:

$$\delta u_{02} = V_{f1}\delta\gamma \cos\Delta\varphi_{f1} - V_{f1} \sin\Delta\varphi_{f1}$$

$$\delta(r_{02}\omega_{02}) = V_{f1}(\cos\Delta\varphi_{f1} - 1) + \delta V_{f1}\cos\Delta\varphi_{f1} + V_{f1}\delta\gamma \sin\Delta\varphi_{f1}$$

With the use of equations (B3), (B4), (B8), and (B9), the previous expressions become

$$\delta u_{02} = \left[\left(\frac{b_1}{r_{f1}}\right)\delta u_{f1} - (s_1)\delta\omega_{f1} - \left(\frac{s_1\omega_{f1}}{r_{f1}}\right)\delta r_{f1}\right]\cos\Delta\varphi_{f1} - V_{f1}\sin\Delta\varphi_{f1}$$

$$\qquad (B10)$$

$$\delta(r_{02}\omega_{02}) = \frac{1}{r_{f1}}(s_1\cos\Delta\varphi_{f1} + b_1\sin\Delta\varphi_{f1})\delta u_{f1}$$

$$+ (b_1\cos\Delta\varphi_{f1} - s_1\sin\Delta\varphi_{f1})\delta\omega_{f1}$$

$$+ \frac{\omega_{f1}}{r_{f1}}(b_1\cos\Delta\varphi_{f1} - s_1\sin\Delta\varphi_{f1})\delta r_{f1} + V_{f1}(\cos\Delta\varphi_{f1} - 1) \qquad (B11)$$

If $\Delta\varphi_{f1}$ is very small $\Delta\varphi_{f1} \to \delta\varphi_{f1}$, equations (B10) and (B11) become

$$\delta u_{02} = \left(\frac{b_1}{r_{f1}}\right) \delta u_{f1} - (s_1)\delta\omega_{f1} - \left(\frac{s_1\omega_{f1}}{r_{f1}}\right) \delta r_{f1} - (V_{f1})\delta\varphi_{f1} \qquad (B12)$$

$$\delta(r_{02}\omega_{02}) = \delta V_{f1} \qquad (B13)$$

The variation $\delta\omega_{02}$ is found from (B6) and (B8)

$$\delta\omega_{02} = \left(\frac{s_1}{r_{f1}r_{02}}\right) \delta u_{f1} - \left(\frac{b_1}{r_{02}}\right)\delta\omega_{f1}$$

$$+ \frac{b_1}{r_{f1}r_{02}} (\omega_{02} - \omega_{f1})\delta r_{f1} + \left(\frac{\omega_{02}s_1}{r_{02}}\right) \delta\varphi_{f1} \qquad (B14)$$

REFERENCES

1. Friedlander, Alan L.: A Study of Guidance Sensitivity for Various Low-Thrust Transfers from Earth to Mars. NASA TN D-1183, 1962.

2. Mackay, J. S., Rossa, L. G., and Zimmerman, A. V.: Optimum Low-Acceleration Trajectories for Earth-Mars Transfer. Paper presented at IAS Conf. on Vehicle Systems Optimization, Garden City (N.Y.), Nov. 28-29, 1961.

3. Bliss, G. A.: Mathematics for Exterior Ballistics. John Wiley & Sons, Inc., 1944.

4. Tsien, H. S.: Engineering Cybernetics. McGraw-Hill Book Co., Inc., 1954, ch. 13.

5. Kelley, Henry J.: Gradient Theory of Optimal Flight Paths. ARS Jour., vol. 30, no. 10, Oct. 1960, pp. 947-953.
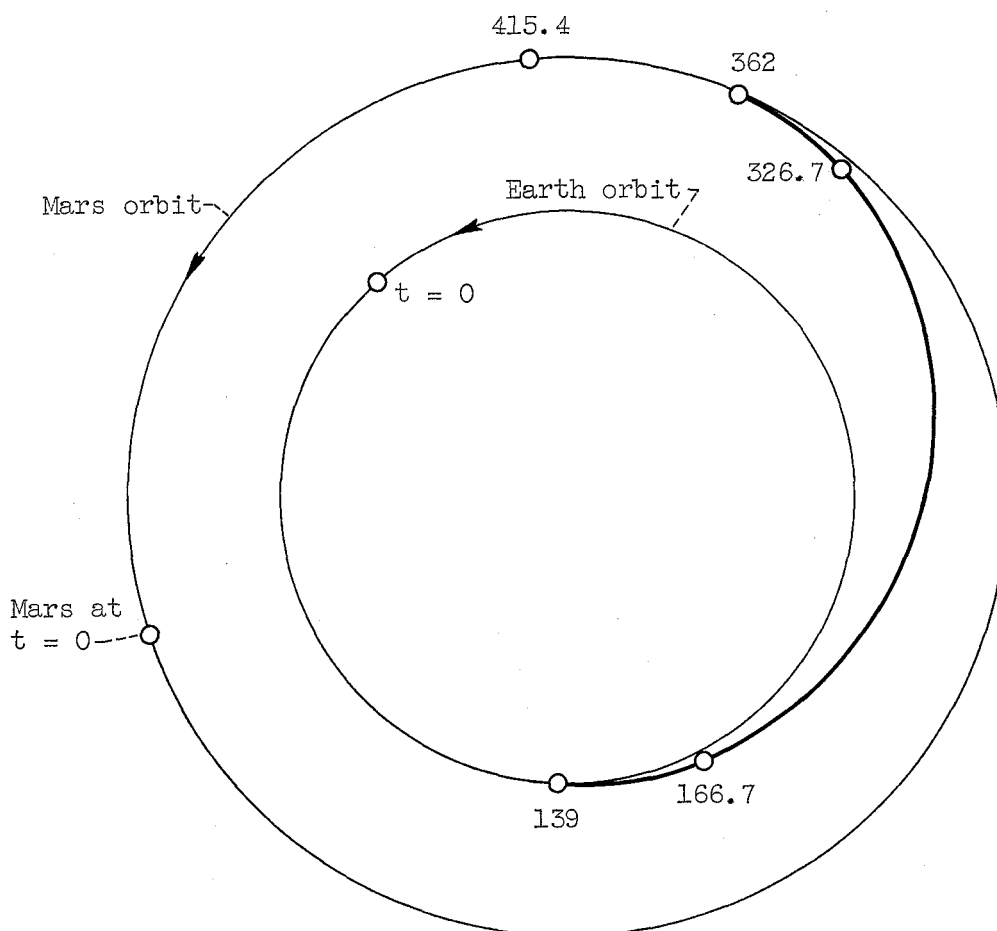
Time, t, days	Event
0	927 km Earth-satellite orbit; initiation of escape spiral
139	Hyperbolic escape condition; initiation of heliocentric transfer
166.7	Initiation of coast period
326.7	Termination of coast period
362	Hyperbolic capture condition; initiation of capture spiral
415.4	927 km Mars-satellite orbit

Figure 1. - Overall interplanetary transfer between Earth and Mars.
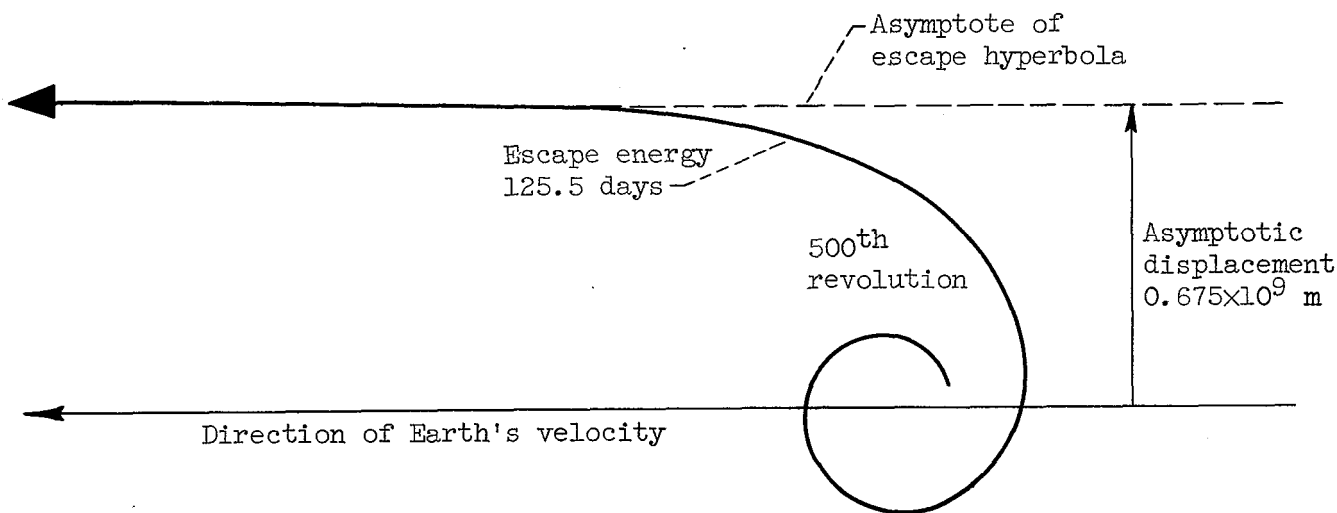
Figure 2. - Escape-spiral trajectory. Hyperbolic-escape conditions: time, 139 days; radial position, 1.899×10^9 meters (298 Earth radii); relative velocity, 1577 meters per second.
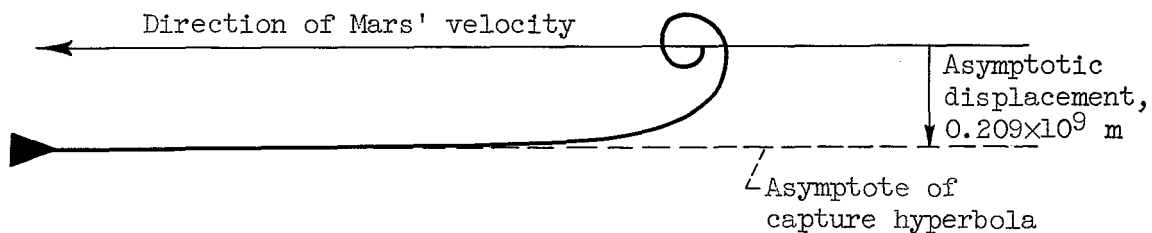
Figure 3. - Capture-spiral trajectory. Hyperbolic-capture conditions: radial position, 1.382×10^9 meters (418 Mars radii); relative velocity, 1454 meters per second.
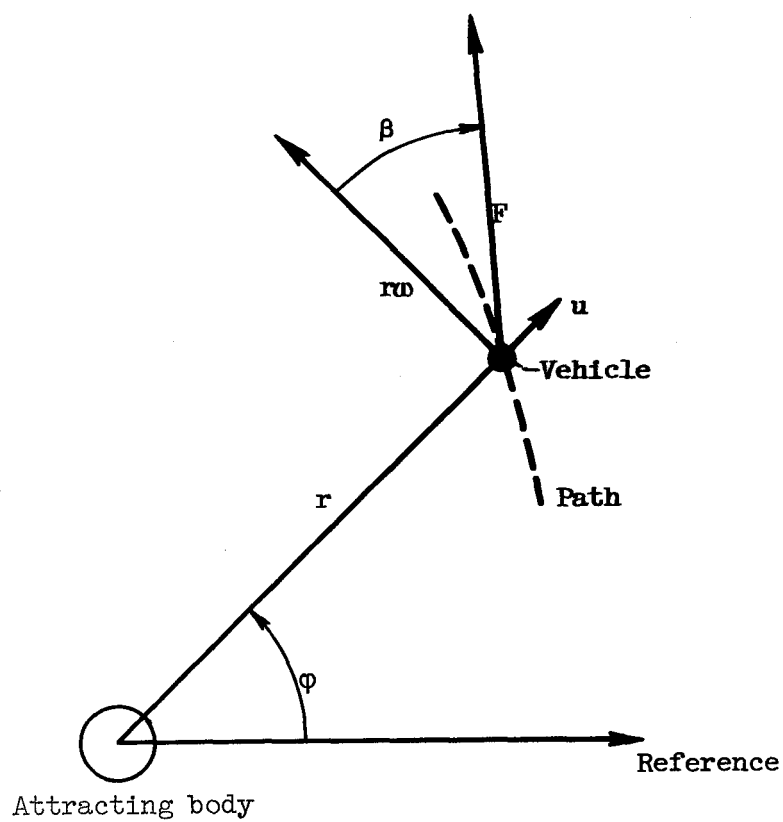
Figure 4. - Coordinate reference schematic
diagram.
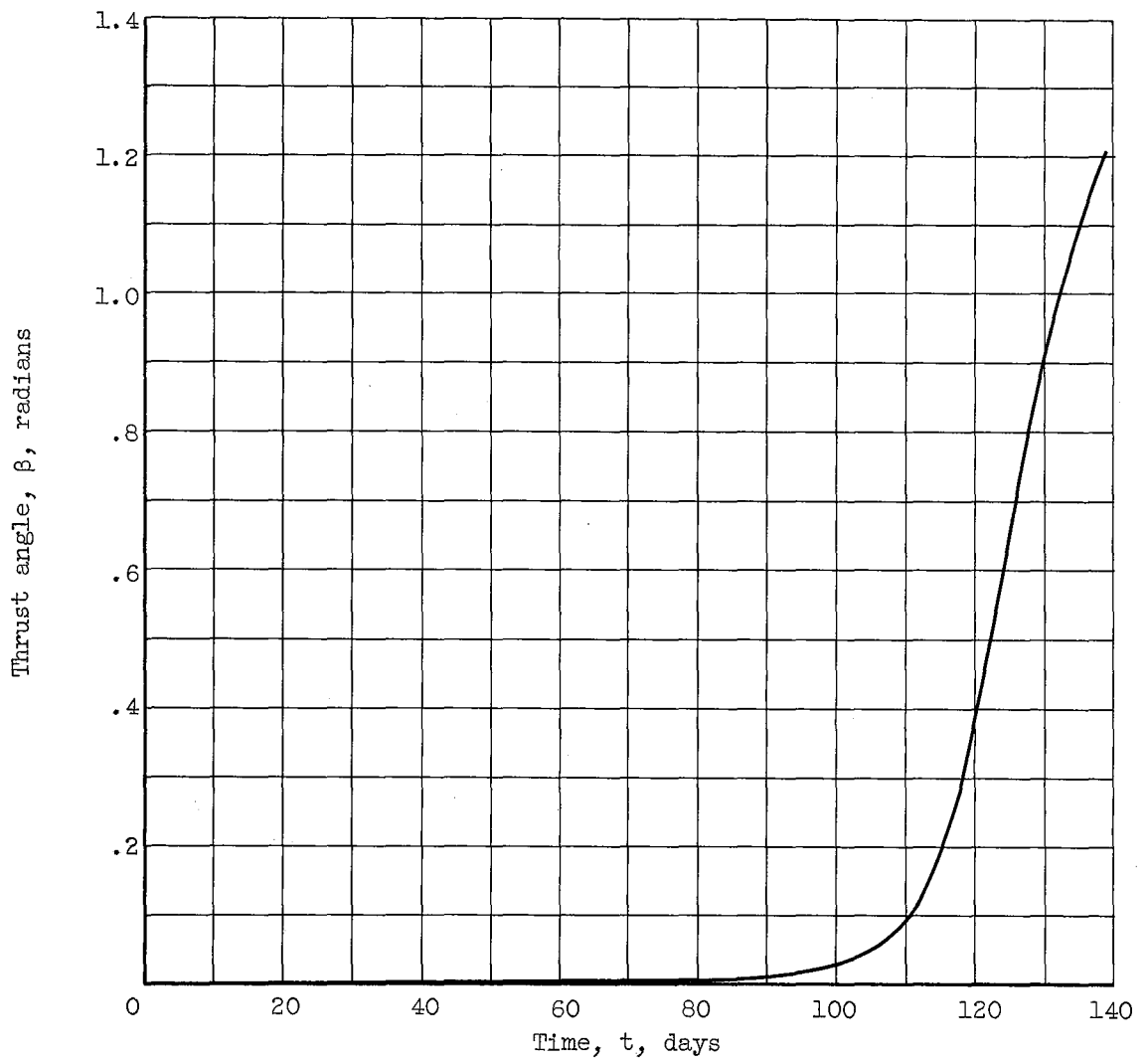
(a) Thrust-angle program.

Figure 5. - Characteristics of escape-spiral reference trajectory.
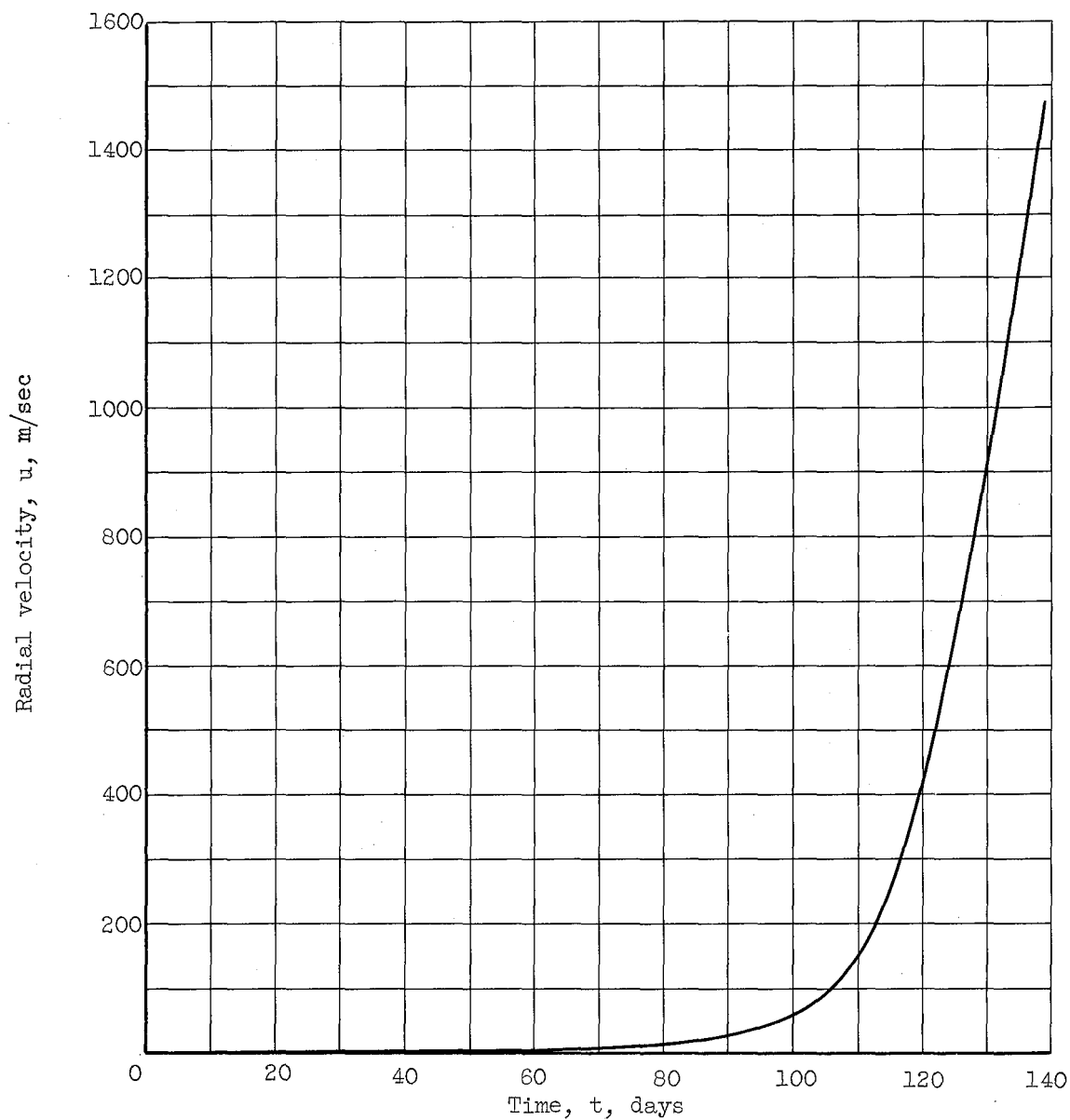
(b) Radial-velocity time history.

Figure 5. - Continued.   Characteristics of escape-spiral reference
   trajectory.
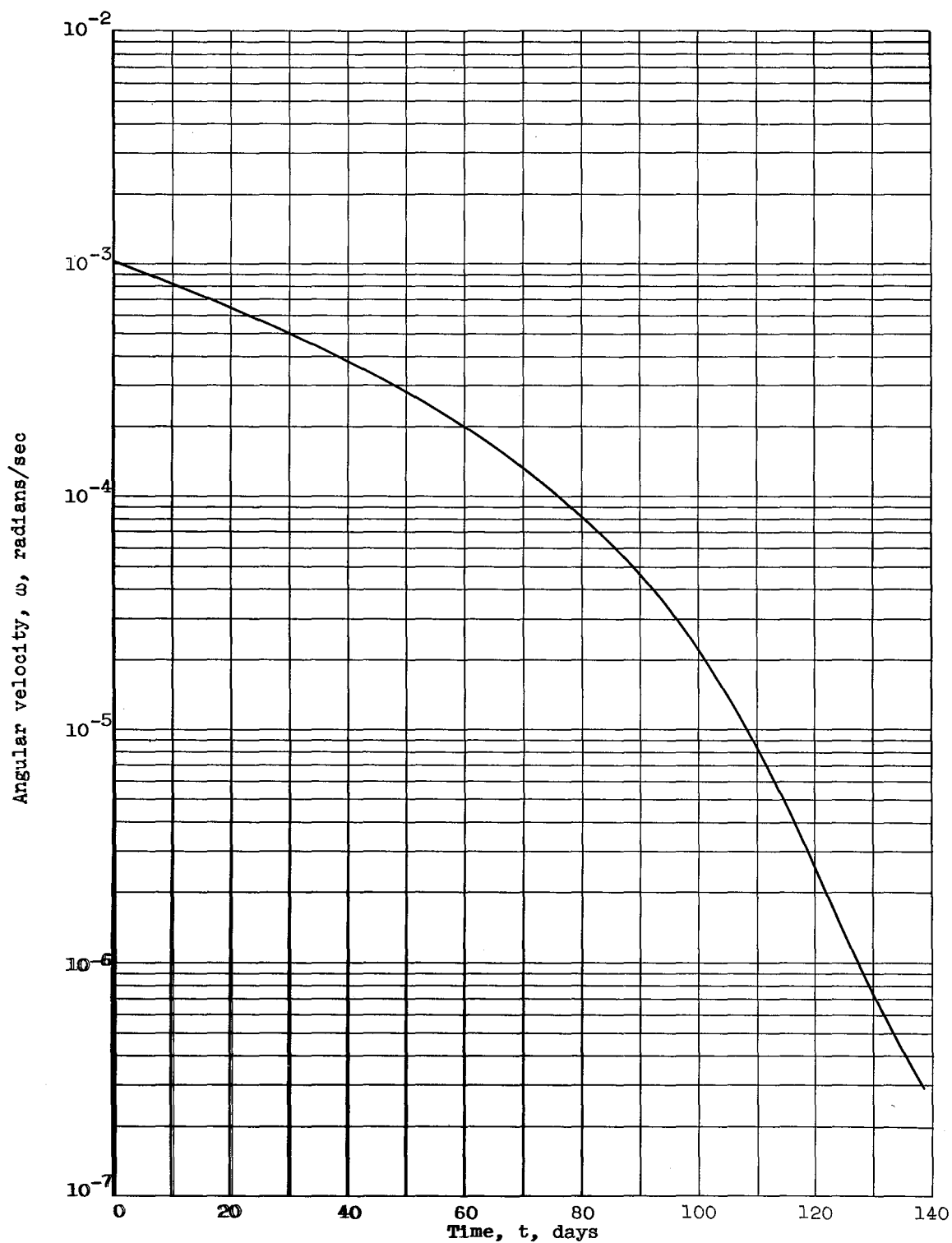
(c) Angular-velocity time history.

Figure 5. - Continued. Characteristics of escape-spiral reference
trajectory.
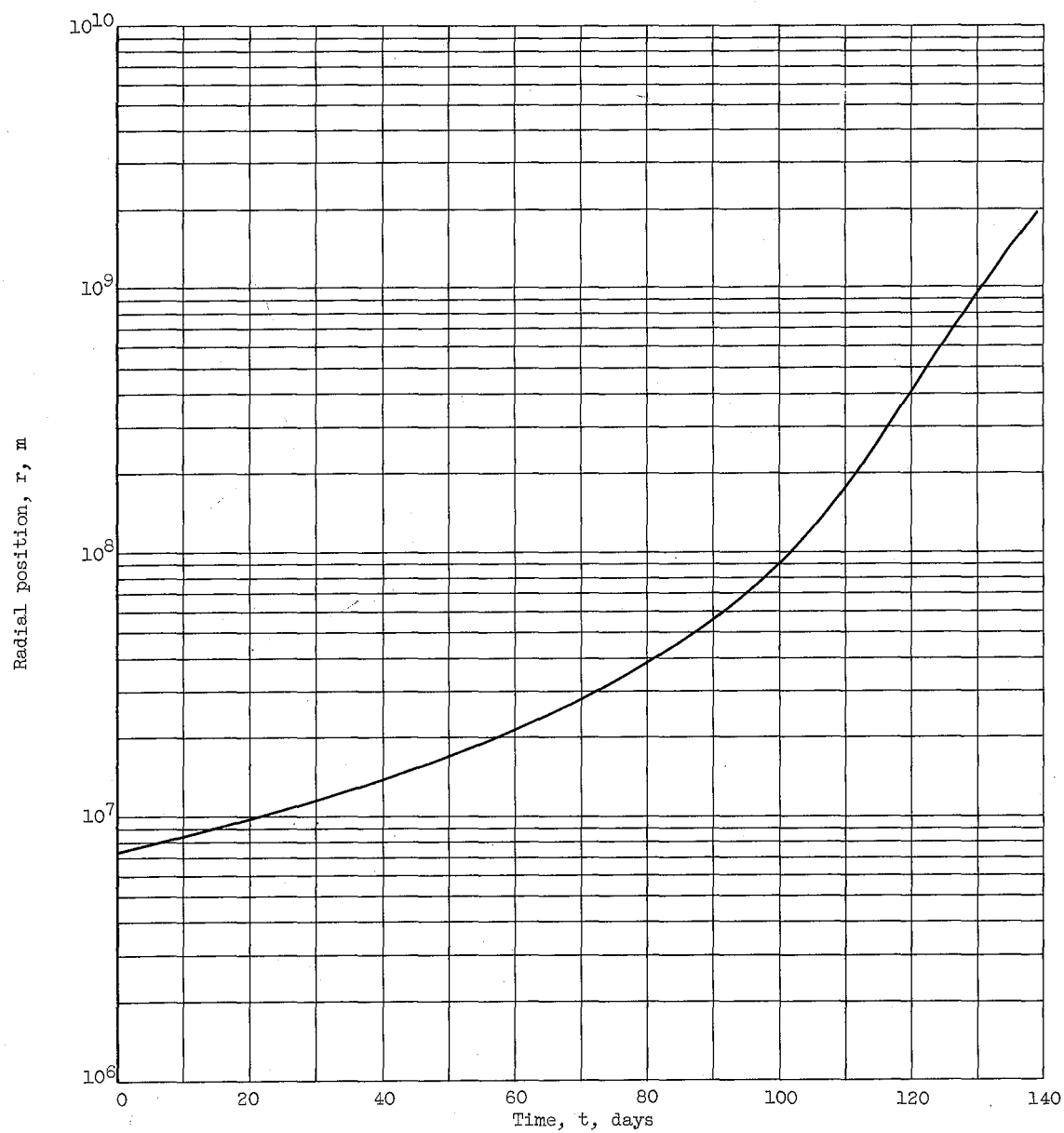
(d) Radial-position time history.

Figure 5. - Continued. Characteristics of escape-spiral reference trajectory.
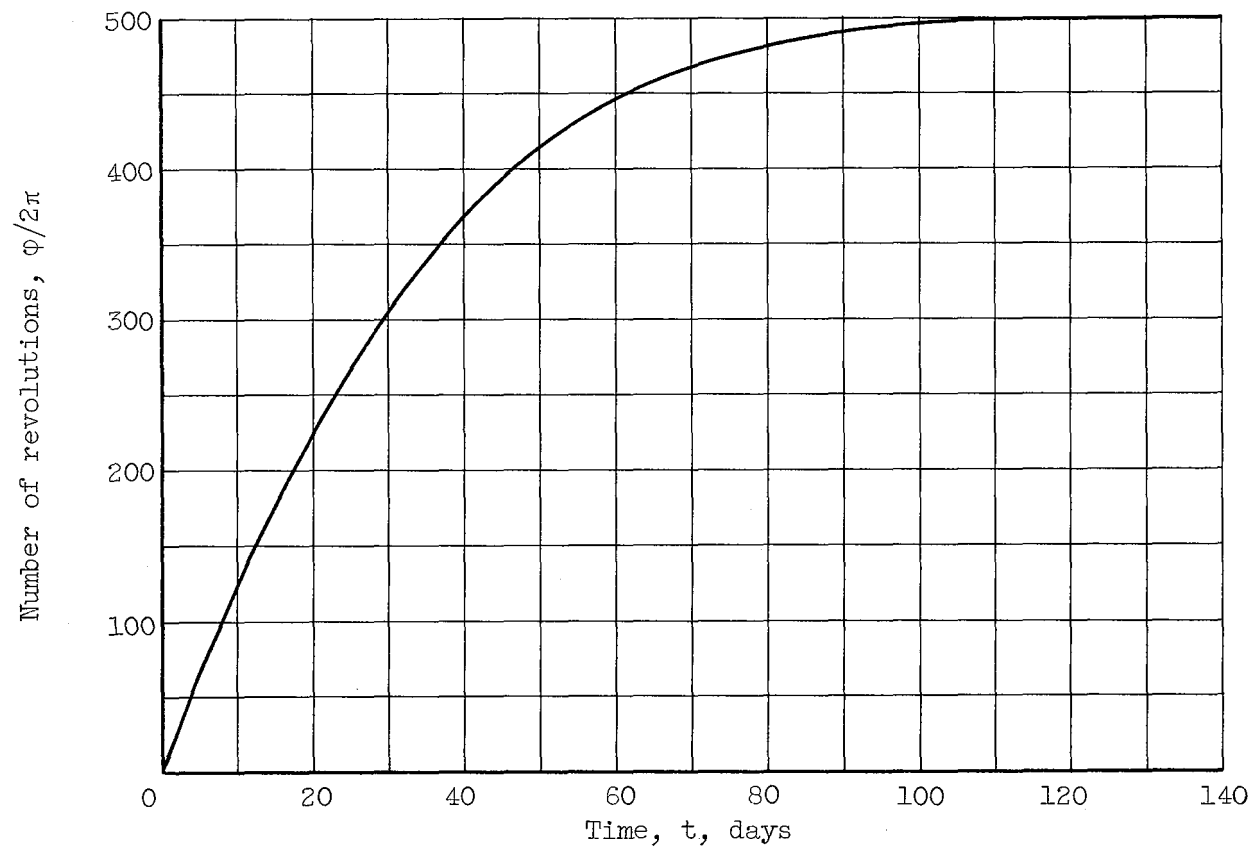
(e) Angular-position time history.

Figure 5. - Concluded.   Characteristics of escape-spiral reference
    trajectory.
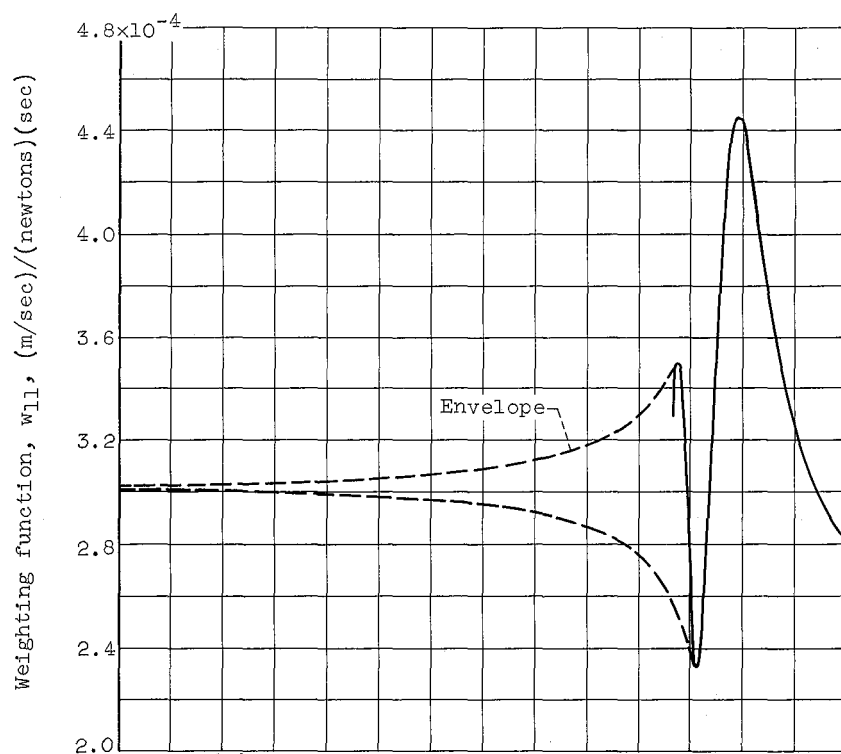
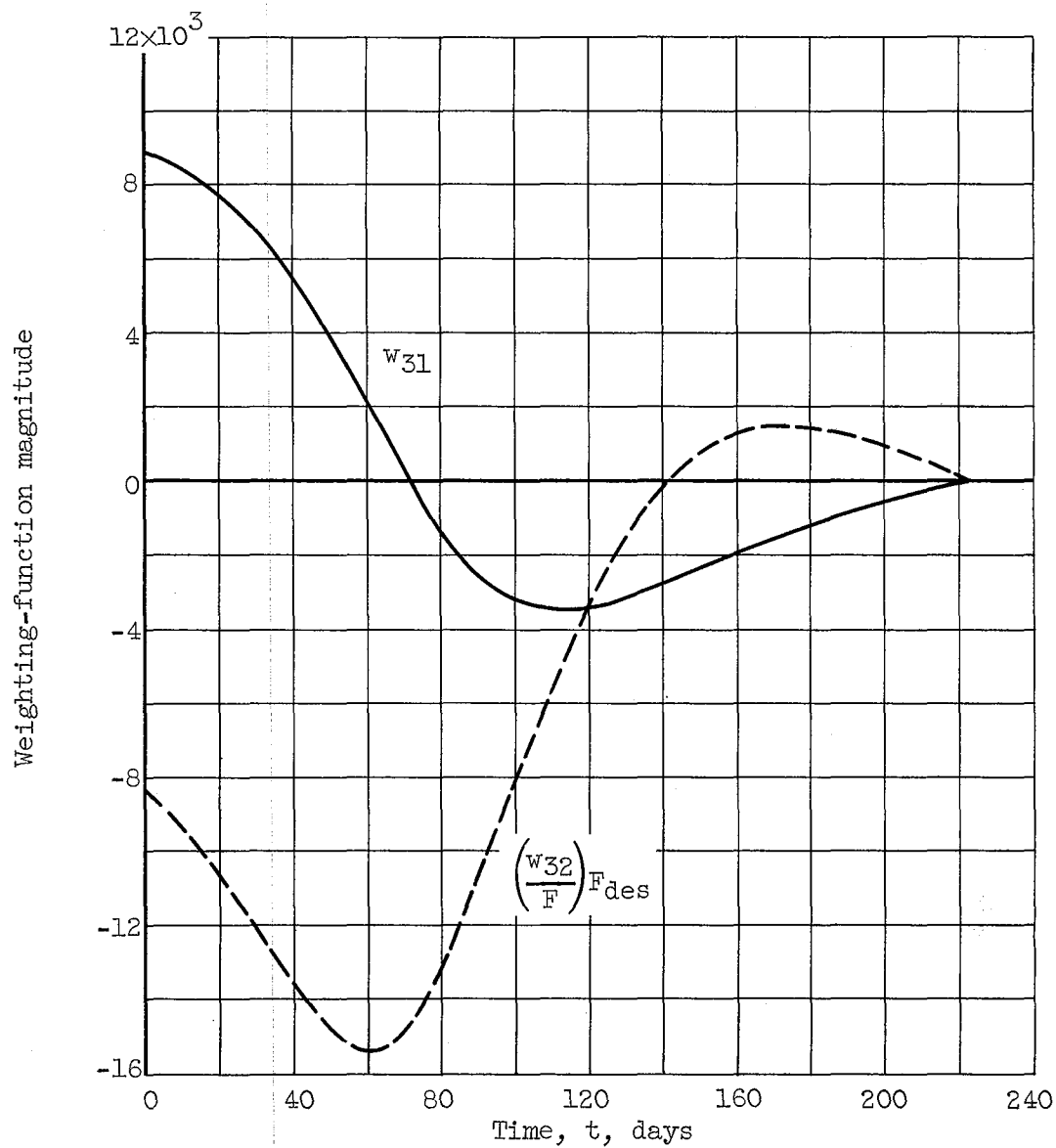(a) Sensitivity of final radial velocity to thrust-magnitude variations.
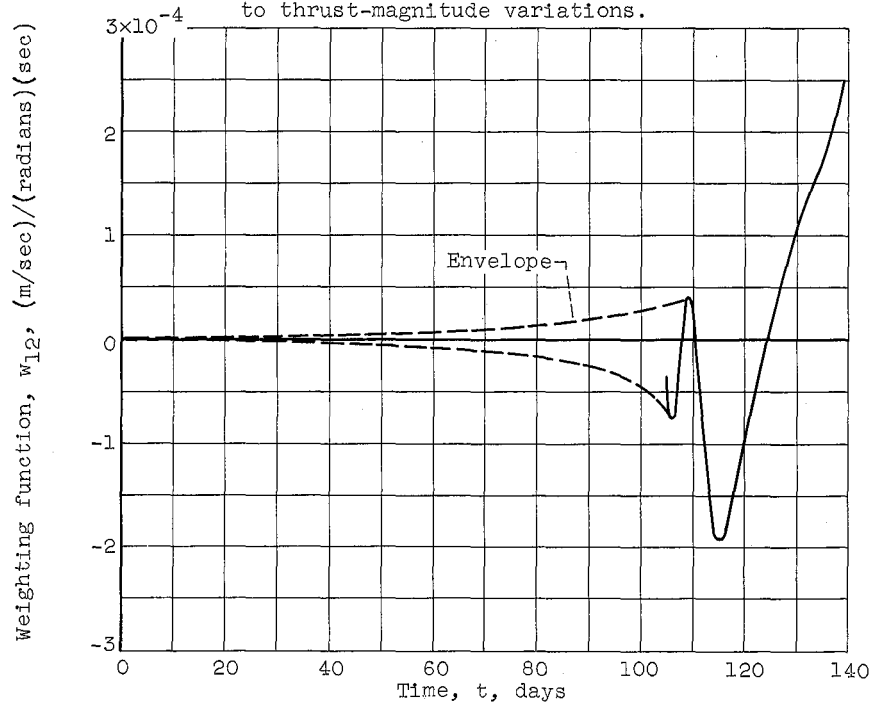
(b) Sensitivity of final radial velocity to thrust-angle variations.

Figure 6. - Thrust-vector weighting functions for escape-spiral phase.

54

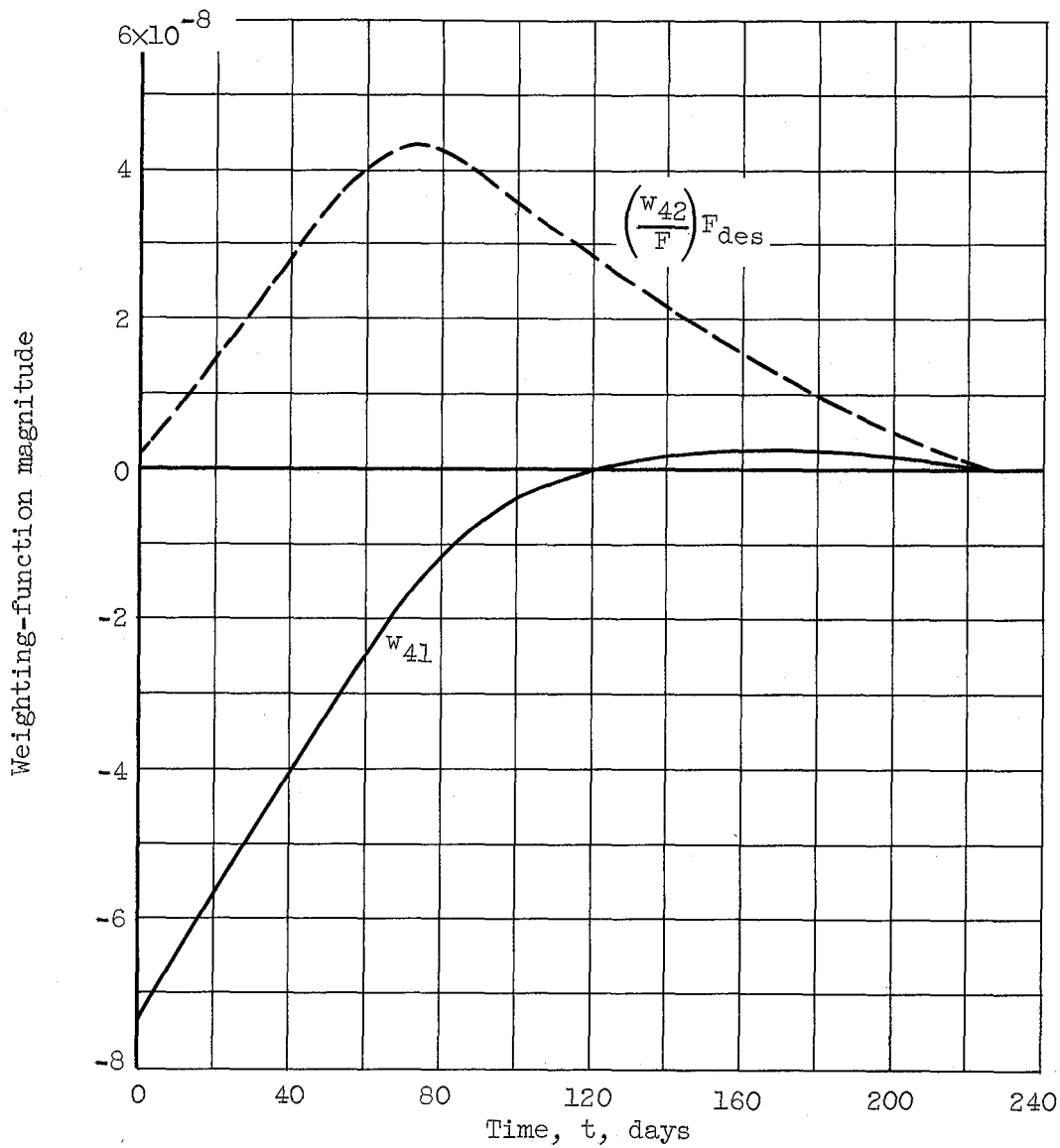(c) Sensitivity of final angular velocity to thrust-
magnitude variations.

(d) Sensitivity of final angular velocity to thrust-
angle variations.
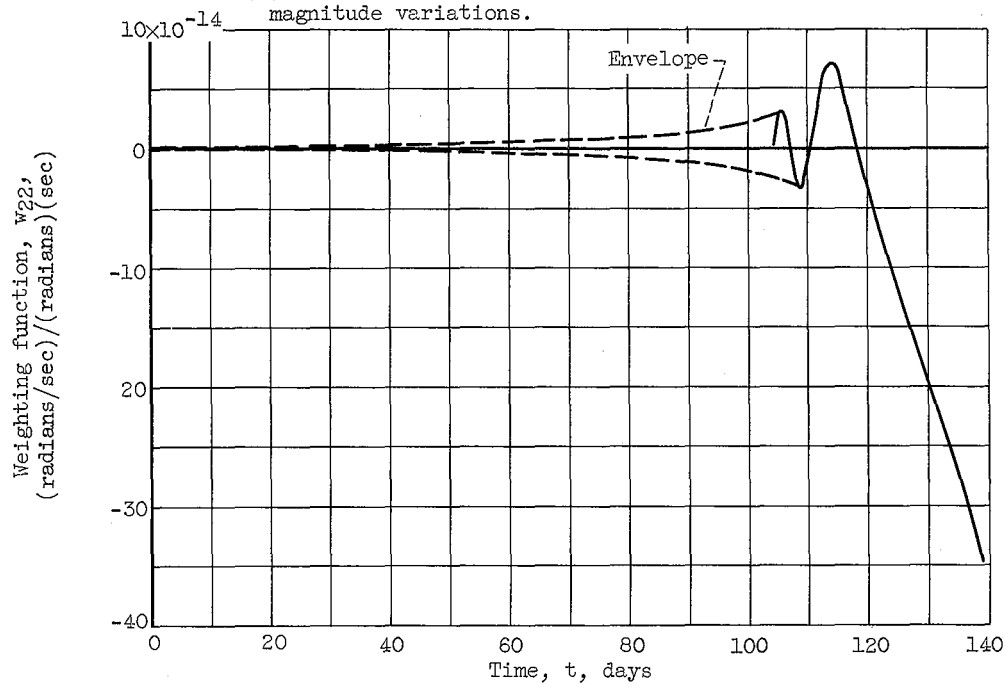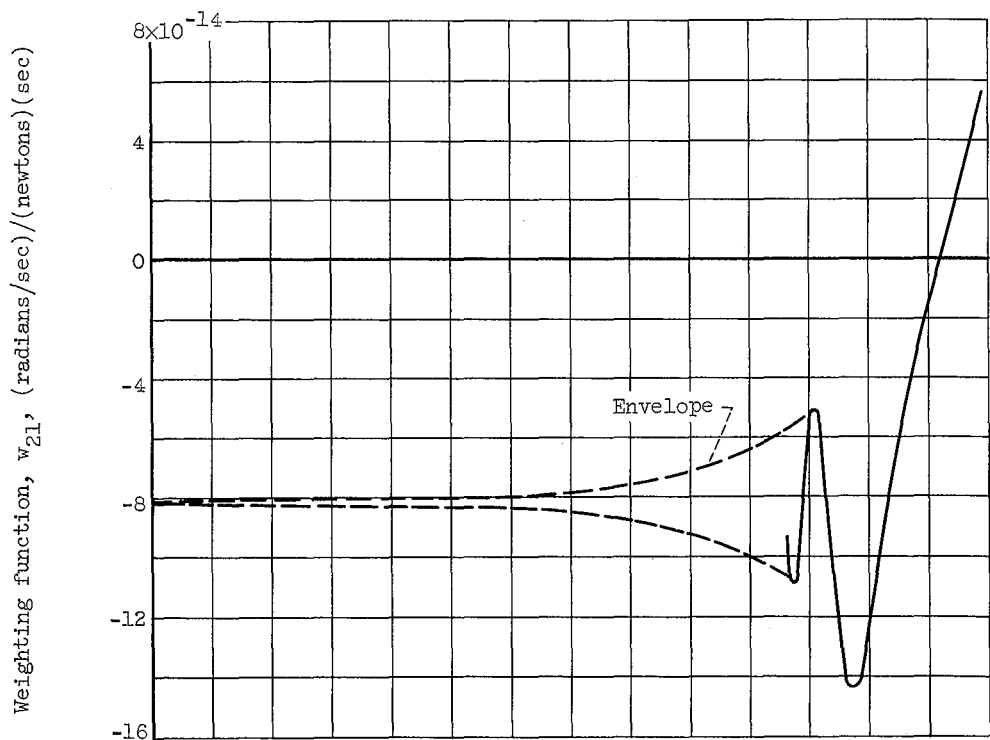
Figure 6. - Continued. Thrust-vector weighting functions
for escape-spiral phase.
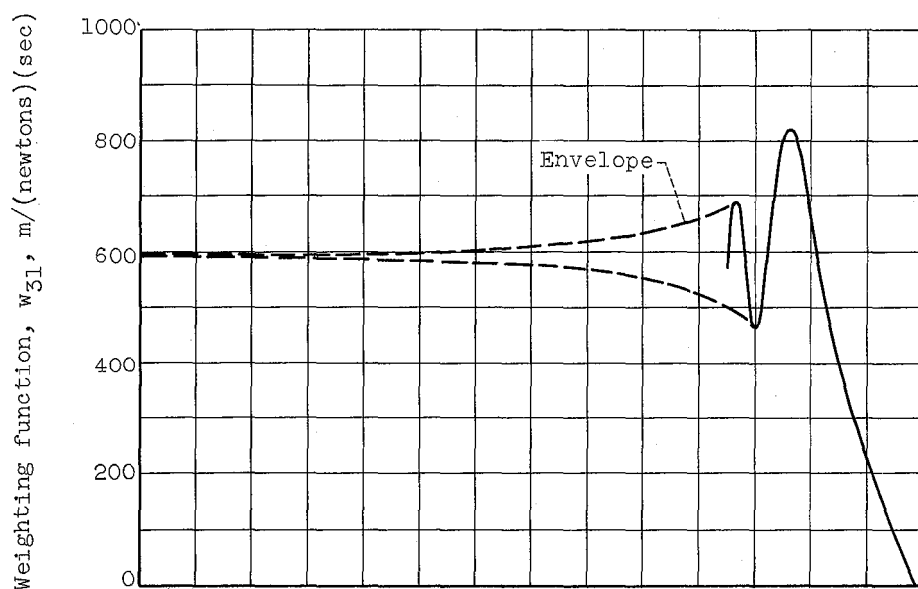
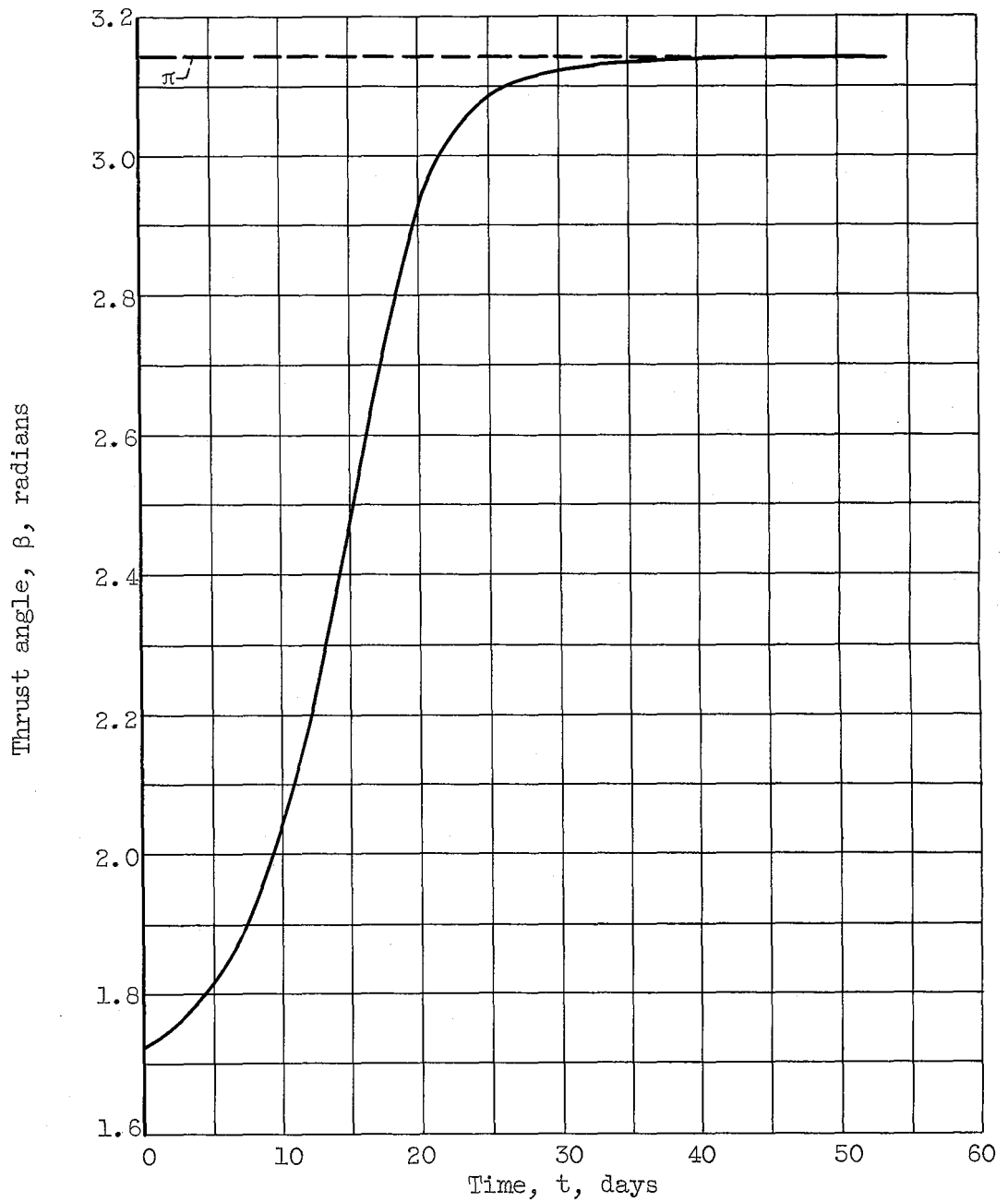(e) Sensitivity of final radial position to thrust-magnitude variations.

(f) Sensitivity of final radial position to thrust-angle variations.

Figure 6. - Continued. Thrust-vector weighting functions for escape-spiral phase.
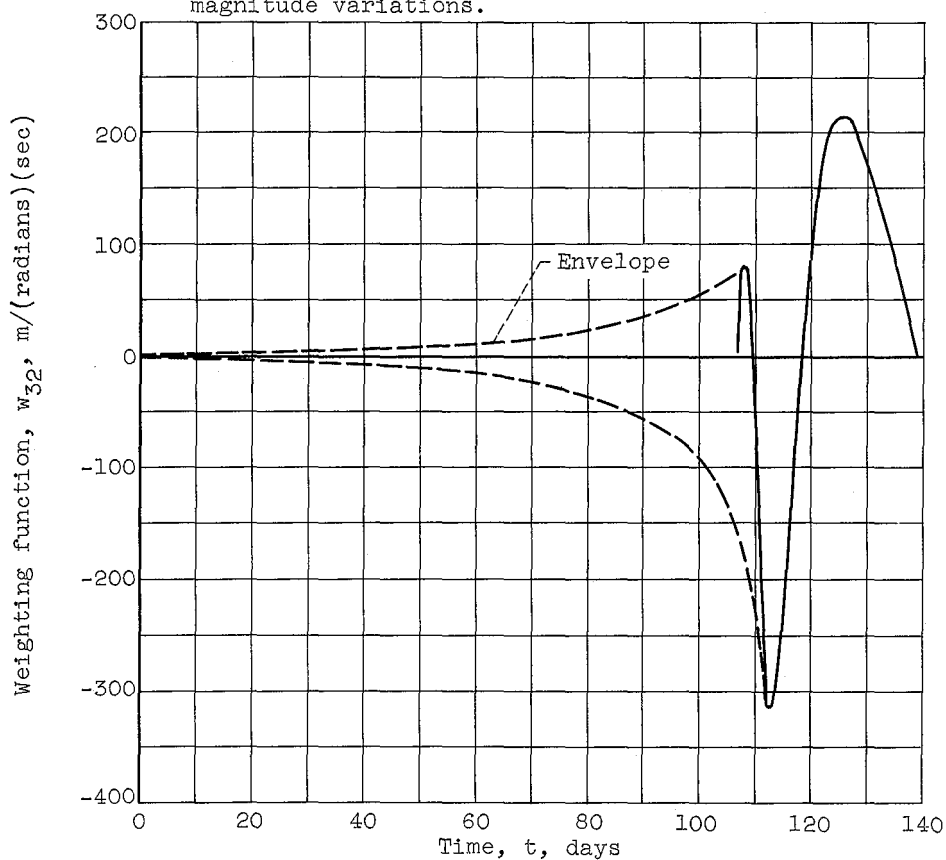
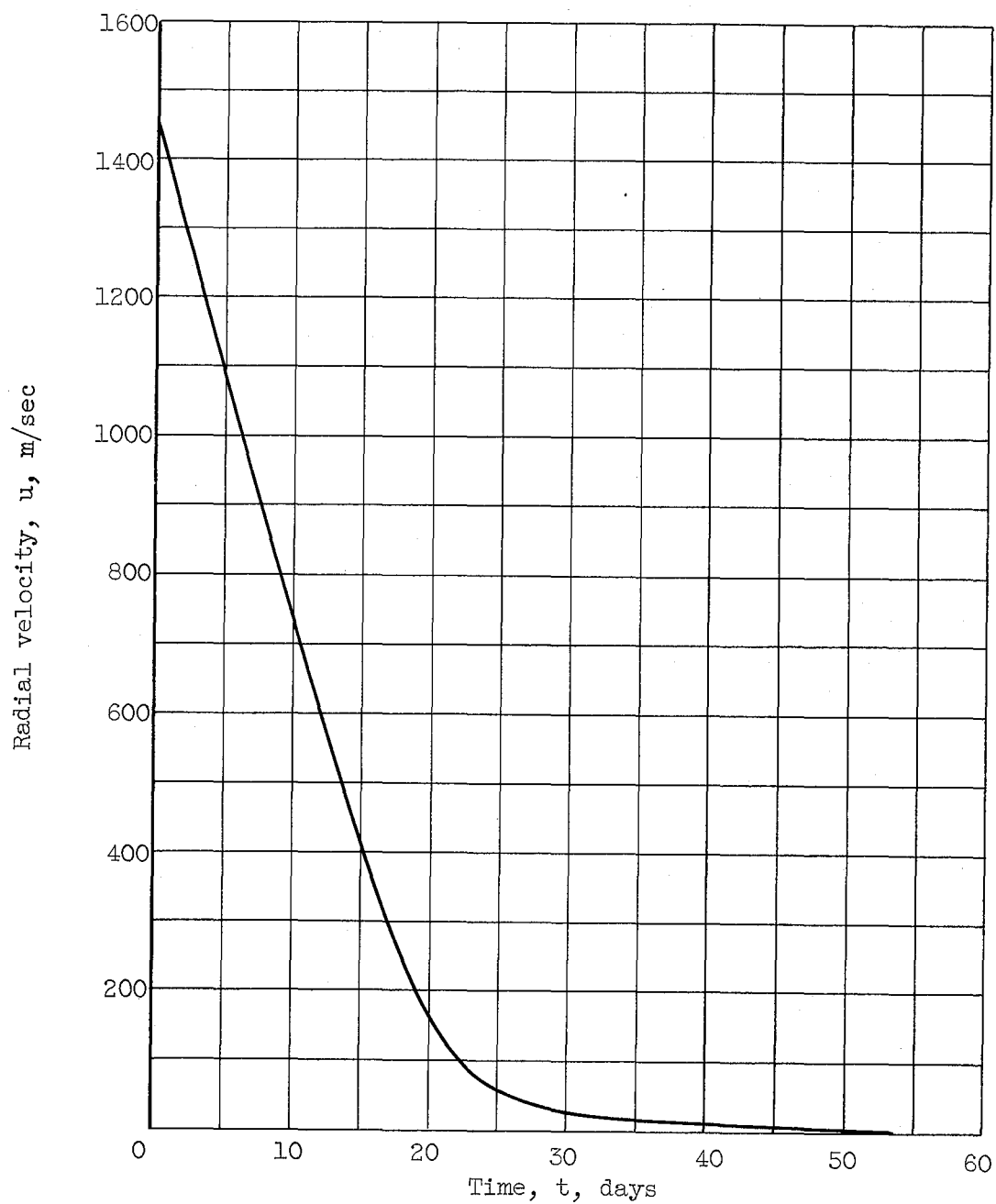(g) Sensitivity of final angular position to thrust-magnitude variations.

(h) Sensitivity of final angular position to thrust-angle variations.
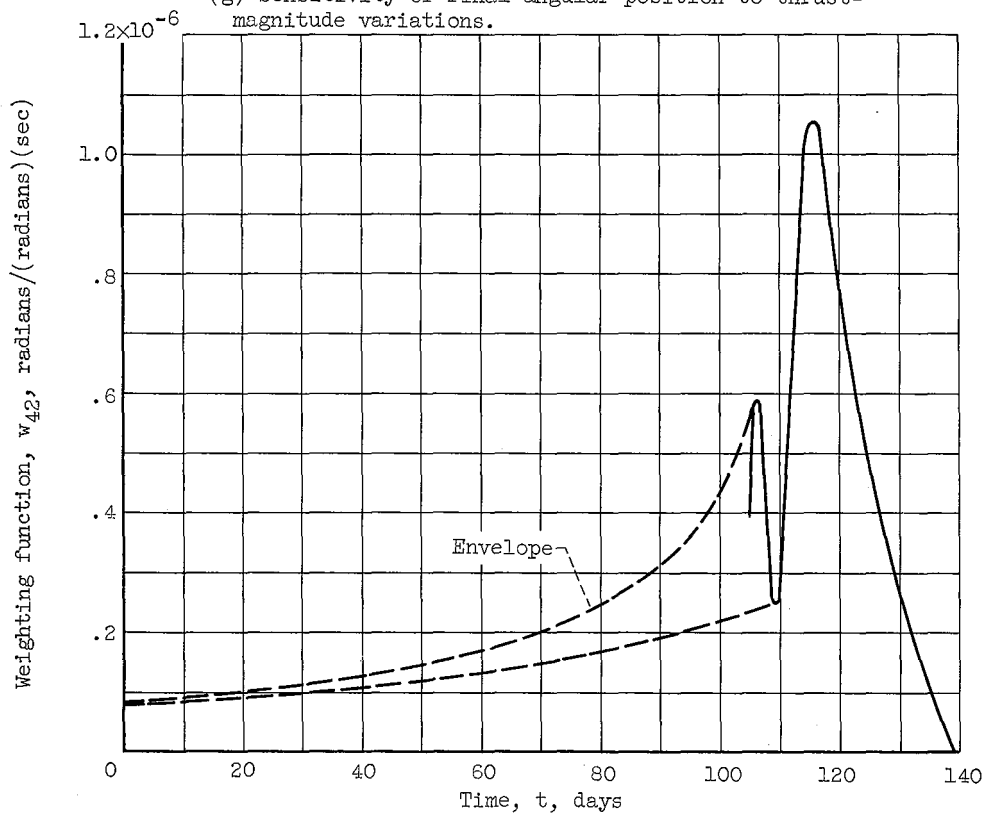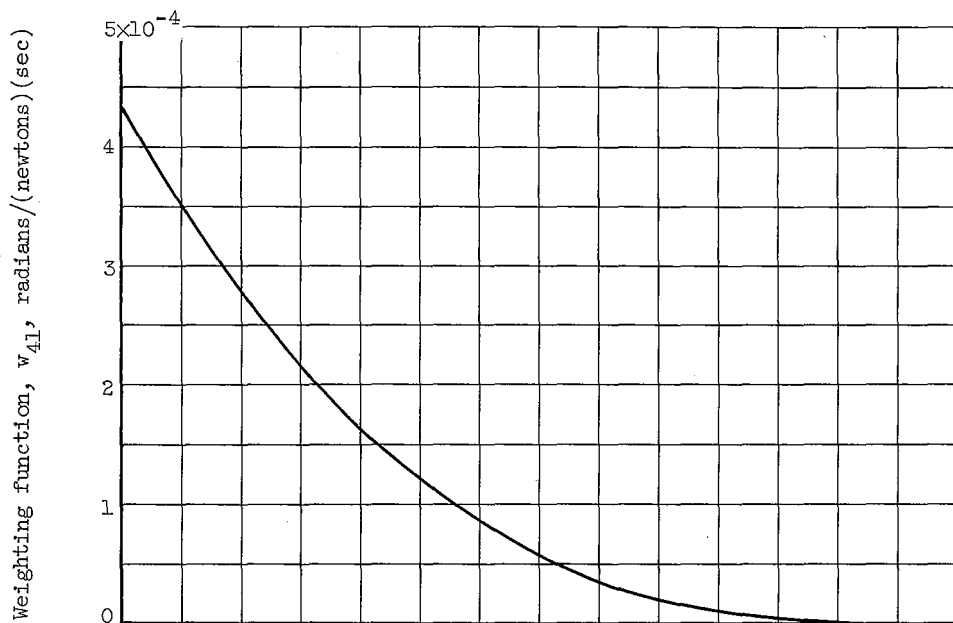
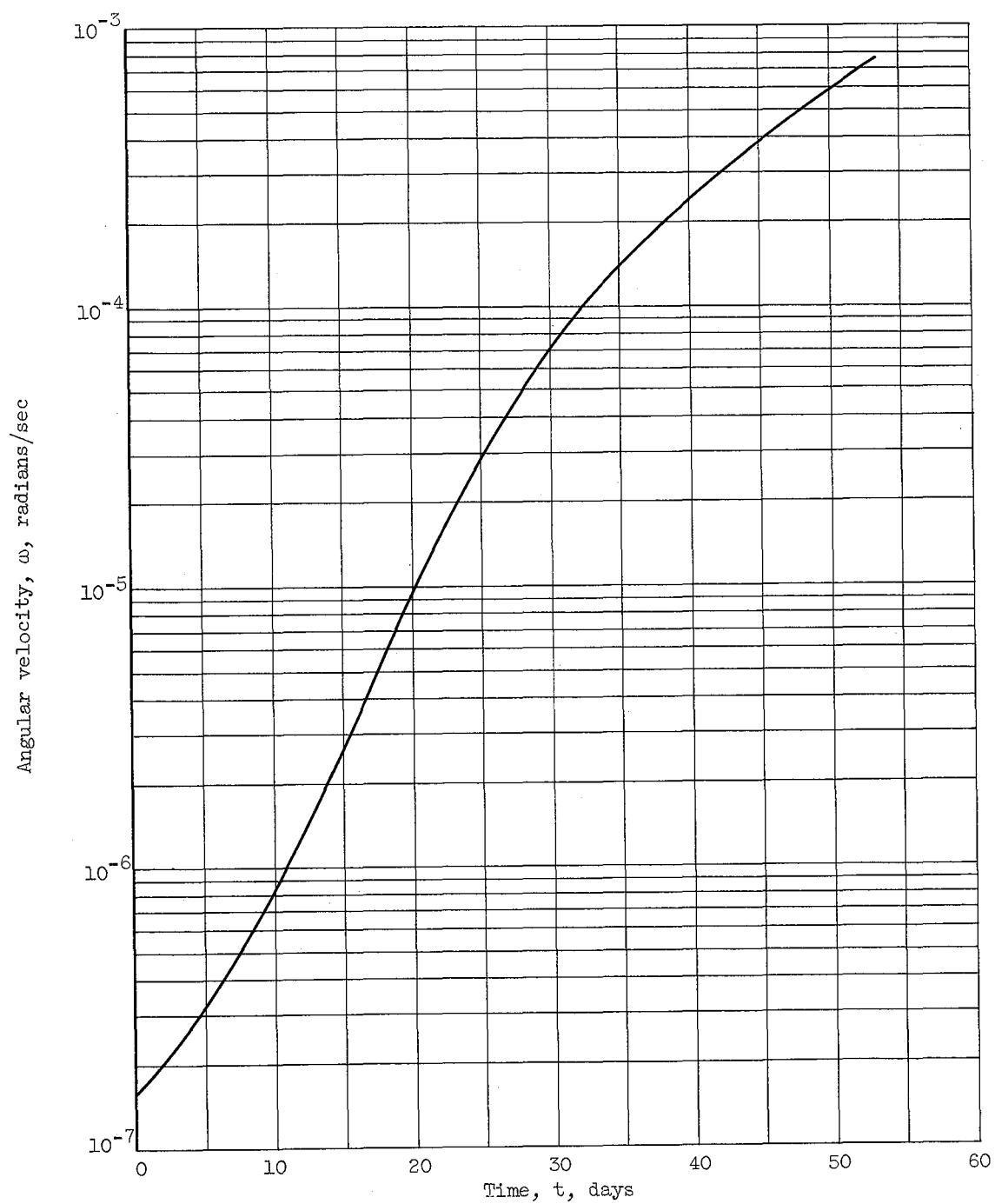Figure 6. - Concluded. Thrust-vector weighting functions for escape-spiral phase.
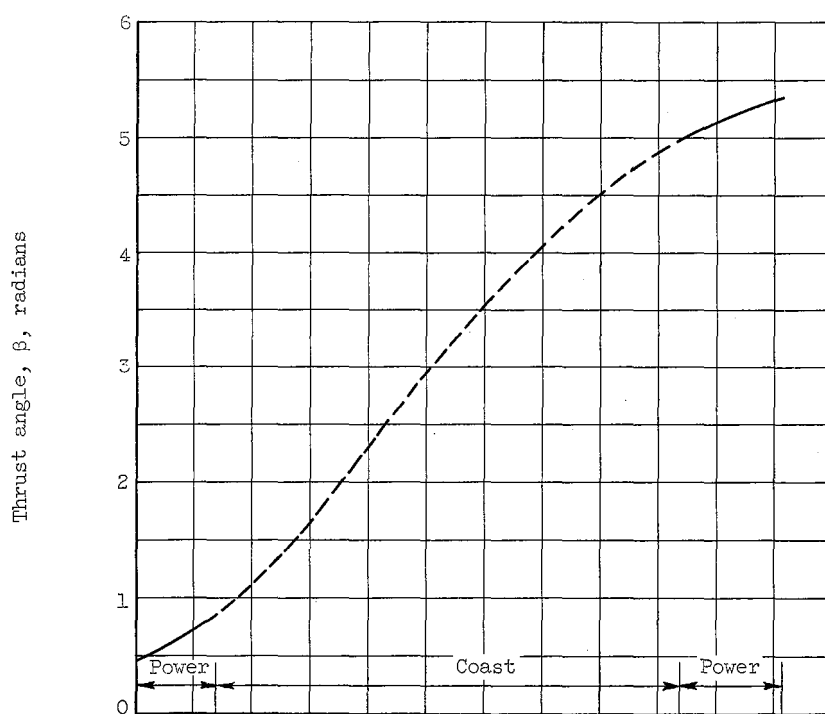
(a) Thrust-angle program.
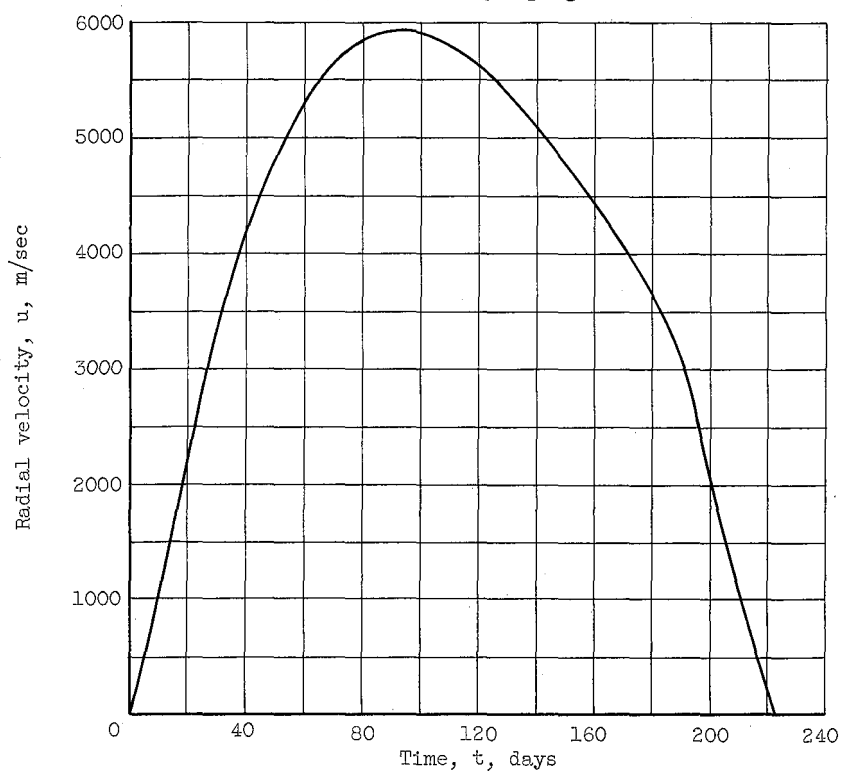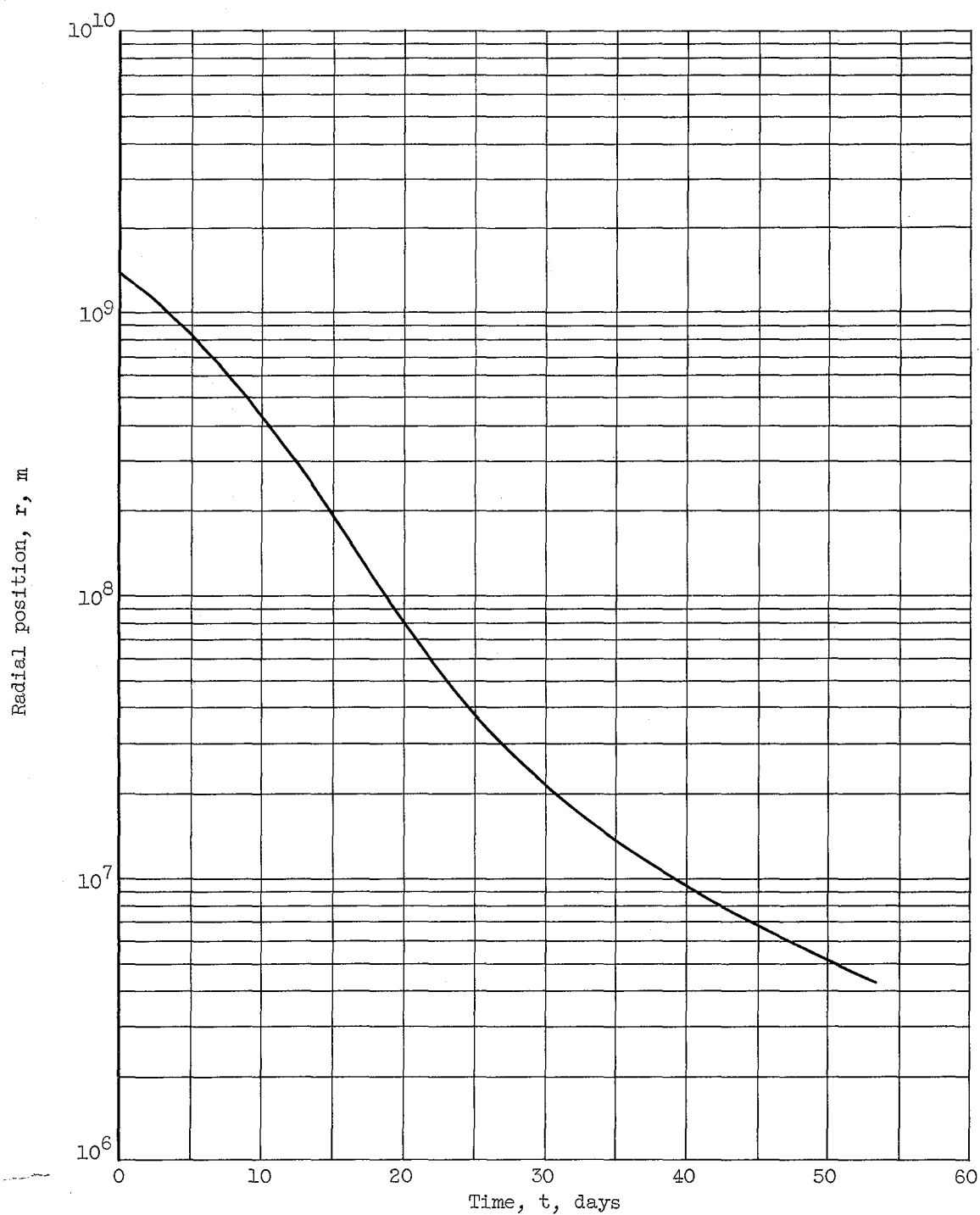
(b) Radial-velocity time history.

Figure 7. - Characteristics of heliocentric reference
trajectory.

(c) Angular-velocity time history.
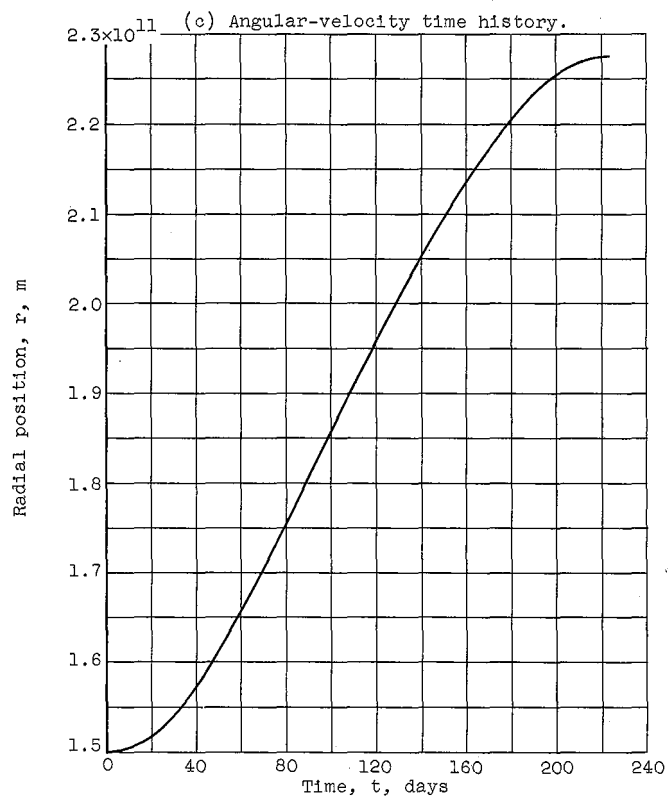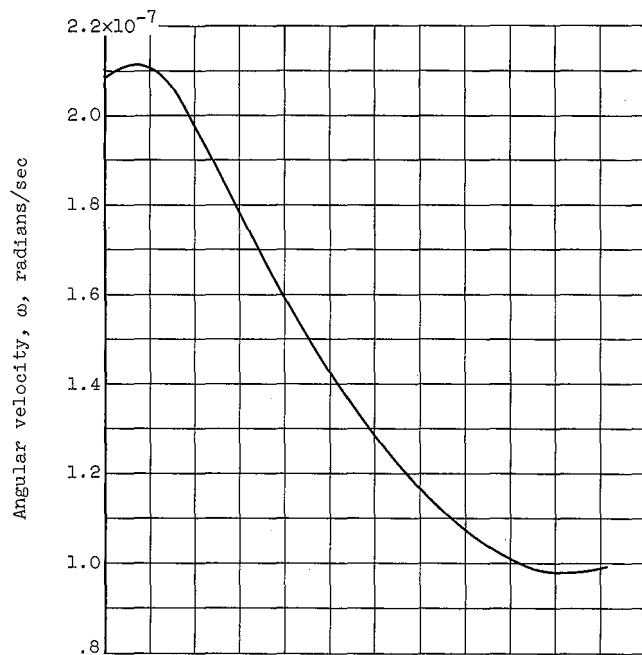
(d) Radial-position time history.

Figure 7. - Continued.   Characteristics of helio-
centric reference trajectory.
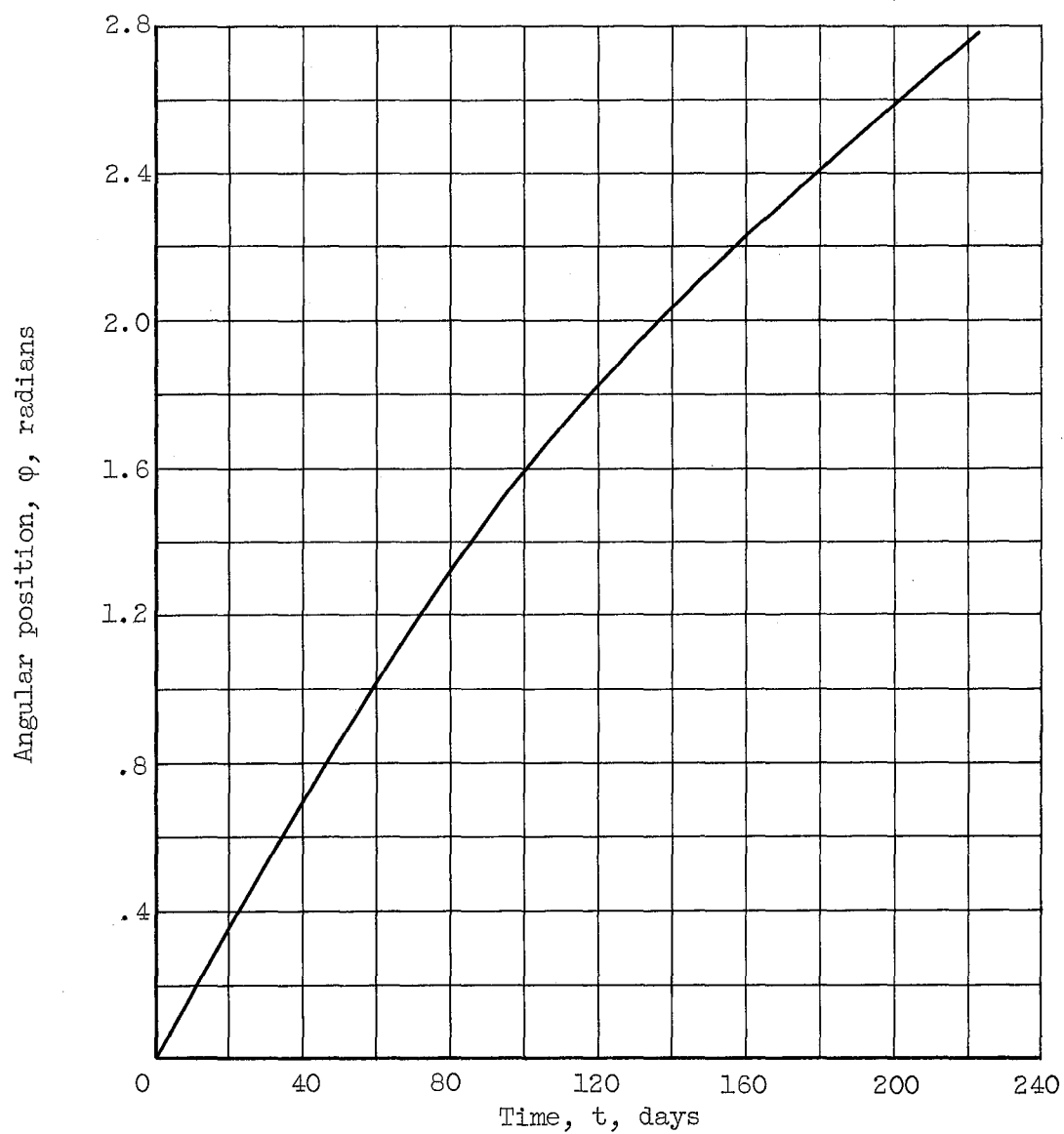
(e) Angular-position time history.

Figure 7. - Concluded. Characteristics of heliocentric
reference trajectory.
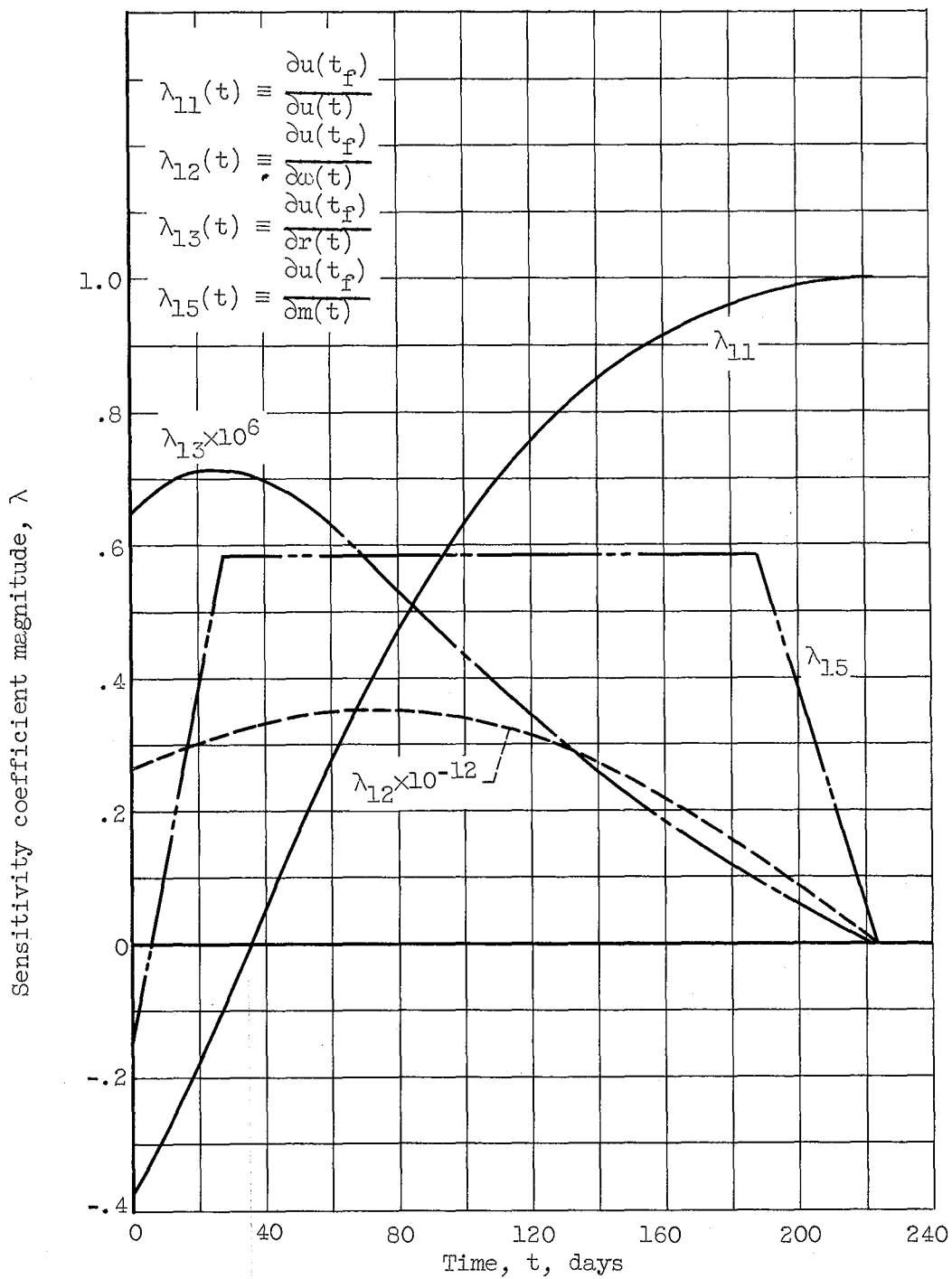
(a) Sensitivity of final radial velocity to variations in velocity, position, and mass.

Figure 8. – Adjoint solution for heliocentric-transfer phase.
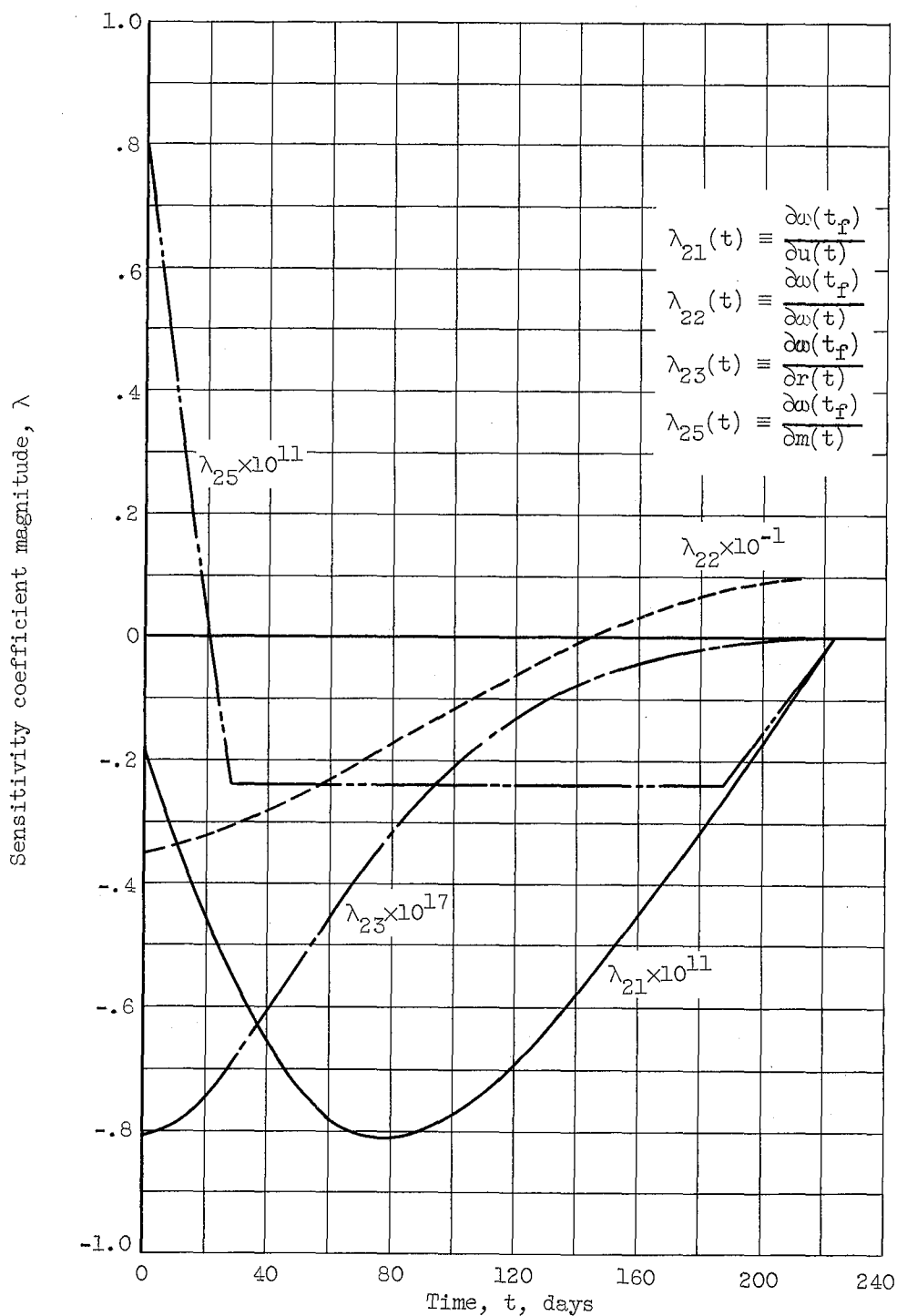
(b) Sensitivity of final angular velocity to variations in velocity, position, and mass.

Figure 8. - Continued. Adjoint solution for heliocentric-transfer phase.
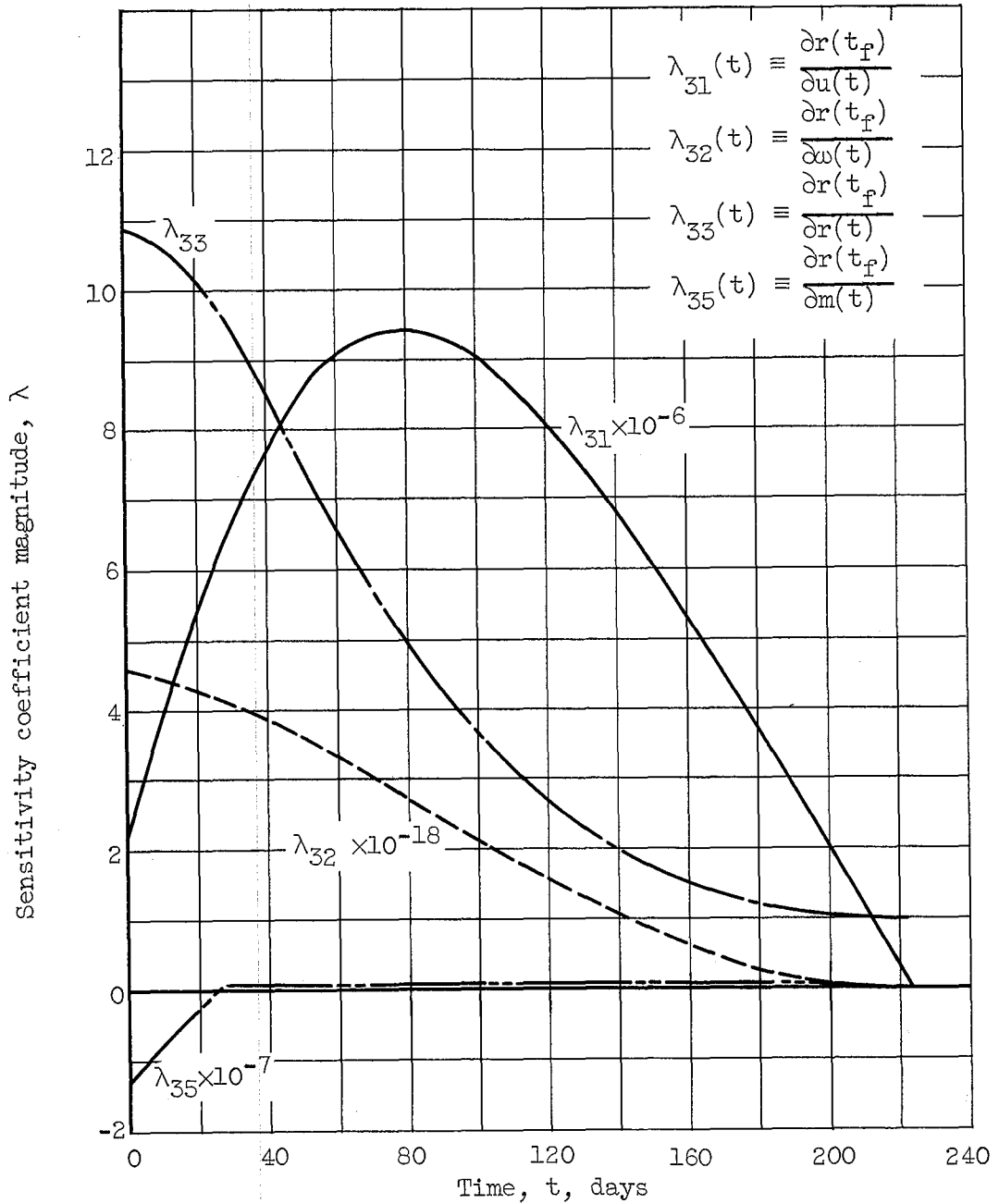
(c) Sensitivity of final radial position to variations
in velocity, position, and mass.

Figure 8. - Continued. Adjoint solution for
heliocentric-transfer phase.
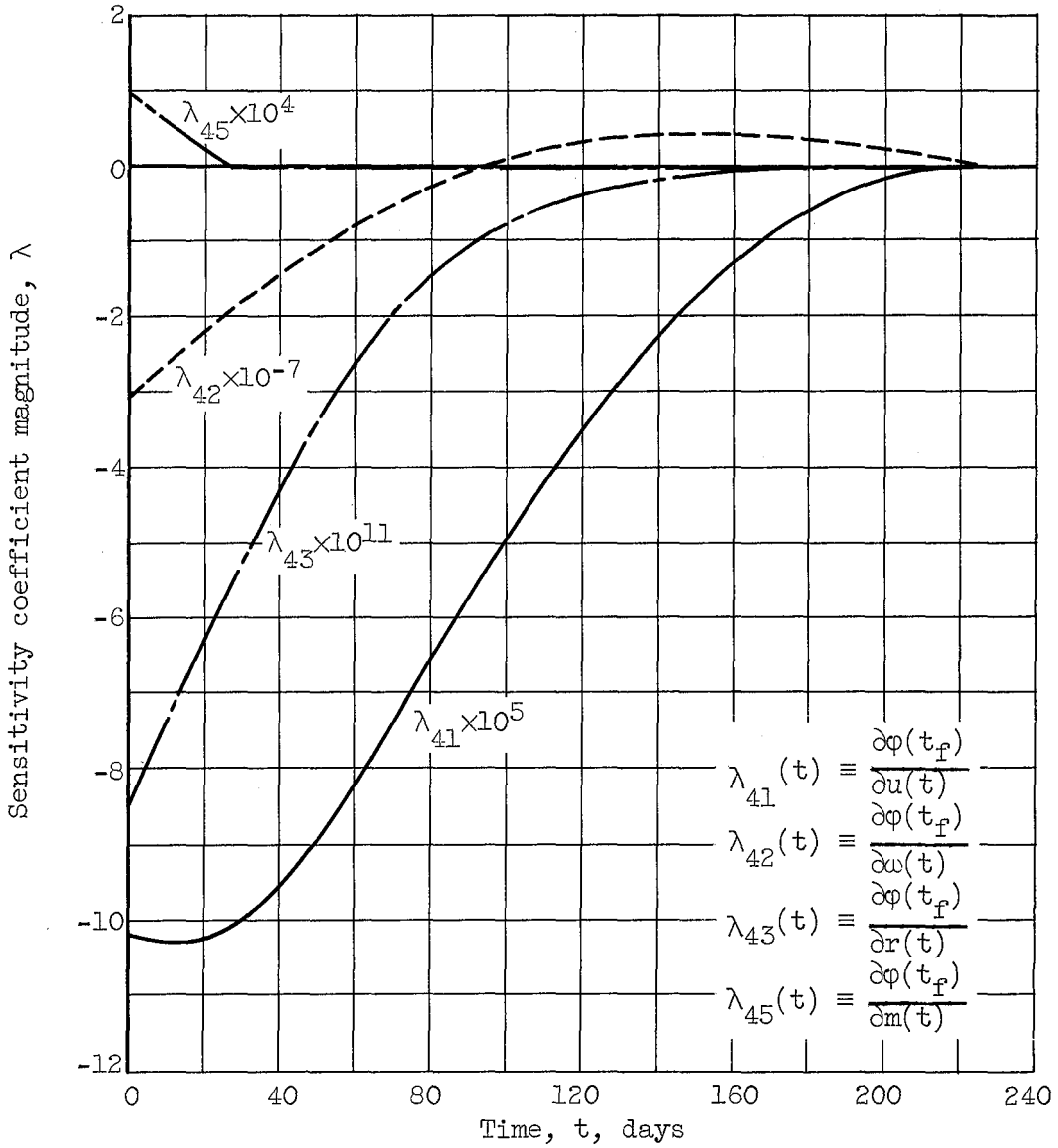
(d) Sensitivity of final angular position to variations in velocity, position, and mass.

Figure 8. - Concluded. Adjoint solution for heliocentric-transfer phase.
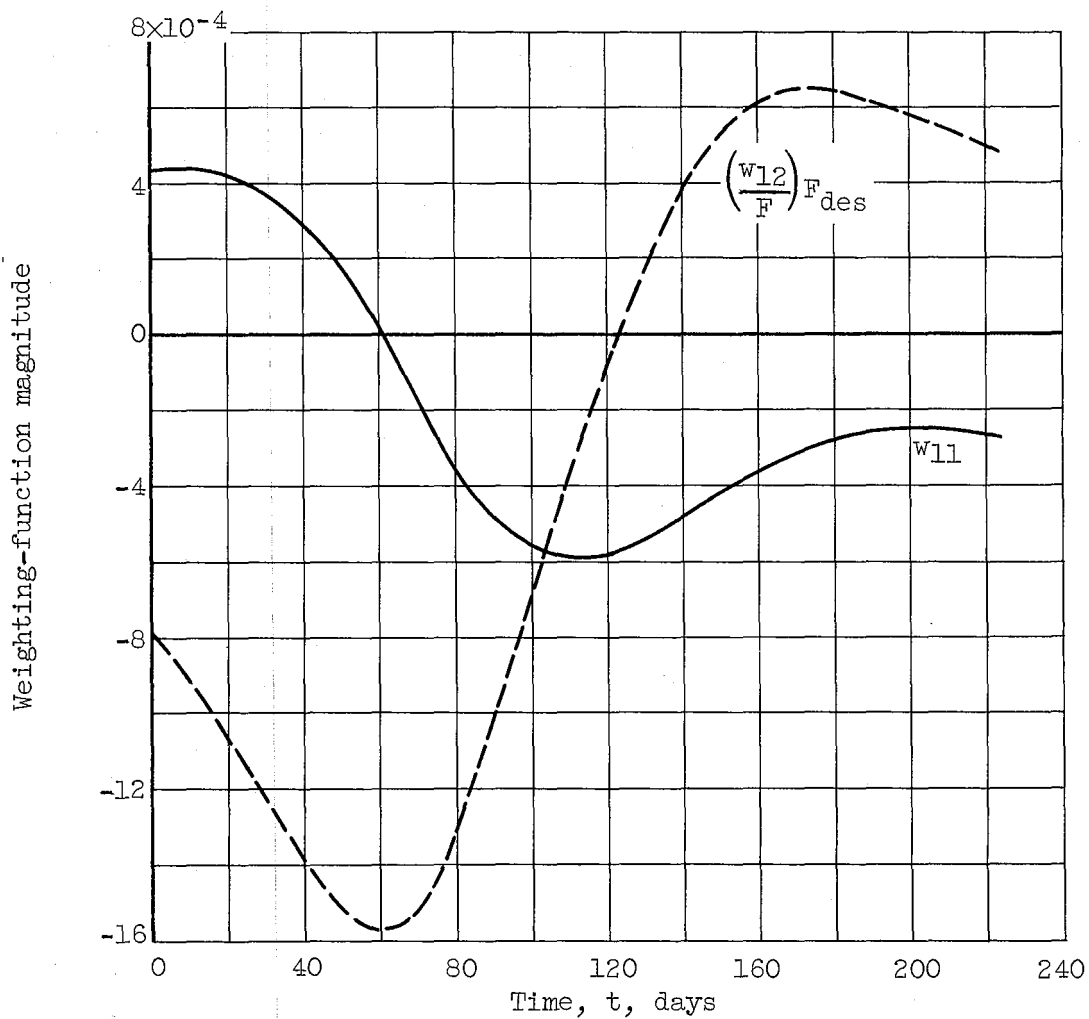
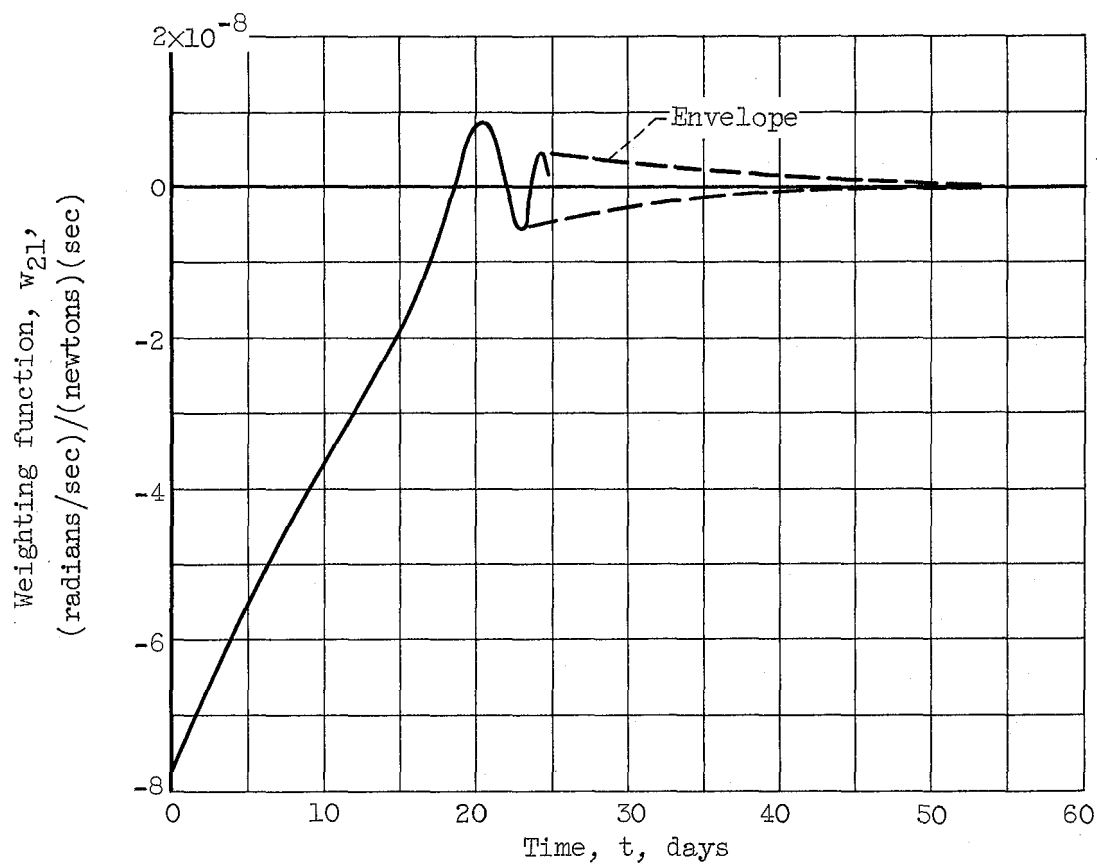(a) Sensitivity of final radial velocity to thrust-
vector variations.

Figure 9. - Thrust-vector weighting functions for
heliocentric-transfer phase.

(b) Sensitivity of final angular velocity to thrust-
vector variations.

Figure 9. - Continued. Thrust-vector weighting functions
for heliocentric-transfer phase.

(c) Sensitivity of final radial position to thrust-
vector variations.

Figure 9. - Continued. Thrust-vector weighting functions
for heliocentric-transfer phase.

6×10^{-8}

Weighting-function magnitude

$\left(\dfrac{w_{42}}{F}\right)F_{des}$

w_{41}

4

2

0

-2

-4

-6

-8

0   40   80   120   160   200   240

Time, t, days

(d) Sensitivity of final angular position to thrust-
vector variations.

Figure 9. - Concluded. Thrust-vector weighting functions
for heliocentric-transfer phase.

(a) Thrust-angle program.

Figure 10. - Characteristics of capture-spiral
reference trajectory.

(b) Radial-velocity time history.

Figure 10. - Continued. Characteristics of capture-
spiral reference trajectory.

(c) Angular-velocity time history.

Figure 10. - Continued. Characteristics of capture-spiral reference
trajectory.

(d) Radial-position time history.

Figure 10. - Continued.   Characteristics of capture-spiral reference
trajectory.
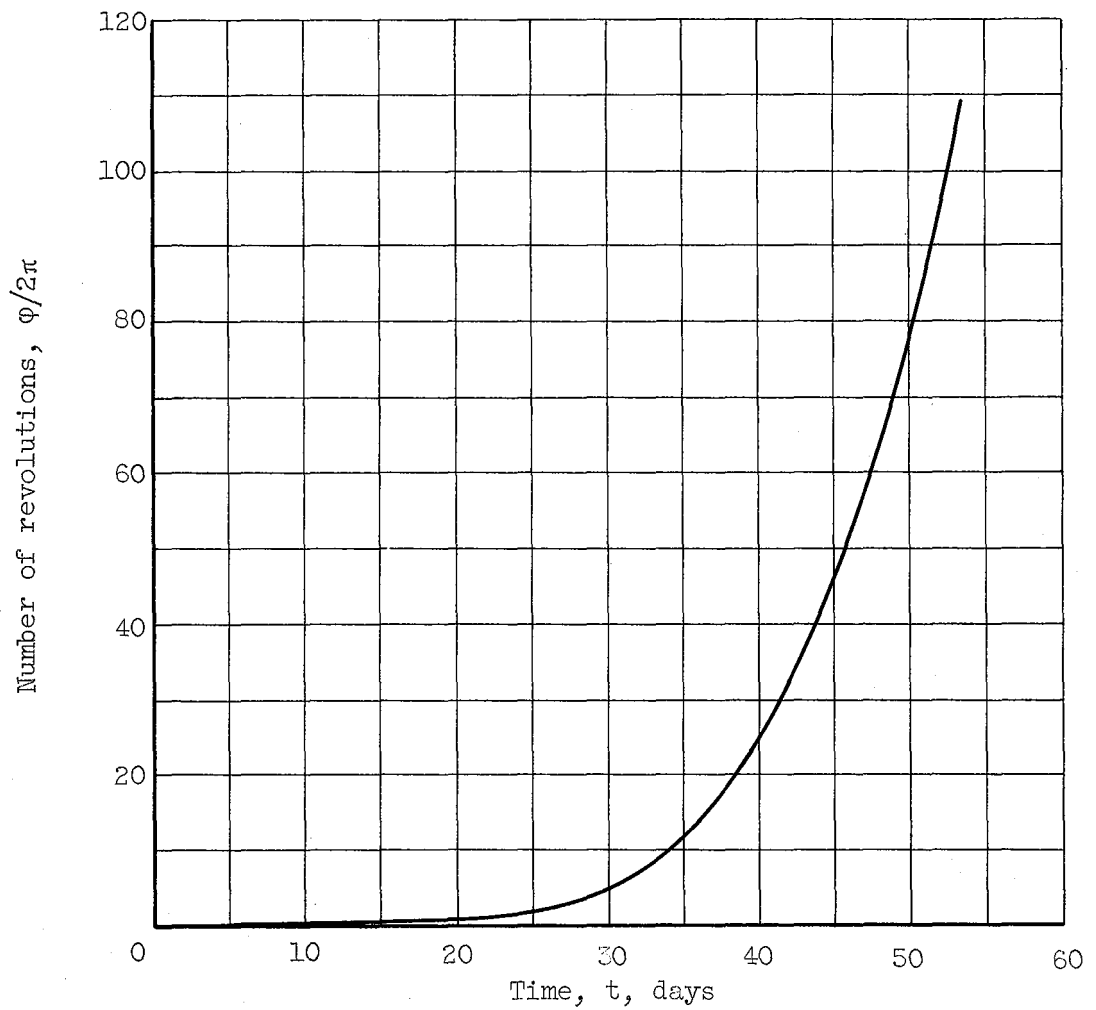
(e) Angular-position time history.

Figure 10. - Concluded.   Characteristics of capture-spiral
reference trajectory.
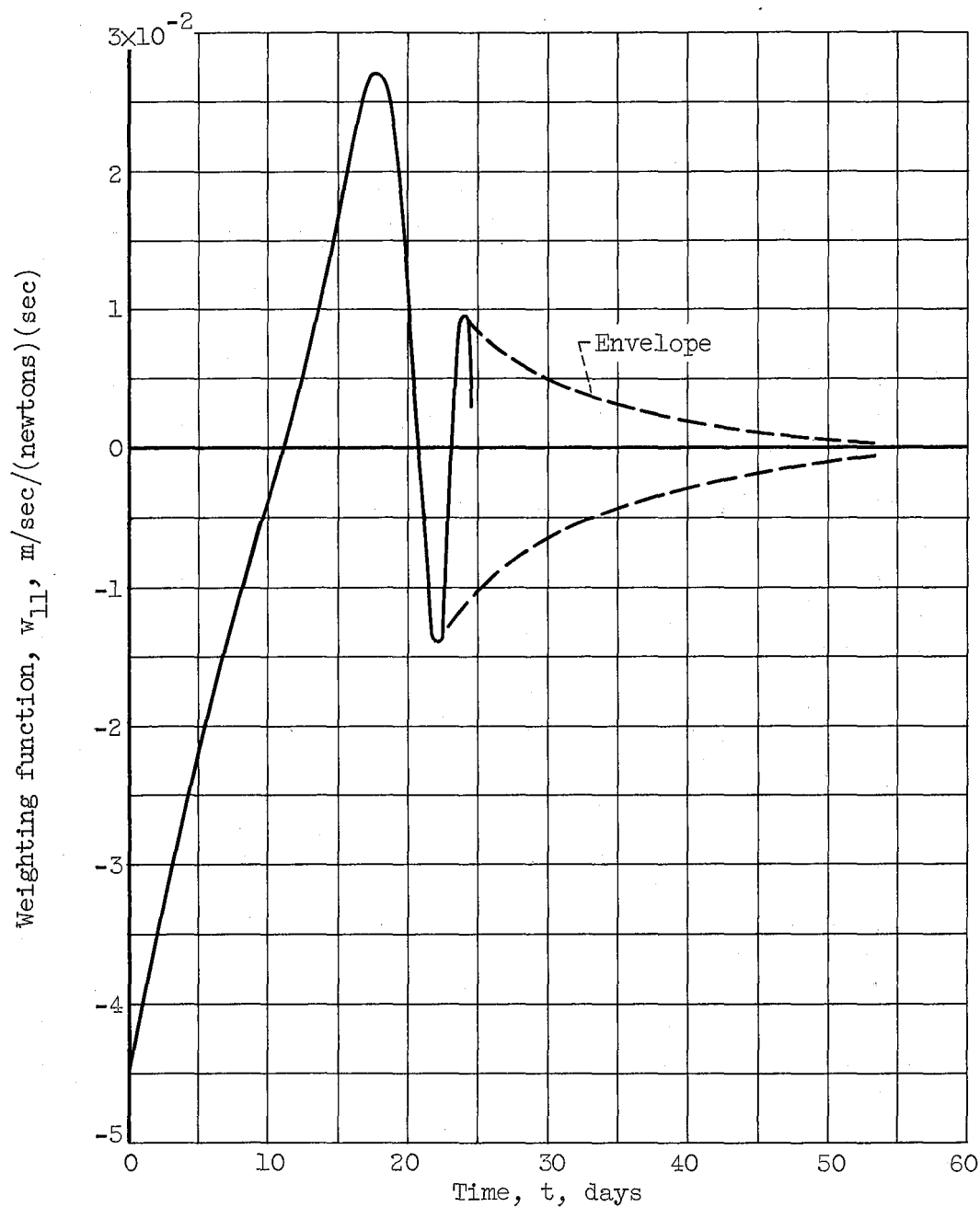
(a) Sensitivity of final radial velocity to thrust-magnitude variations.

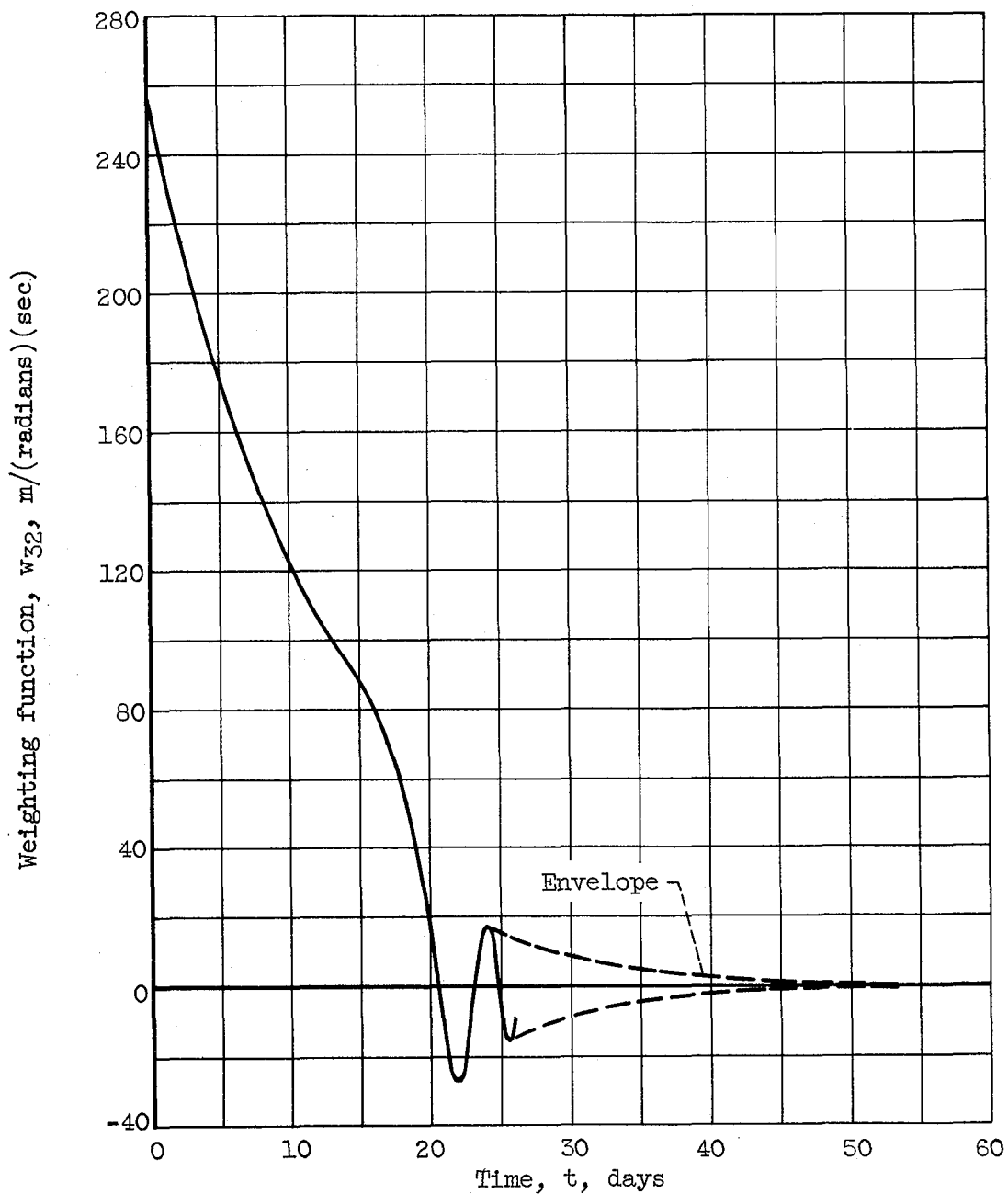Figure 11. - Thrust-vector weighting functions for capture-spiral phase.
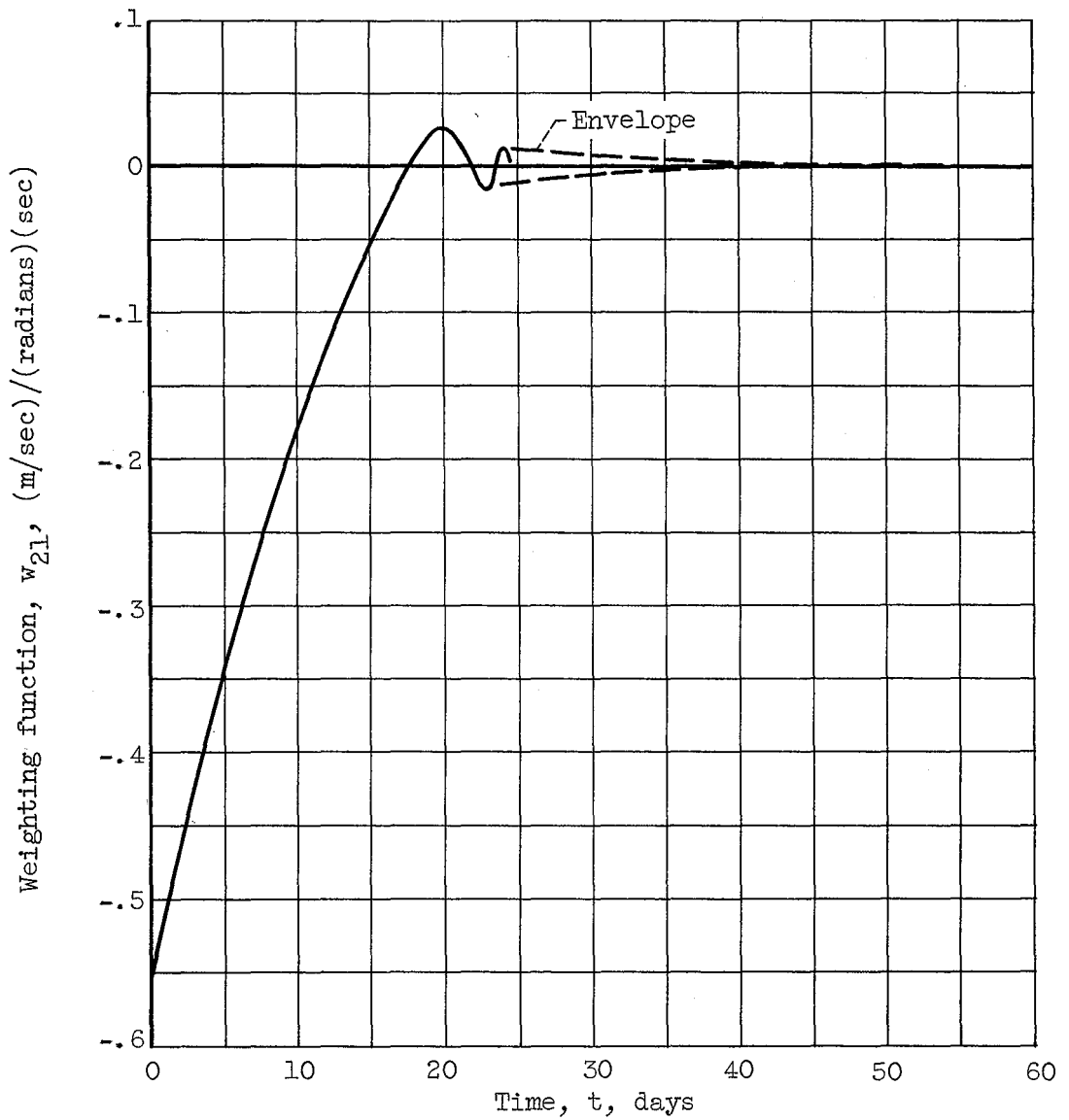
(b) Sensitivity of final radial velocity to thrust-angle variations.

Figure 11. - Continued.   Thrust-vector weighting functions for capture-spiral phase.

(c) Sensitivity of final angular velocity to thrust-magnitude variations.

Figure 11. - Continued.   Thrust-vector weighting functions for capture-spiral phase.
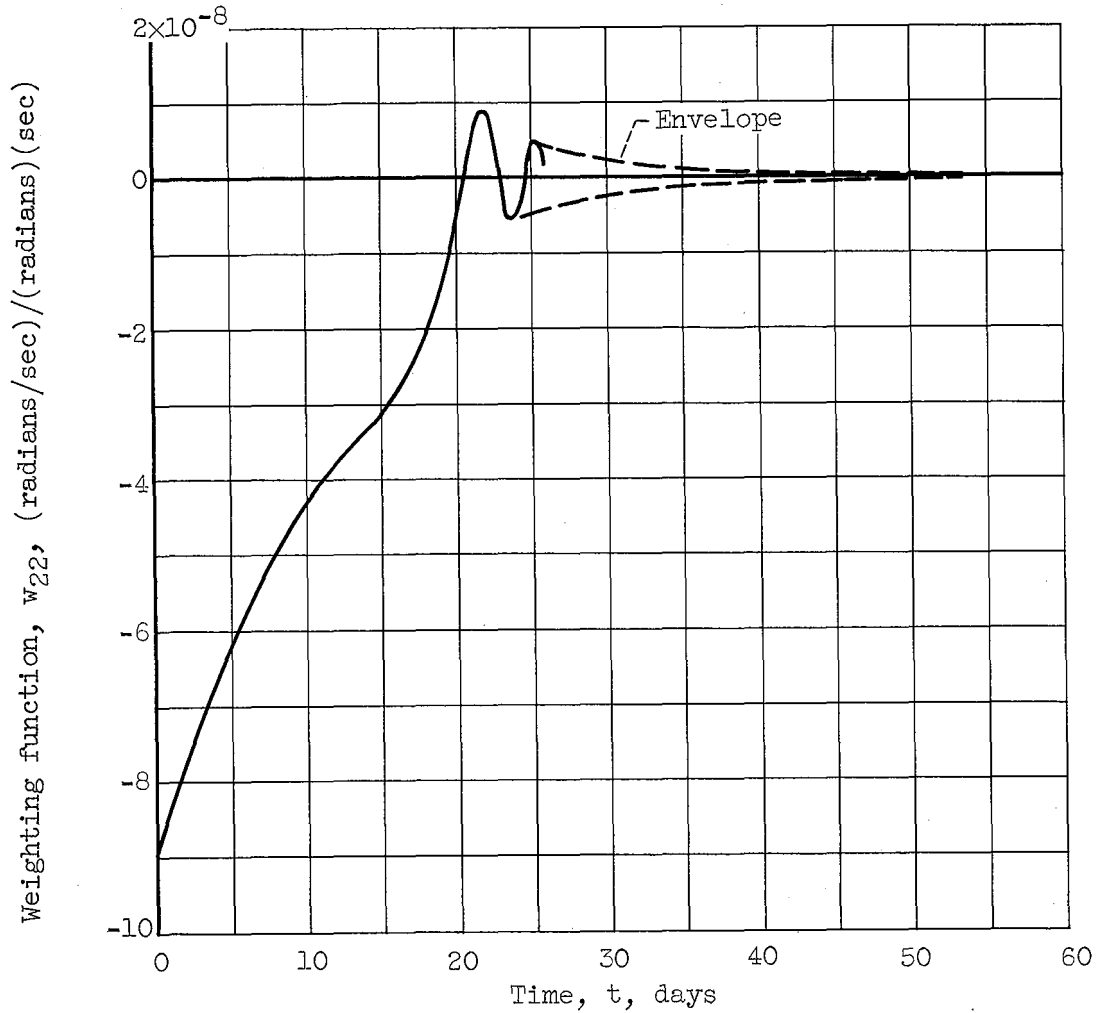
(d) Sensitivity of final angular velocity to thrust-angle variations.

Figure 11. - Continued. Thrust-vector weighting functions for capture-spiral phase.
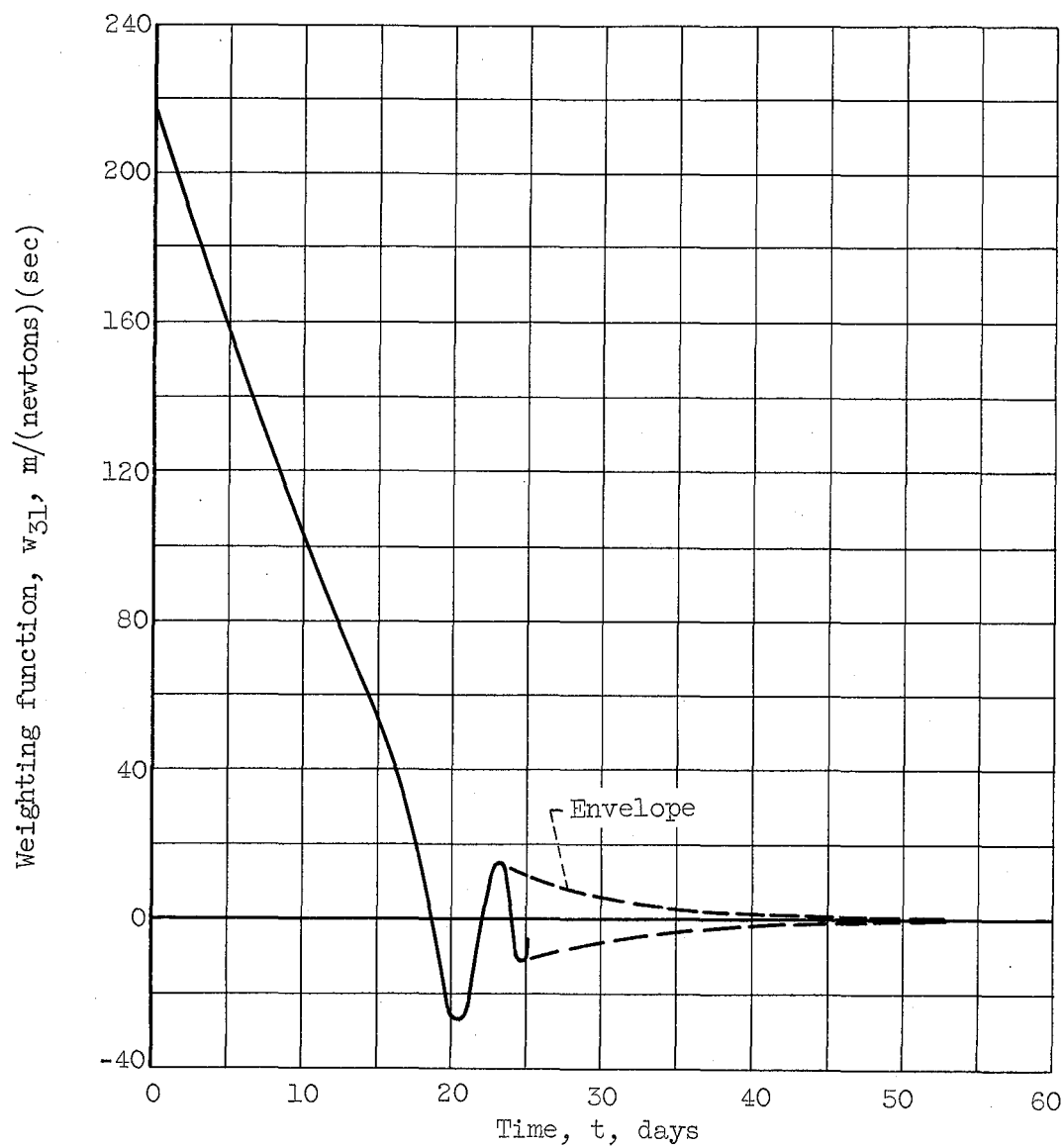
(e) Sensitivity of final radial position to thrust-magnitude variations.

Figure 11. - Continued. Thrust-vector weighting functions for capture-spiral phase.
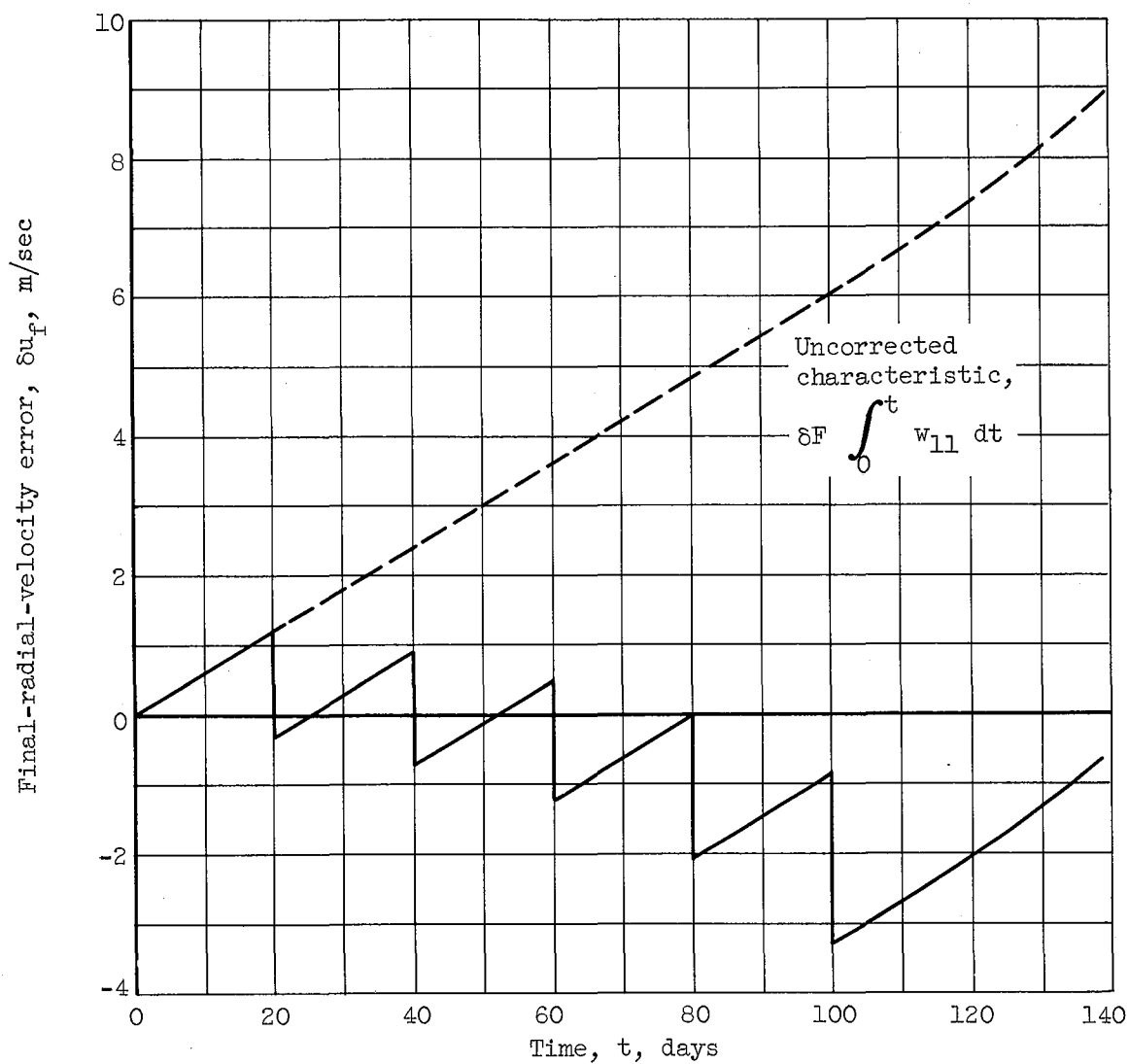
(f) Sensitivity of final radial position to thrust-
angle variations.

Figure 11. - Concluded. Thrust-vector weighting
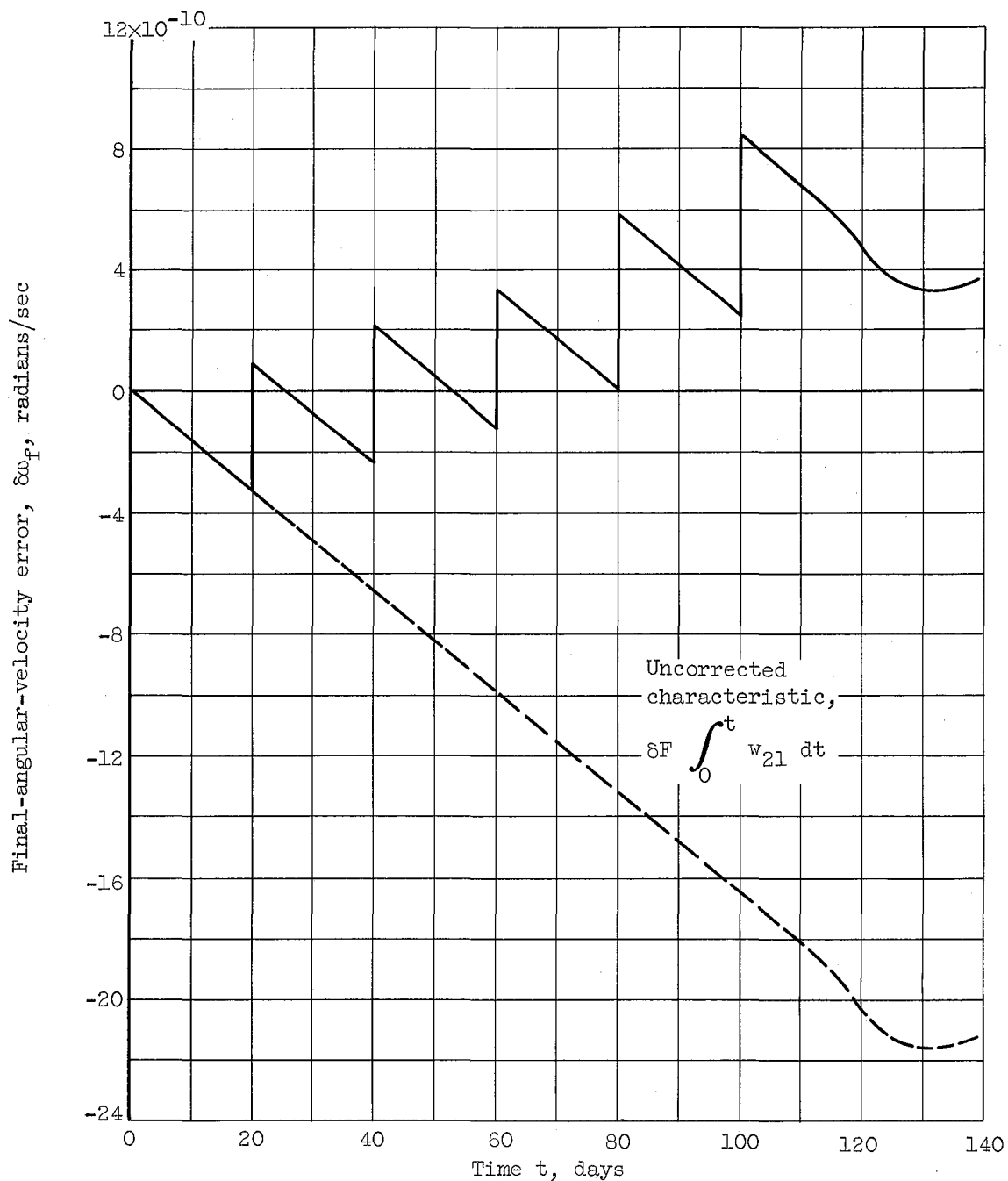functions for capture-spiral phase.
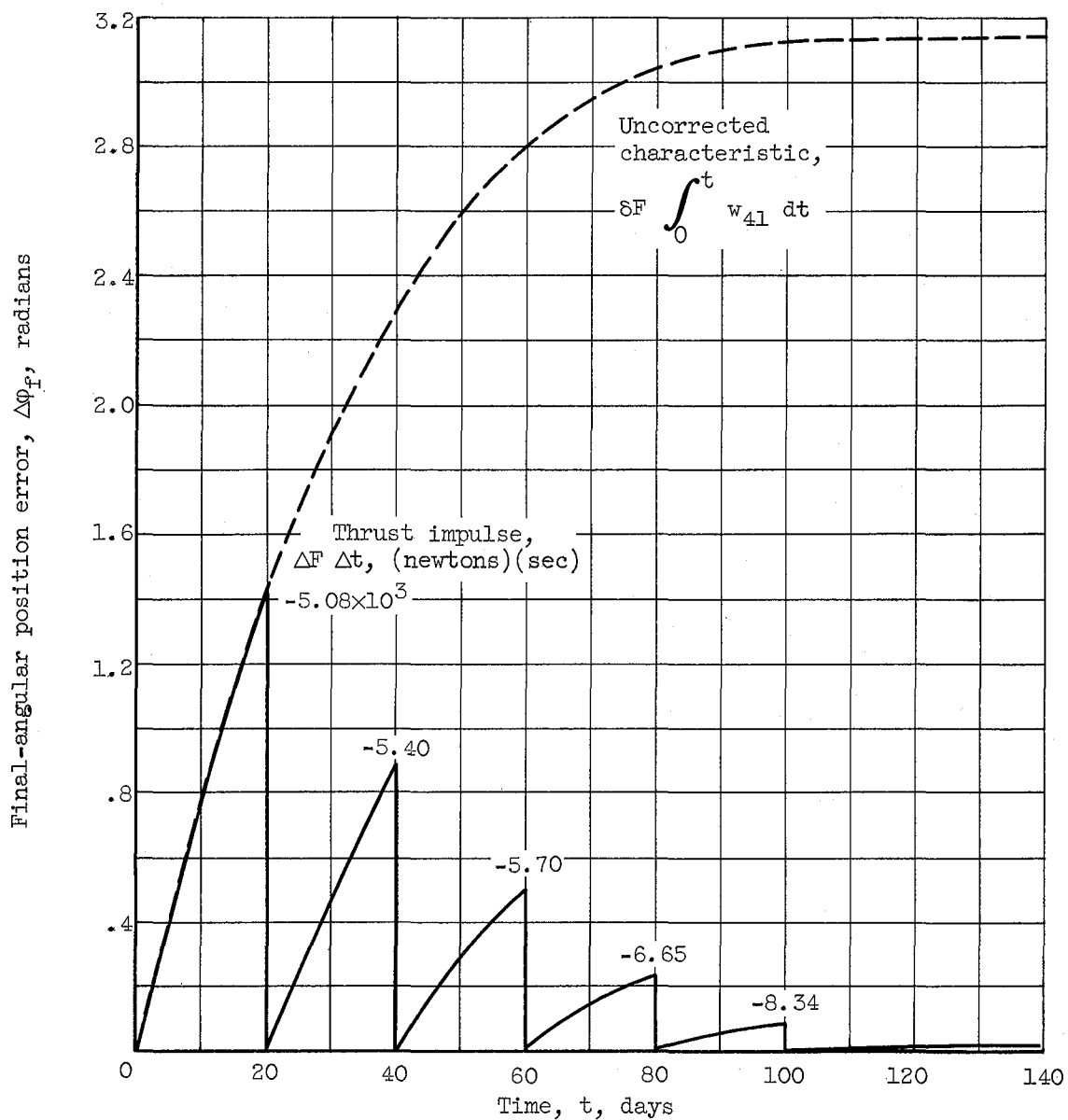
(a) Final-angular-position characteristic.

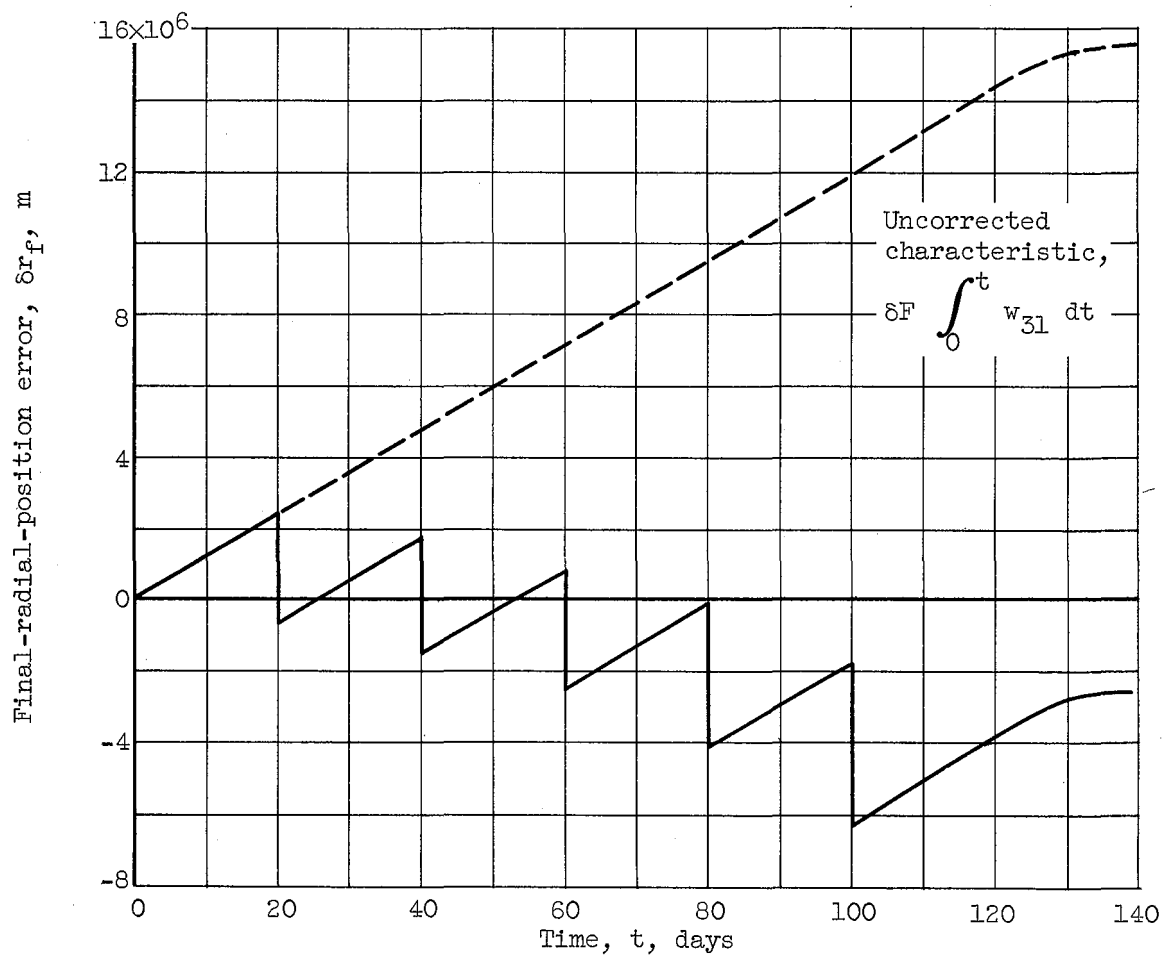Figure 12. - Simulated escape guidance maneuver; thrust-magnitude perturbation, δF, 2.32×10^{-3} newton.

(b) Final-radial-velocity characteristic.

Figure 12. - Continued. Simulated escape guidance maneuver; thrust-magnitude perturbation, δF, 2.32×10^{-3} newton.

(c) Final-angular-velocity characteristic.

Figure 12. - Continued. Simulated escape guidance maneuver; thrust-magnitude perturbation, δF, 2.32×10^{-3} newton.

(d) Final-radial-position characteristic.

Figure 12. - Concluded. Simulated escape guidance maneuver; thrust-magnitude perturbation, δF, 2.32×10^{-3} newton.